

UNCLASSIFIED

AD NUMBER
AD451357
NEW LIMITATION CHANGE
TO Approved for public release, distribution unlimited
FROM Distribution authorized to U.S. Gov't. agencies and their contractors; Administrative/Operational Use; 22 oct 1964. Other requests shall be referred to Army Missile Command, Restone Arsenal, AL.
AUTHORITY
CFSTI per RSIC Center, 4 Nov 1965

THIS PAGE IS UNCLASSIFIED

UNCLASSIFIED

AD. 4 5 1 3 5 7

DEFENSE DOCUMENTATION CENTER

FOR

SCIENTIFIC AND TECHNICAL INFORMATION

CAMERON STATION ALEXANDRIA, VIRGINIA



UNCLASSIFIED

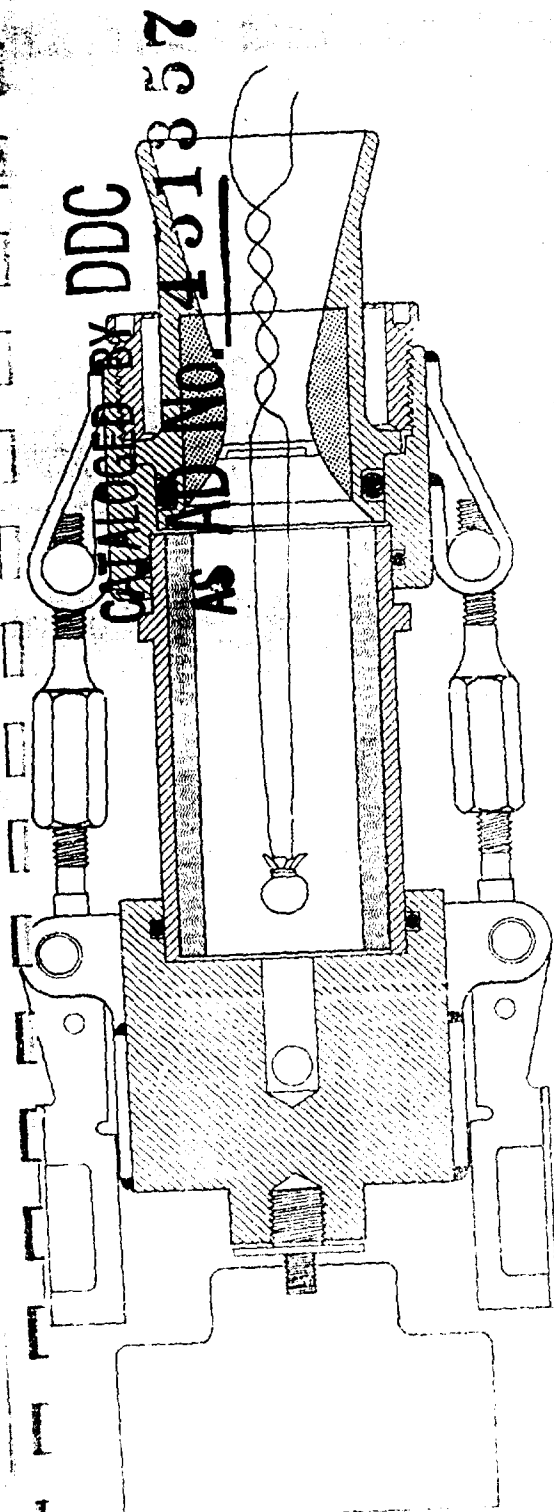
NOTICE: When government or other drawings, specifications or other data are used for any purpose other than in connection with a definitely related government procurement operation, the U. S. Government thereby incurs no responsibility, nor any obligation whatsoever; and the fact that the Government may have formulated, furnished, or in any way supplied the said drawings, specifications, or other data is not to be regarded by implication or otherwise as in any manner licensing the holder or any other person or corporation, or conveying any rights or permission to manufacture, use or sell any patented invention that may in any way be related thereto.

ROHM & HAAS COMPANY
REDSTONE ARSENAL RESEARCH DIVISION
HUNTSVILLE, ALABAMA

S-49
Copy No. 1
Nov. 1964



BALLISTIC EVALUATION OF PROPELLANTS IN MICRO-MOTORS



451357

DDC
NOV 24 1964
DDC-IRA C

U.S. ARMY MISSILE COMMAND
DA-01-021 ORD-11876
DA-01-021 ORD-11909

Best Available Copy

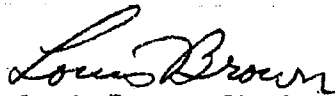
ROHM & HAAS COMPANY

REDSTONE ARSENAL RESEARCH DIVISION
HUNTSVILLE, ALABAMA

Report No. S-49

BALLISTIC EVALUATION OF PROPELLANTS IN MICRO-MOTORS

Approved:


Louis Brown, Head
Ballistics Section


O. H. Loeffler
General Manager

Written by:

Byron L. Cockrell

Contributing Staff:

J. L. Chaille

B. L. Cockrell

J. E. DeMore

T. E. Stonecypher

B. E. Sturgis

October 22, 1964

The work done herein was
carried out under Contracts:

DA-01-021 ORD-11878(Z)

DA-01-021 ORD-11909(Z)

ROHM & HAAS COMPANY

REDSTONE ARSENAL RESEARCH DIVISION
HUNTSVILLE, ALABAMA

BALLISTIC EVALUATION OF PROPELLANTS IN MICRO-MOTORS

ABSTRACT

Development of a 10-gm micro-motor for ballistic evaluation of novel propellants was initiated by this Division in early 1960. Several thousand micro-motors containing a variety of propellant formulations were fired demonstrating that reliable precise ballistic data could be obtained if proper experimental techniques were used.

An extensive series of static tests showed that specific impulse could be scaled when corrections were made for heat-loss and two-phase-flow effects. These scaling factors could be obtained from a series of micro-motor tests requiring as little as 2 pounds of propellant.

This report is a summary of all previous reports on the development of micro-motors and small-scale testing and it is directed toward those groups which might wish to use the Rohm & Haas micro-motor system for propellant evaluation purposes. Accordingly, the areas of system design features, motor preparation and assembly, ignition, data acquisition, data reduction, scaling effects, scaling-factor determination, and specific-impulse prediction have been treated in considerable detail. Sufficient information is provided to allow interested agencies to duplicate the hardware system, conduct static tests, obtain valid ballistic data on scaling factors, and make specific-impulse predictions.

TABLE OF CONTENTS

BALLISTIC EVALUATION OF PROPELLANTS IN MICRO-MOTORS

	Page No.
1. INTRODUCTION	1
2. SYSTEM DESIGN FEATURES	2
2.1 General	2
2.2 Motors	3
2.2.1 Thread-Type .75C.50 Motors	3
2.2.2 Clamp-Type .75C.50 Motors	3
2.2.3 Clamp-Type 2C1.5-4 Motors	6
2.3 Remote Casting Equipment and Facilities	9
2.3.1 .75C.50 Motor Casting Fixtures	9
2.3.2 2C1.5-4 Motor Casting Fixtures	11
2.4 Remote Motor -Assembly and Firing Facility	16
2.5 Self-Propelled Hazardous-Materials Carrier	20
2.6 .75C.50 Motor Shielded Transport Containers	20
3. EXPERIMENTAL TECHNIQUES	22
3.1 Motor Preparation and Physical Measurements	22
3.1.1 Steel-Motor Cleaning	22
3.1.2 Fiberglass-Motor Cleaning	24
3.1.3 Lining	24
3.1.4 Casting	24
3.1.5 Motor Cleanup	25
3.1.6 Grain Trimming and Inspection	25
3.1.7 Weighing	25
3.1.8 Grain and Nozzle Measurements	26

Table of Contents, continued

	Page No.	
3.2	Motor Assembly	26
3.2.1	Threaded .75C.50 Motors	26
3.2.2	Clamp-Type .75C.50 Motors	27
3.2.3	Clamp-Type 2C1.5-4 Motors	27
3.3	Ignition	28
3.3.1	Ignition of .75C.50 Motors	28
3.3.1.1	General	28
3.3.1.2	Nozzle Closures	28
3.3.1.3	Igniters	30
3.3.1.4	Effect of Ignition on Specific-Impulse Measurements	31
3.3.1.5	Effect of Ignition on P-K-r Measurements	33
3.3.2	Ignition of 2C1.5-4 Motors	33
3.3.2.1	General	33
3.3.2.2	Nozzle Closures	33
3.3.2.3	Igniters	34
3.4	Insulation of .75C.50 Motors	34
3.5	Instrumentation	37
3.5.1	General	37
3.5.2	Special Consideration for .75C.50 Motors	38
3.6	Data Reduction	43
4.	DATA INTERPRETATION	48
4.1	Specific Impulse Data	48
4.1.1	Theoretical Scaling Considerations and Equations	48
4.1.1.1	Heat-Loss Effects	49
4.1.1.2	Two-Phase-Flow Effects	51
4.1.1.3	Combined Heat-Loss and Two-Phase-Flow Effects	52

Table of Contents, continued

	Page No.
4.1.2 Calculation of Fractional Velocity Lag (Δ)	54
4.1.3 Determination of Scaling Factors	55
4.1.4 Prediction of Large-Motor Specific-Impulse	59
4.2 P-K-r and Temperature-Coefficient Data	59
BIBLIOGRAPHY	65
APPENDICES	
A. Data-Reduction Definitions and Procedures	
B. Calculation of Velocity Lag in Two-Phase Flow	
C. FORTRAN Program for the Calculation of Velocity Lag	
D. Velocity-Lag Curves for RH-P-112 Propellant	
E. Examples of Scaling-Factor Determination and Specific-Impulse Prediction	
F. Heat-Loss-Surface-Area Determination	

BALLISTIC EVALUATION OF PROPELLANTS IN MICRO-MOTORS

1. Introduction

Over the past several years there has been a general trend in propellant research toward the use of smaller motors for ballistic-evaluation purposes. Many factors have contributed to this, including (a) a large number of new contractors in the field of propellant research, most of whom have an upper restriction on propellant quantity, (b) increasing toxicity and/or sensitivity of new formulations, and (c) limited availability or excessive costs of novel propellant ingredients. These factors make ballistic evaluation of propellants in small motors either highly desirable or mandatory, and have caused many groups to reevaluate their ideas concerning motor size and ballistic measurements.

Early in 1960 the Redstone Arsenal Research Division of Rohm & Haas Company initiated the development of a ten-gram micro-motor for solid propellant static-test purposes. The resulting motor was a small-scale model (.75-in. I. D. X 1.5-in. long) of the Division's standard 6C5-11.4 test motor. Additional .75-in.-I. D. micro-motors in lengths of 2.5 and 3.5 inches were subsequently developed. Static tests of several thousand micro-motors containing a variety of propellant formulations demonstrated that reliable, precise ballistic data could be obtained if proper experimental techniques were used.

Concurrent with the micro-motor development, a parallel investigation of the specific-impulse scaling phenomena of solid propellants was being conducted by this Division. An extensive series of static tests showed that specific impulse could be scaled when corrections were made for heat-loss and two-phase-flow effects. Specifically, it was found that experimental scaling factors relating to heat flux and condensed-phase particle diameter could be extracted from data obtained by static testing

a propellant in a series of small-motor configurations, that these scaling factors could be used to accurately predict the specific impulse of the propellant in any other untested motor configuration, and that these scaling factors could be obtained from a series of micro-motor tests requiring as little as two pounds of propellant.

Most recently, the micro-motor hardware and casting equipment were redesigned to allow completely remote operation, and remote casting and firing facilities were designed and constructed. These modifications allow evaluation of very hazardous materials.

This report is a summary of all previous reports on the development of micro-motors and small-scale testing and is directed toward those groups who might wish to use the Rohm & Haas micro-motor system for propellant evaluation purposes. Accordingly, the areas of system design features, motor preparation and assembly, ignition, data acquisition, data reduction, scaling effects, scaling-factor determination, and specific impulse prediction have been treated in considerable detail. Sufficient information is provided to allow interested agencies to duplicate the hardware system, conduct static tests, obtain valid ballistic data and scaling factors, and make specific-impulse predictions. Details of previous scaling data and prediction results for specific propellants may be obtained from the material listed in the Bibliography.

2. Design Features

2.1 General

The standard Rohm & Haas motor designation used throughout this report is as follows: reading from left to right, the first number represents motor I. D., the letter group designates grain design, the next number represents grain I. D., and the last number represents motor chamber length. As an illustration the .75C.50-1.5 motor has a case I. D. of 0.75 in., a cylindrical grain design, a grain I. D. of 0.50 in., and a motor case length of 1.5 in.

2.2 Motors

2.2.1 Thread-Type .75C.50 Motor¹

The threaded .75C.50 motor (Fig. 1) is attached to its associated hardware with machine threads and was designed for non-remote assembly. The motor bodies are 1.000-in. O. D. x 0.750-in. I. D. mild steel tubes with 1-1/8 - 12 NF male threads on each end. The standard motor lengths are 1.5, 2.5, and 3.5 in. The nozzle is mild steel with a graphite insert and is threaded on the exit end for attachment of a nozzle-closure retainer. The other end of the motor attaches to a special pressure transducer and squib-lead sealing assembly which is in turn attached to a load cell. Squib leads are sealed by a gland nut and Teflon packing.

Several motors may be connected together with threaded couplings to obtain greater lengths. Threaded connections provide adequate sealing for all joints in the motor system.

Motors have been hydrostatically tested to 13,000 psi without failure, indicating that a working pressure of 10,000 psi can be considered safe. However, an all-steel nozzle is required for pressures about 6000 psi to prevent failure of the graphite insert.

2.2.2 Clamp-Type .75C.50 Motor

The clamp type .75C.50 motor (Fig. 2) was designed for remote casting, assembly, and firing but is also used for non-remote operations. The motor is attached to its associated firing hardware with cam-action container latches. The motor dimensions are 0.750-in. I. D. x 0.950-in. O. D. with the same lengths as for the threaded motors. Shoulders are machined on the outer surface near the motor ends to facilitate casting-equipment disassembly. Motors are currently fabricated from both stainless steel and phenolic-glass-fiber tubes.²

¹Detailed shop drawings of all hardware and components are available upon request.

²The glass-fiber motors were purchased from Dynetics, Inc., 34 Crestview Road, Mountain Lakes, New Jersey.

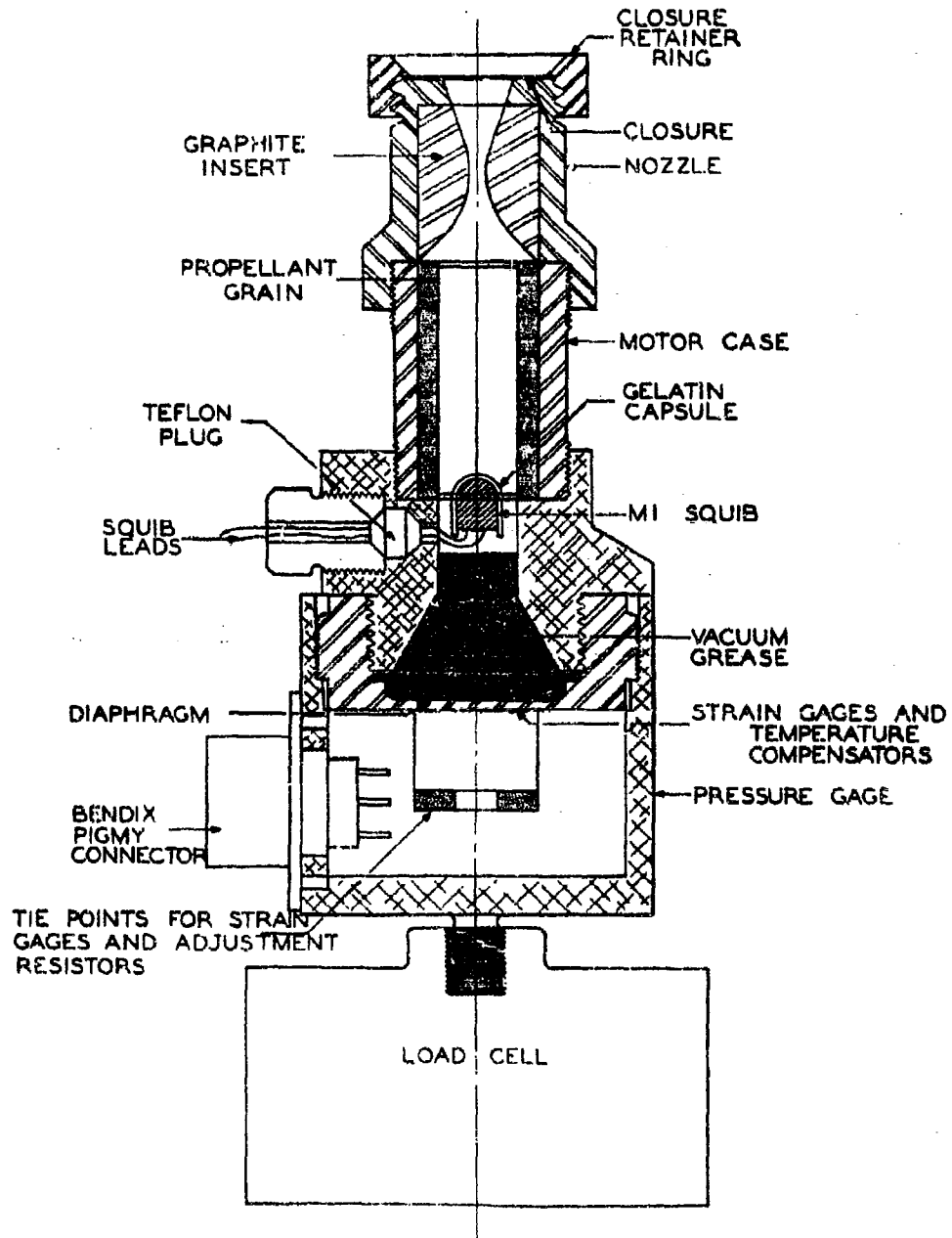


Fig 1 Threaded .75C 50-15 motor firing assembly.

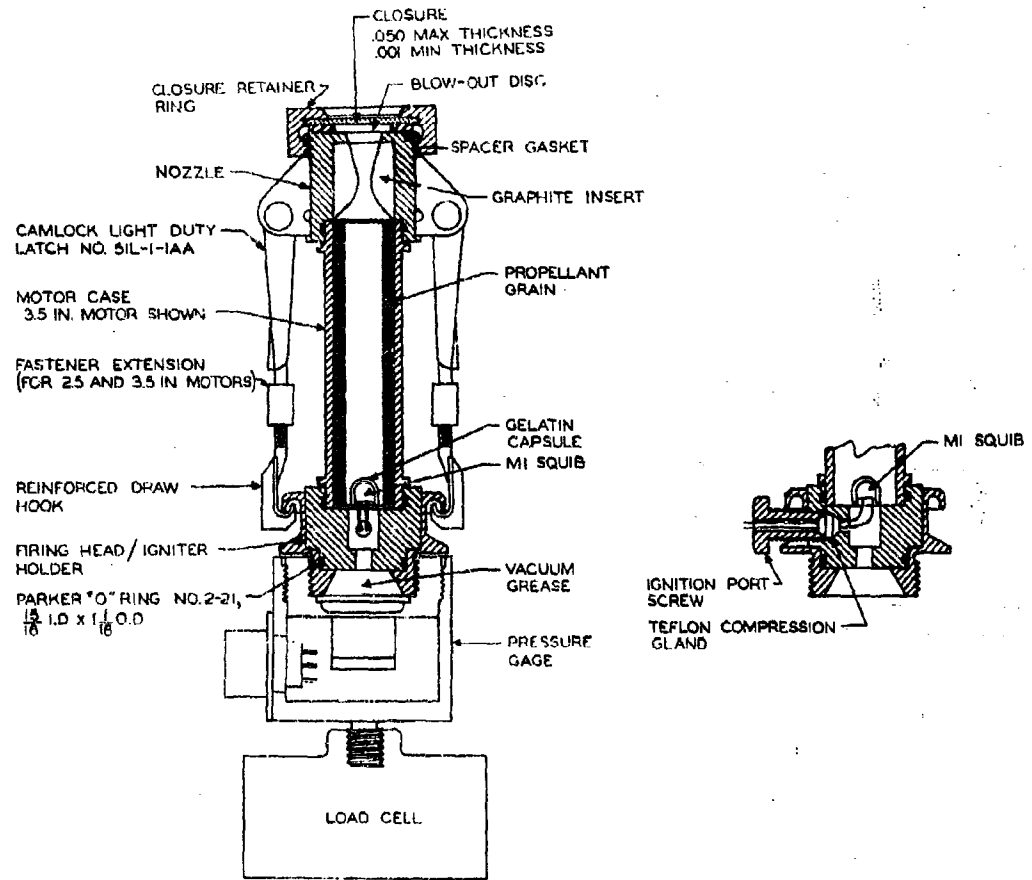


Fig.2 Clamp-type .75C.50-3.5 motor firing assembly.

The firing head and nozzle each contain a counterbore with a radial groove for O-ring sealing on the external motor surface. The nozzle throat inserts are graphite. Another O-ring seals the firing head to the pressure transducer.

Two Camloc light-duty container latches¹ are bolted to the nozzle and are used to clamp the motor assembly together during firing (Fig. 2). Extensions on the Camloc latches permit the use of motors having different lengths, and reinforcing ribs welded to the hooks permit operation at a maximum motor-chamber pressure of 2000 psi.

A special nozzle-closure assembly provides reproducible blow-out pressures. The design includes the use of closure discs having thicknesses from 0.001 to 0.050 in., a metal blow-out slug which must shear a plug from the closure before escaping, and a closure retainer which screws onto the nozzle exit. Blow-out pressures are controlled by the selection of closure-disc material and thickness.

Stacking sleeves are used with standard motors to obtain additional lengths as required, but a special-length clamp extension is required for each combination. A dummy load cell machined from stainless steel is used with a commercial pressure transducer when firing new propellants which have unknown sensitivity characteristics.

2.2.3 Clamp-Type 2Cl.5 - 4 Motor

The 2Cl.5 - 4-clamp-type motor (Fig. 3) was designed primarily for remote operations, but its ease of assembly and good grain-dimension reproducibility makes it equally useful for routine operations. When new materials having unknown sensitivity characteristics are being tested and remote operation is required, a motor² made of filament-wound epoxy-glass tubing is used to minimize potential fragment hazards from malfunctions. These motors are wound and machined to 2.000-in. I. D. x 2.258-in. O. D. x 4-in. long with a shoulder near one end to hold

¹Part No. 51L-1-1AA, Camloc Fastener Corporation, Paramus, New Jersey.

²Purchased from Lamtex Industries, Inc., of Farmingdale, Long Island, New York.

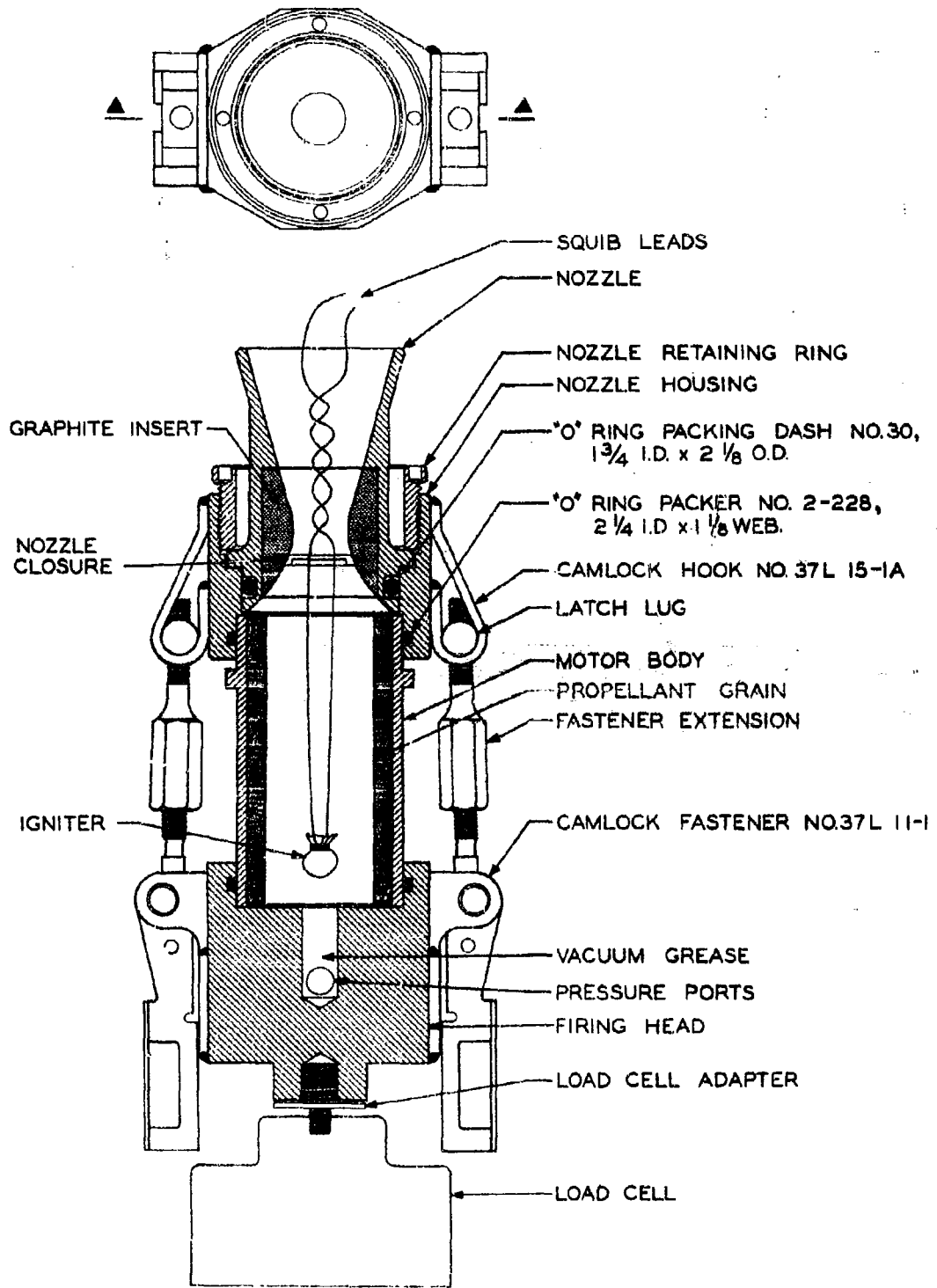


Fig.3 Clamp-type 2CI 5-4 motor firing assembly.

the motor during casting-equipment disassembly. The outer surface of the motor is used as an O-ring seal and casting-fixture-alignment surface. For non-remote operation a motor made of 2.000-in.-I. D. stainless steel tubing having dimensions similar to those of the glass fiber motor may be used.

The firing head contains a counterbore with an O-ring groove for inserting one end of the motor, two threaded ports for installing commercial pressure transducers, a threaded boss for mounting to a commercial load cell, and two Camloc heavy-duty container latch¹ assemblies for clamping the motor firing assembly together. Two mating Camloc hooks² are welded to the nozzle housing which also contains a counterbore with an O-ring groove for inserting the other end of the motor. Both firing head and nozzle housing are made of mild steel. Steel nozzle inserts containing press-fitted graphite throats are sealed in the nozzle housing with O-rings and are retained by a threaded steel ring.

The Camloc latch as received from the manufacturer will function at a maximum chamber pressure of 1700 psi, but the maximum chamber pressure can be increased to 2000 psi by replacing the latch shear pins with hardened steel bolts. Latch extension arms serve as turnbuckles for adjusting the latch length and are fabricated in length increments required for use with 4-in., 8-in., 12-in., and 16-in. motor combinations. All motors are cast in 4-in. lengths; the additional lengths, which are used only for non-remote firings, are obtained by coupling the motors end to end through the use of O-ring-sealed short sleeves which provide a $\frac{1}{16}$ -in. gap between motor sections. The use of turnbuckle-type extensions requires fabrication of latch lugs with left-hand threads. Both the lugs and extensions are fabricated from Type 4130 steel and heat treated.

¹Camloc Part No. 37L11-1B.

²Camloc Part No. 37L15-1A.

A special firing head and nozzle housing, with the latch assembly replaced by $\frac{1}{2}$ -in. steel tie rods, are used for non-remote assembly of motors when chamber pressures from 2000 to 3000 psi are anticipated. A dummy load cell is used when firing novel propellants which have unknown characteristics.

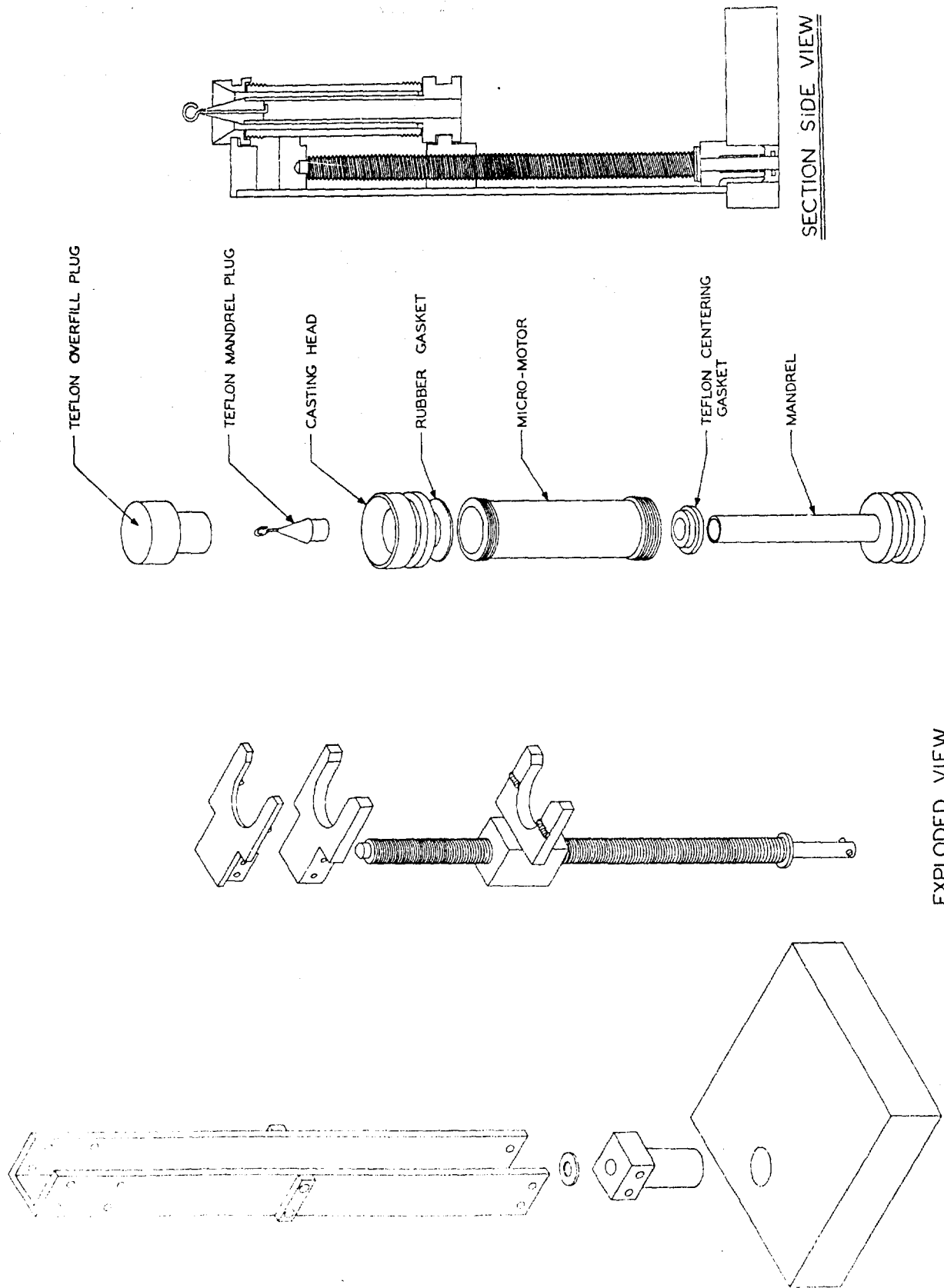
2.3 Remote Casting Equipment and Facilities

2.3.1 .75C.50 Motor Casting Fixtures

Casting fixtures (Fig. 4) for both the threaded- and clamp-type .75C.50 motors are assembled and disassembled using a screw-clamp fixture. Two stationary yokes at the top of the clamp hold the motor shoulder and casting head, and a screw-actuated yoke holds the one-piece casting base and mandrel. Mandrel alignment is provided by a Teflon gasket at the mandrel base, and by a spacer at the top, which is inserted temporarily during assembly and removed immediately prior to casting. The clamp, with the screw manually driven by a hand crank or remotely driven by a geared air motor, disassembles the motor and casting fixtures. A Teflon plug fits into the upper end of a 0.50-in.-O. D. hollow mandrel during the filling operation. When filling is completed, the plug is removed and a Teflon overfill plug is inserted which forces the excess propellant into the hollow portion of the mandrel. The overfill plug in conjunction with a gasket at the base of the mandrel provides a $\frac{1}{32}$ -in. grain recess at each end of the motor.

2.3.2 2C1.5-4 Motor Casting Fixtures

Casting fixtures for the 2C1.5 motor (Fig. 5) consist of a casting head, a one-piece casting base and mandrel, a break-off ring, and two tie rods. Small wooden cross pins are used on the bottom ends of the tie rods to act as shear pins during remote disassembly. A shoulder on the base of the mandrel, and the break-away ring provide a $\frac{1}{16}$ -in. grain recess at each end of the motor. A remote casting-fixture disassembly device (Fig. 6) actuated by a double-acting air-draulic



Best Available Copy

Fig. 4 Casting equipment for .75C.50 motors.

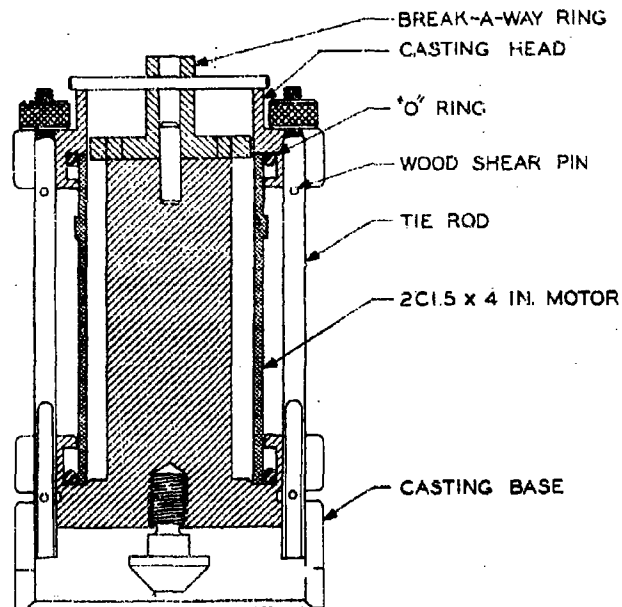


Fig. 5 Casting equipment for 2C1.5-4 motors.

cylinder is used to disassemble the motor. The casting fixture is set on the jig in an inverted position. As the moveable portion comes down, two fingers press against the tie rods, removing them, the casting head, and the break-off ring. The puller jaw engages a button on the end of the mandrel, and the mandrel is extracted on the upward stroke.

2.3.3 Remote Casting Facilities

Three facilities, differing primarily in size and propellant-handling capacities, were designed and constructed for mixing and casting hazardous propellants. Two small facilities were built to handle up to 250 g of propellant. Operations are carried out behind a semicircular steel shield (Figs. 7 and 8) having a radius of three feet with two AMF Mini-Manip manipulators¹; a rectangular Plexiglas² sight port provides for direct viewing. The air within each shield may be maintained at a dew point of -50°C , thus allowing the processing of hygroscopic materials.

¹Part No. 89-63-R1000, AMF Atomics, A Division of American Machine & Foundry Company, 140 Greenwich Ave., Greenwich, Conn.

²Rohm & Haas Company, Philadelphia, Pennsylvania.

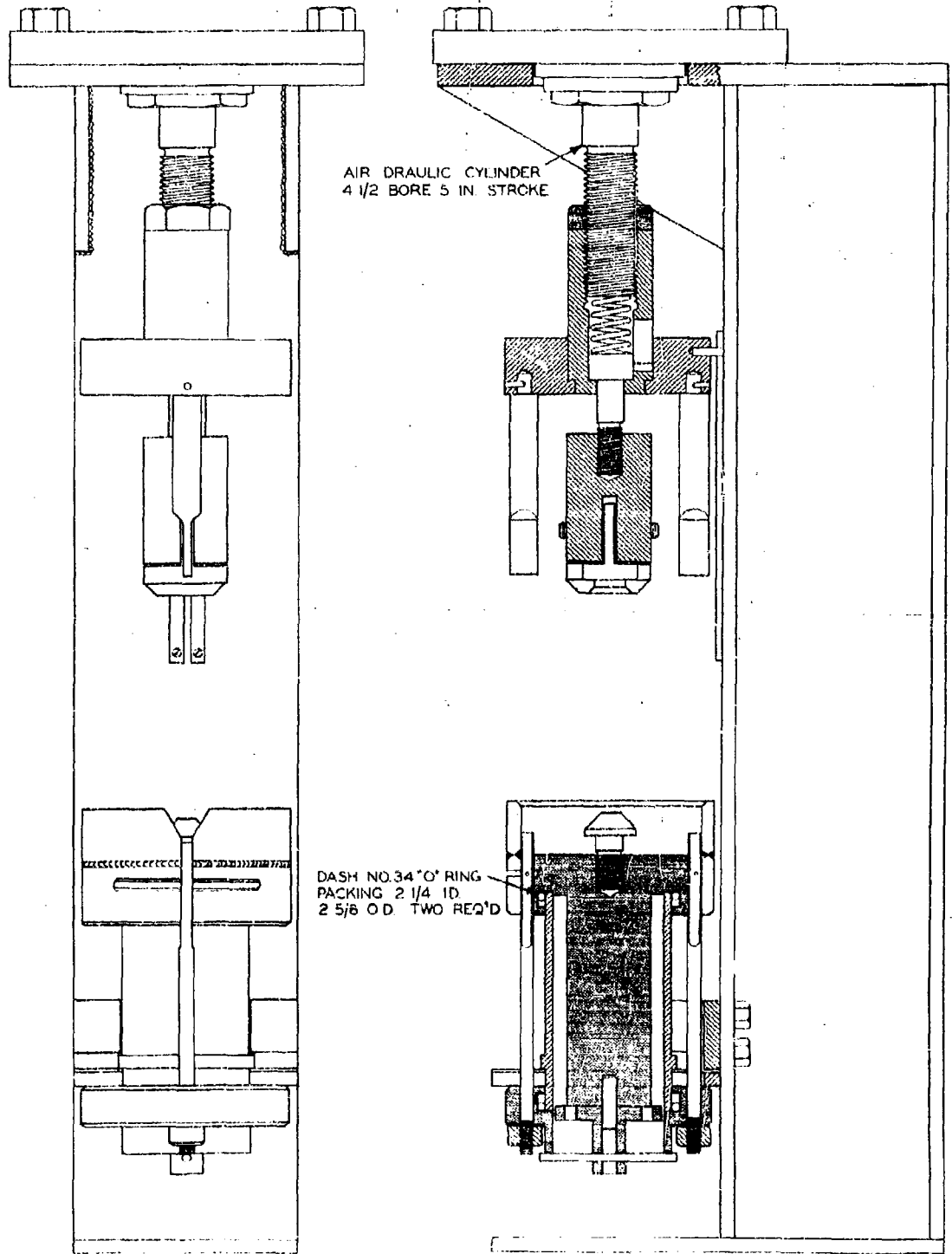


Fig 6 2CI.5-4 motor remote mandrel puller.



Fig. 7 250-gram remote casting facility-front view.

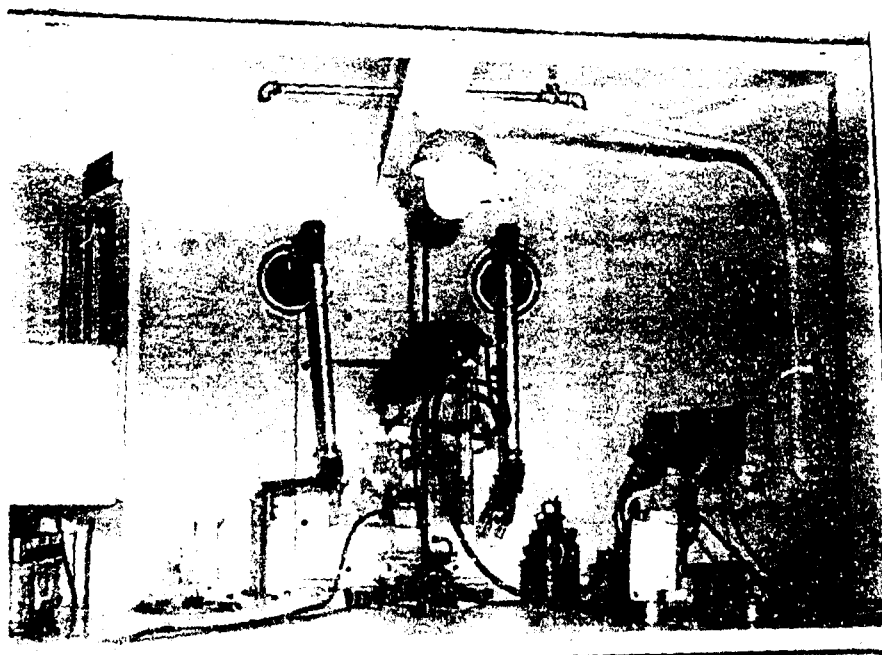


Fig 8 250-gram remote casting facility-rear view.

Best Available Copy

One shield was designed for casting .75C.50 motors and the other was designed for casting both .75C.50 and 2Cl.5 motors.

The third facility (Figs. 9 and 10) was designed to handle up to 2 lbs of propellant. Mixing, casting, curing, and motor disassembly are carried out remotely in a concrete cell. Transfer operations are handled with two AMF Model 8 extended-reach standard-duty manipulators while processing equipment is operated with compressed air or hydraulically. A sight-port containing a 3-in. block of Plexiglas is used for direct viewing, and close-up views of equipment and controls are provided with a closed-circuit television camera.

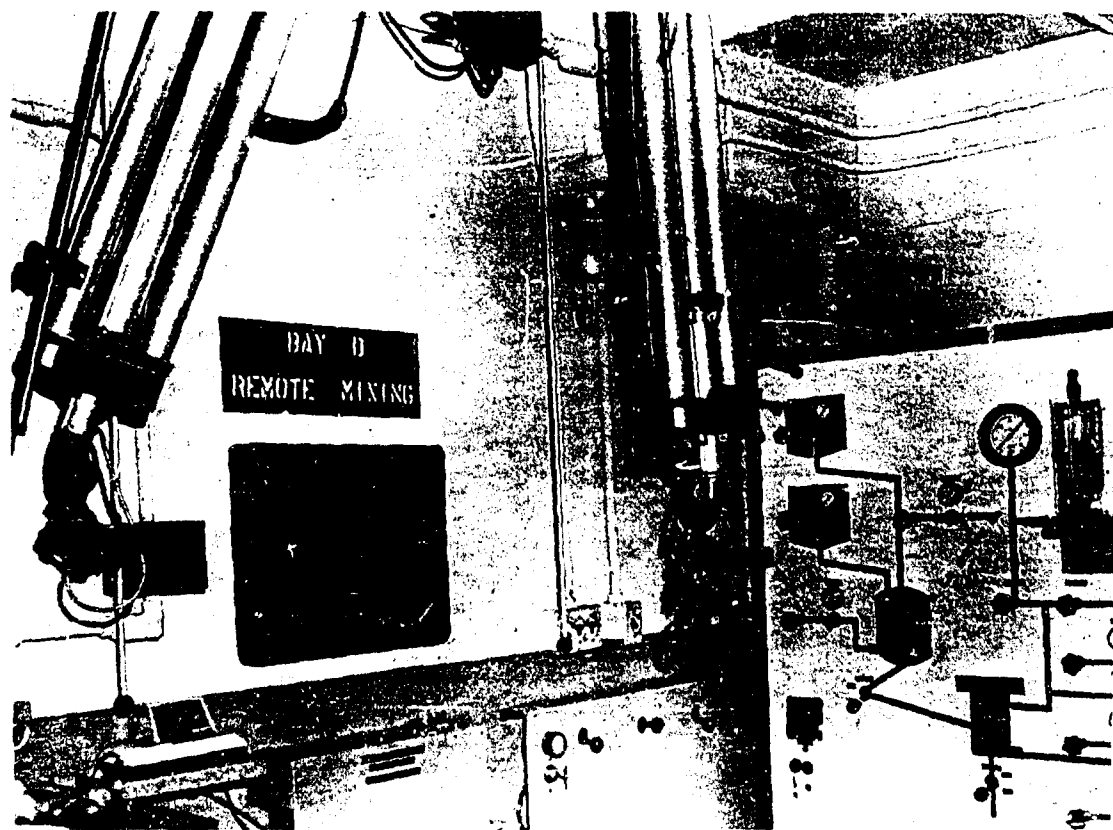


Fig 9 Operating control area for 2-lb. remote mixing and casting facility.

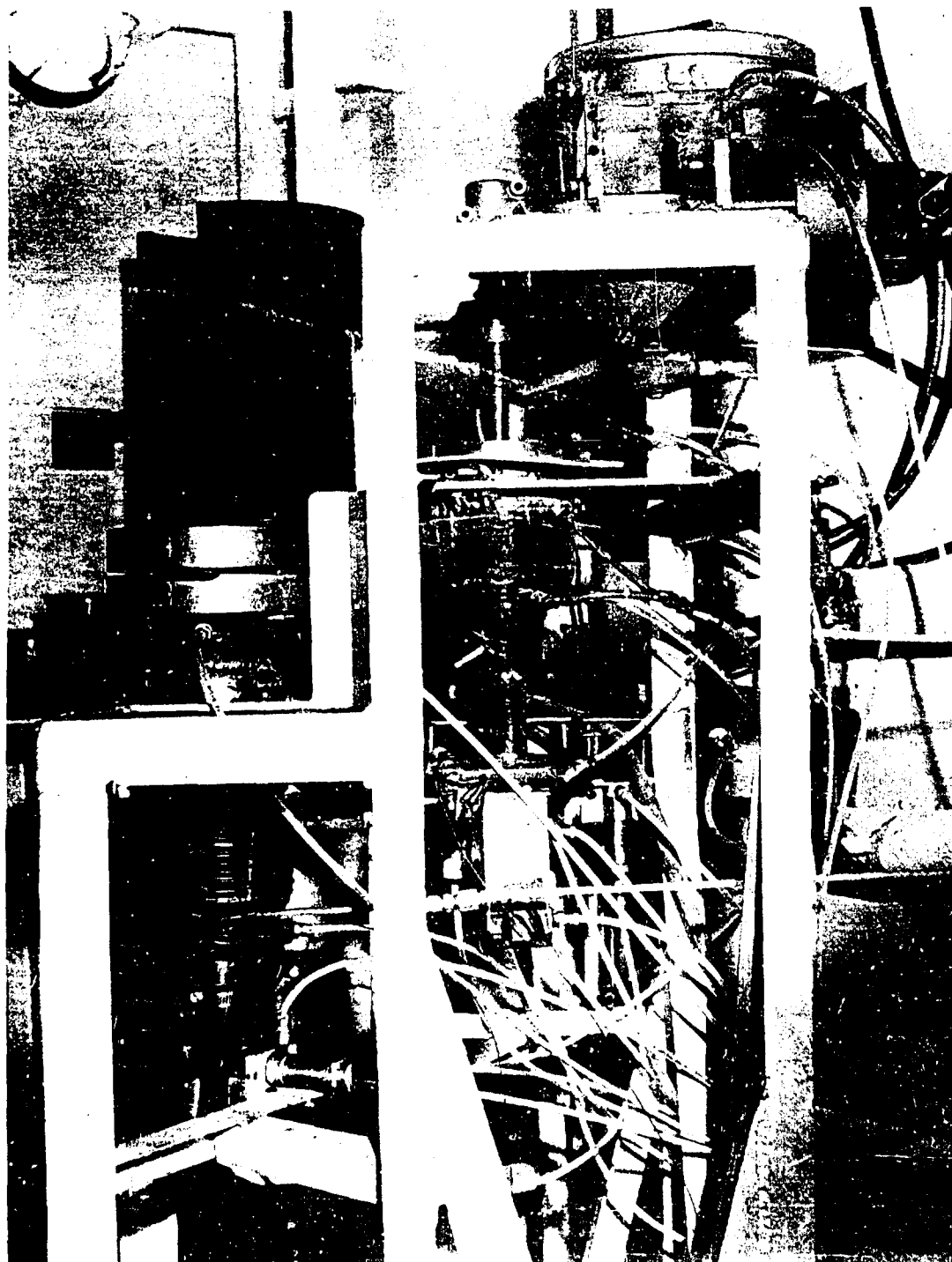


Fig.10 Two pound mixer in remote facility.

Best Available Copy

2.4 Remote Motor Assembly and Firing Facility

The remote motor assembly and firing facility was designed for installation within an existing static-firing-range bunker. The facility provides for completely remote assembly, firing, or disassembly of .75C.50 and 2Cl.5-4 clamp-type motors without personnel exposure.

A thrust plate for firing motors in a vertical position is mounted at table-top level on a reinforced concrete block. A 1-in. -thick steel shield is set in front of the stand and a heavy wire-mesh screen extends from the top of the shield to the bunker ceiling to protect the operator while the motor is being set on the firing stand. Transfer operations within the test cell are handled with a Mini-Manip manipulator which is set in the upper right-hand corner of the shield while motors are prepared for firing. A 14-in.-wide X 22-in.-high opening is provided in the shield for a movable Plexiglas sight-port which also serves as an access door. The door is air-powered and is remotely actuated.

Motors are brought to the stand for firing in an armoured transporter. An air-cylinder-actuated retracting cup on the stand is automatically actuated by door movements. When the door is opened, the cup swings toward the door opening. The motor is transferred from the transporter to the cup with a Mini-Manip on the transporter. The door is closed, and the cup and motor are retracted inside the shield. Fig. 11 shows an outside view of the shield with the door open and the manipulator installed. With the shield door closed, the operator assembles the motor remotely, removes the manipulator, and leaves the bay before the motor is fired.

The .75C.50-motor assembly and disassembly fixtures use a pivoted motor-clamping yoke and a pivoted unlatching hook in conjunction with the manipulator. Fixtures for the remote assembly and disassembly of 2Cl.5 - 4 motors are clamped and unclamped by ropes extending through the front of the shield. Figs. 12 and 13 illustrate some steps in the assembly of .75C.50 and 2Cl.5 clamp-type motors.

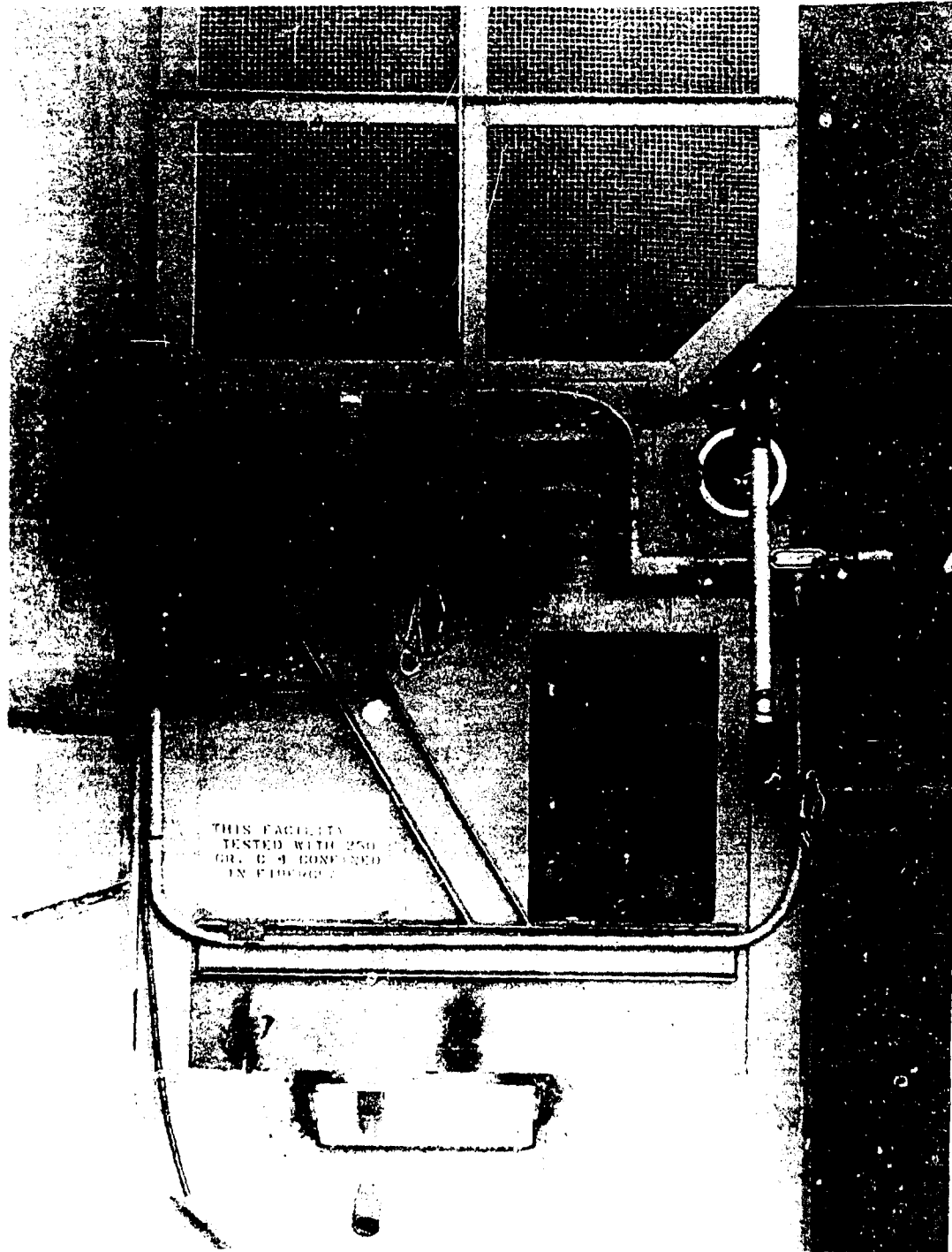
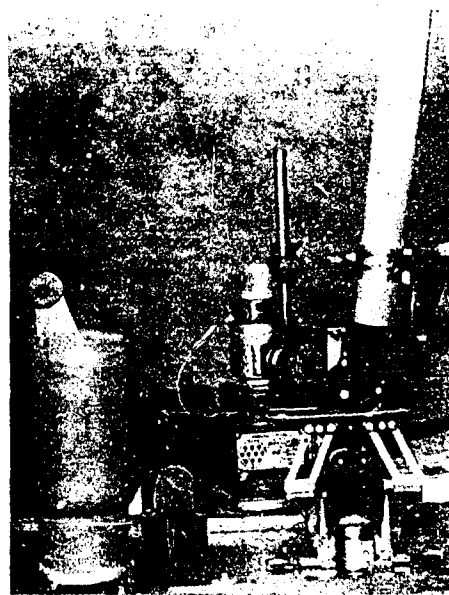


Fig. II Remote static test facility.

Best Available Copy



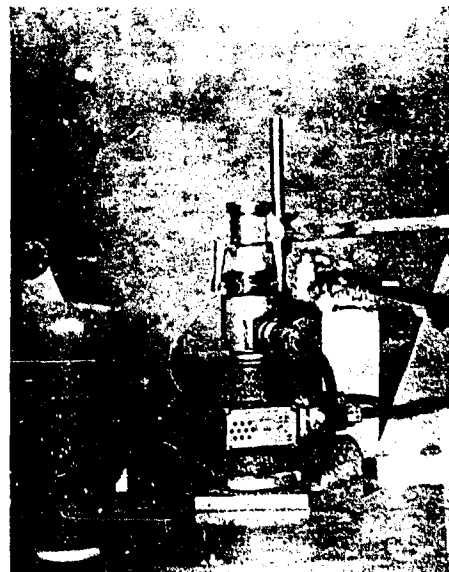
(A) GAUGES, FIRING HEAD AND IGNITER IN PLACE



(B) MOTOR INSERTED INTO FIRING HEAD



(C) NOZZLE ASSEMBLY



(D) COMPLETE ASSEMBLY, READY TO FIRE

Fig.12 Steps in the assembly of the .75C.50 micro-motor for firing in the static test stand.

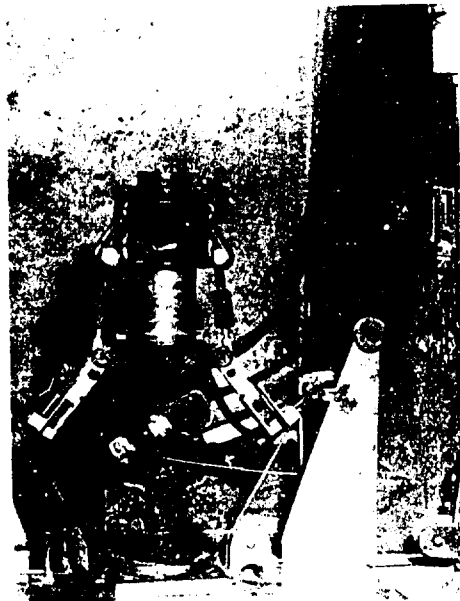
Best Available Copy



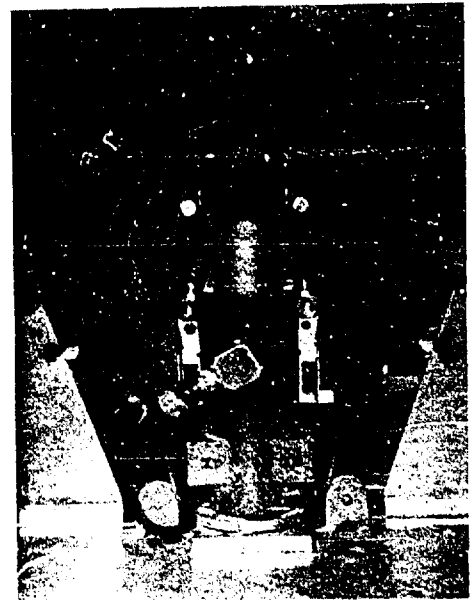
(A) GAUGES AND FIRING HEAD IN PLACE



(B) MOTOR CASE IN PLACE, NOZZLE BEING TRANSFERRED.



(C) NOZZLE ASSEMBLY



(D) COMPLETE ASSEMBLY, READY TO FIRE.

Fig.13 Steps in the assembly of the 2C1.5-4 motor for firing on the static test stand

The facility was tested by detonating 250 g of C-4 explosive confined in a 2Cl.5-4 fiberglass motor located at the position of normal motor firing. The sight-port withstood a separate test with 250 g of C-4 in a fiberglass motor located 3 in. from the inside pane.

2.5 Self-Propelled Hazardous Materials Carrier

A powered vehicle (Fig. 14) capable of safely transporting 1 lb of hazardous material from the remote-casting facilities to the remote-firing facility without exposure of personnel was designed, fabricated, and tested. The design was patterned after a hazardous material vehicle designed and built by the E. I. duPont de Nemours & Company, Inc.¹ The vehicle consists of a warehouse-type electric truck chassis² upon which is mounted a 30-in. sphere made of 1.5-in. steel. The vehicle is operated from a shielded cab.

The sphere is equipped with hydraulically actuated devices which open an inwardly swinging lid and extend a cup into which hazardous material is placed. Transfer operations are handled remotely with a modified Mini-Manip manipulator, installed in the front of the cab. The walls of the cab are 1 in. thick in front (the surface most directly exposed to the sphere) and $\frac{1}{2}$ in. thick on the sides and top. Aluminum doors in the rear protect the operator from blast overpressure in the event of an explosion outside of the sphere.

2.6 .75C.50 Motor Shielded Transport Containers

Two types of portable containers are used to transport .75C.50 motors: a thick-wall closed vessel, and an open-end pipe-section carrier (Figs. 15 and 16).

¹Explosives Department, Repauno Development Laboratory, Gibbstown, New Jersey.

²Model No. RW-41136, Automatic Transportation Company, Chicago, Illinois.

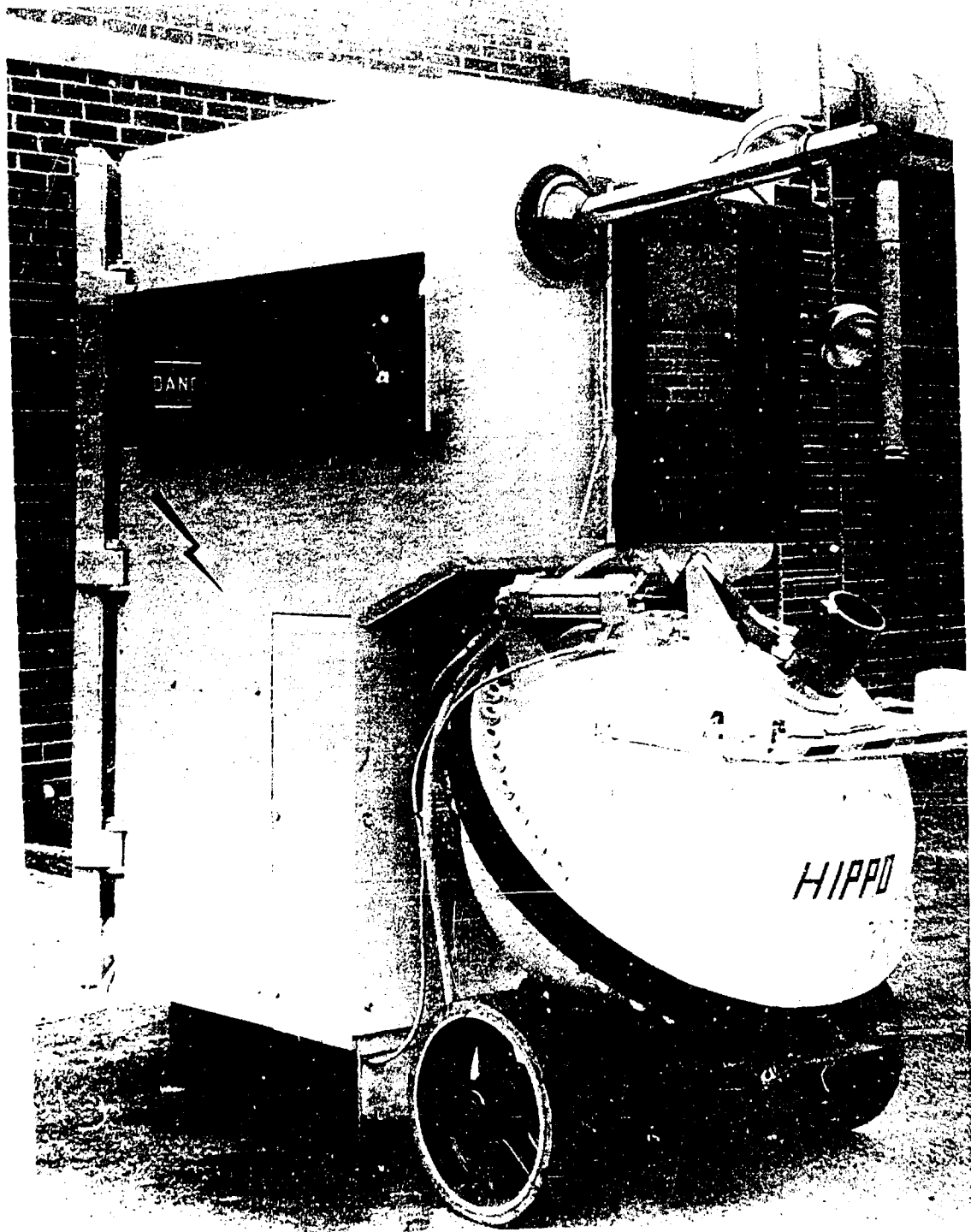


Fig 14. Self-propelled, hazardous materials carrier.

Best Available Con

3. Experimental Techniques

3.1 Motor Preparation and Physical Measurements

3.1.1 Steel Motor Cleaning

Steel motor cases are hydroblasted thoroughly, rinsed with water to remove all grit, dipped in acetone to remove the water, and quickly transferred to a trichloroethylene-vapor degreaser. After remaining in the degreaser for several minutes, the motors are removed, capped on each end with plastic cap-plugs, and stored at a temperature of +140° F until required for use.

3.1.2 Fiberglass Motor Cleaning

Fiberglass motors are hydroblasted very lightly to remove the surface glaze. The remaining operations are the same as for the steel motors, except that time in the degreaser is reduced to about 30 seconds.

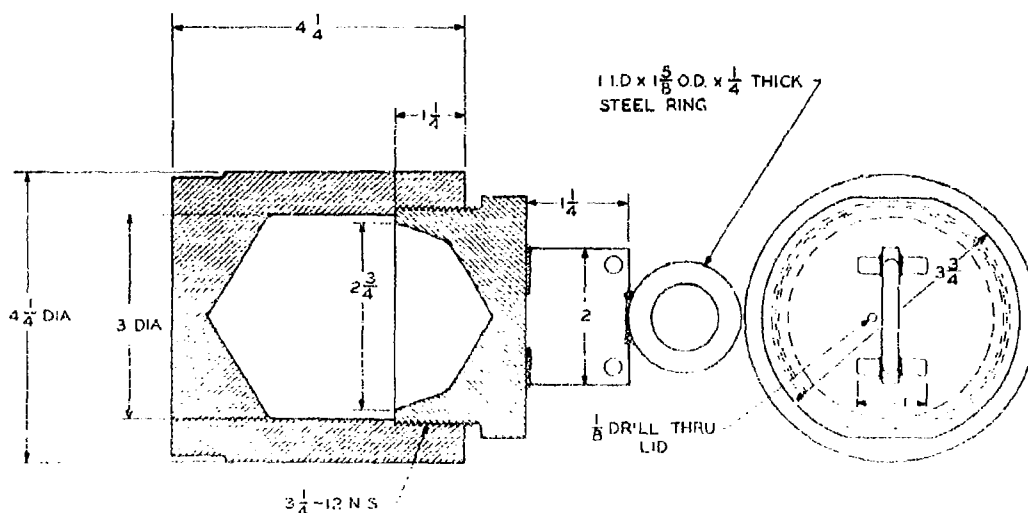


Fig 15 Detonable sample container.

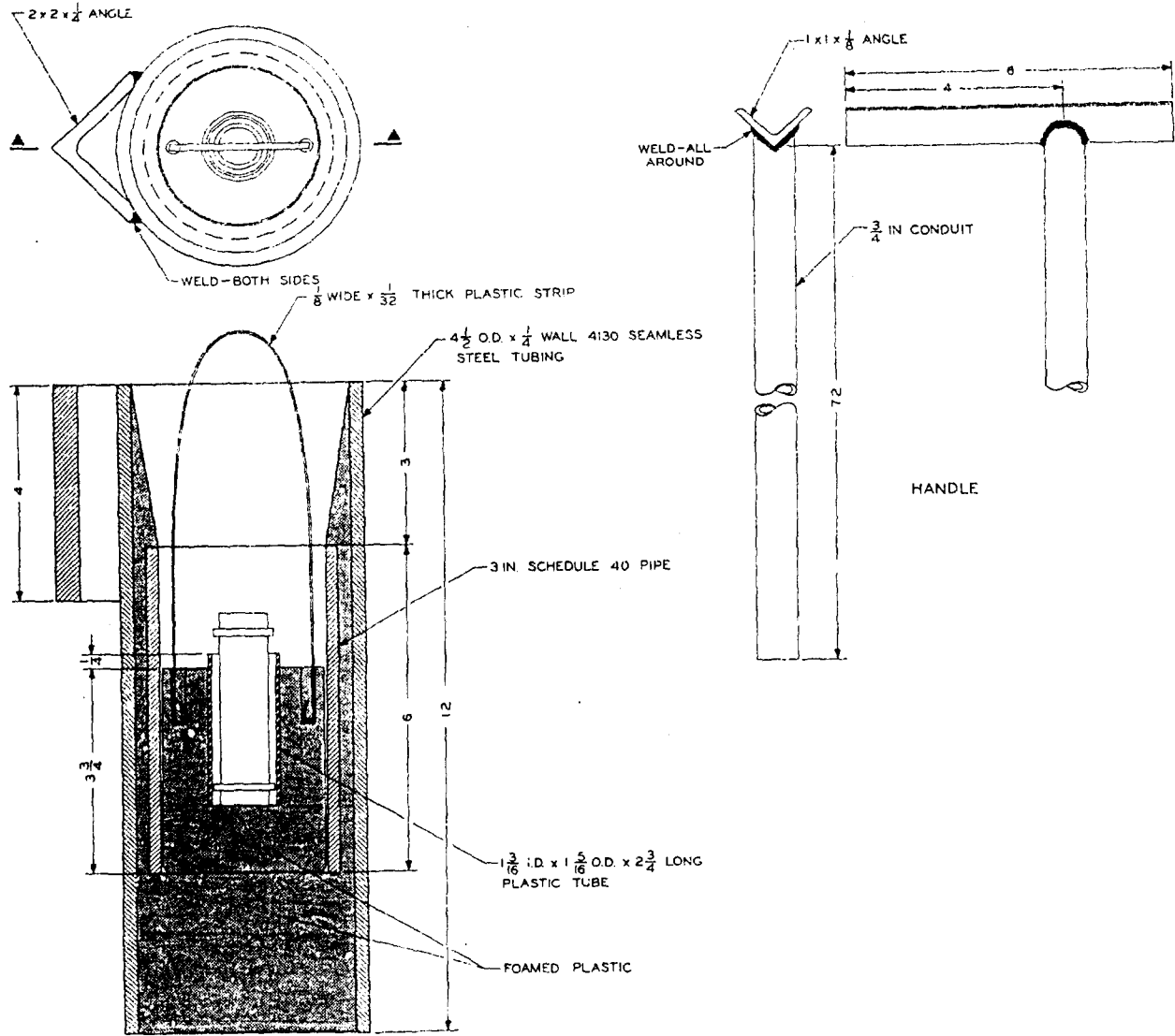


Fig.16 Open-end micro-motor carrier.

Best Available Copy

3.1.3 Lining

The motor liner depends on the type of propellant to be cast. For composite double-base plastisol propellants, the cases are sprayed with an extremely thin film of Rohm & Haas PL-1 liner (Table I). Many experimental propellants will bond adequately to the clean steel or fiberglass motor cases, and no liner is required. Any liner must be thin and uniform to avoid errors in burning rate measurements, as well as efficiency losses associated with long tail-offs.

Table I

Composition of PL-1 Liner

<u>Constituent</u>	<u>% by Weight</u>
Cellulose Acetate (Powdered) ^a	4.57
Triphenyl Phosphate Flakes	2.88
Santicizer M-17 ^b	1.74
Red Lead (Pb ₃ O ₄)	.02
Tolylene Diisocyanate (Hylene TM) ^c	.23
Acetone Tolyene	46.39
Methyl Cellosolve Acetate ^d	44.17

^aType 384, Tennessee Eastman Co., Kingsport, Tenn.

^bMonsanto Chemical Co., St. Louis, Mo.

^cE. I. duPont de Nemours Co., Wilmington, Del.

^dEthylene Glycol Monomethyl Ether Acetate, Union Carbide Chemical Co., New York, N. Y.

3.1.4 Casting

While propellant charges for micro-motors could be formed in a number of ways, all motors tested by this Division have been loaded by casting the propellant directly into the motor case and curing it in place.

Casting techniques vary widely depending on the specific propellant composition. For example, compositions which are very fluid may be cast easily, while extremely viscous compositions present

special problems. Specific casting techniques are described in two series of reports of this Division: Quarterly Progress Reports on Chemical and Propellant Processing, and Quarterly Progress Reports on ARPA Projects.

3.1.5 Motor Cleanup

A certain amount of motor cleanup is usually required after the grain has been cast. All external motor surfaces, especially those which mate with the nozzle and head closure, must be thoroughly cleaned. A solvent such as acetone is usually used for this purpose.

3.1.6 Grain Trimming and Inspection

The goal during casting is the production of a perfect, cast-to-length grain. However, it is sometimes necessary to trim the grain to remove end flaws. In this event the motor is clamped in a vise and a small 90° knife is used to trim the grain ends, using a special trimming jig as the knife guide. After trimming and cleaning, the motor is visually inspected for propellant voids, cracks, case-bond failures or other irregularities.

3.1.7 Weighing

Motor cases are weighed after lining, before firing (after trimming), and after firing. The .75C.50 motors are weighed on a 200-gram direct-reading Mettler electric analytical balance which can be read to 0.1 milligram. The 2C1.5-4 motors are weighed on a similar 800-gram Mettler balance which can be read to 0.01 gram. Due to the small size of the motors, weights must be determined with extreme accuracy to provide accurate specific-impulse measurements. Consequently, particular care must be taken to insure that the motor case before and after firing is unaltered with the exception of propellant and liner consumed.

3.1.8 Grain and Nozzle Measurements

Grain length is measured to 0.01 inch with a standard steel rule. Grain web thickness is measured to 0.001 inch from measurements of the grain I. D. before firing and case I. D. after firing; the motor is not cleaned before the latter measurement. Nozzle-throat diameters are measured to 0.001 inch before firing, after firing on top of any material deposited in the nozzle, and after removal of deposits in the nozzle. Small expanding-ball-type hole gauges and standard micrometers are used for throat-diameter measurements. Nozzle exit diameter is measured to 0.001 inch using an inside-reading caliper micrometer.

Extreme care must be taken to determine such physically measured quantities as web thickness, nozzle throat and exit diameter, and charge weight, in order to obtain acceptable ballistic data. Due to the small magnitude of these quantities, allowable tolerances on measurements are inherently small and difficult to maintain.

3.2 Motor Assembly

3.2.1 Threaded .75C.50 Motors

For threaded .75C.50 motors, the special pressure gauge serves as the motor head-closure and contains the squib wire pass-through port. The igniter is installed by passing the squib wires down into the center of the gauge and out through the igniter port, threading the wires through the close-tolerance holes in the Teflon compression gland, pulling the igniter well down to position it at the motor head end, and inserting and tightening the ignition port screw to provide the pressure seal. A disc-type nozzle closure is installed at the nozzle exit using a closure-retaining ring which threads onto the nozzle aft end. The pressure gauge and nozzle are threaded onto the ends of the motor to complete the loading operations. A sectioned view of the loaded motor is shown in Fig. 1.

3.2.2 Clamp-Type .75C.50 Motors

For the clamp-type .75C.50 motors, the igniter is installed in the motor firing head in a manner completely analogous to that used for igniter installation into the threaded motor pressure gauge. The disc-type nozzle closure is similarly retained at the nozzle exit by a threaded retainer ring. Two types of nozzle-closure-retainer ring assemblies are available: one clamps the closure to the exit (as for the threaded motor), and one utilizes a coin-type slug to rupture the closure, allowing better control of closure rupture pressure. The reinforced draw hooks are attached to the nozzle clamp arms (with or without extensions, depending on motor length) and adjusted in length for proper assembly tension. Final assembly is made by inserting the firing head into the special clamp-type pressure gauge, inserting one end of the motor into the firing head, pushing the nozzle down over the motor end, placing the draw-hook feet under the rim of the pressure gauge (clamp levers in a raised position), and seating the clamp levers. The O-rings and the outer motor ends should be lightly coated with a light vacuum grease and care must be taken not to pinch the nozzle and firing-head O-rings during this operation. Since the pressure seal is made by the O-rings on the motor case O.D., clamp-arm tension is not critical and need only be sufficient to provide a snug assembly. A sectioned view of the assembled motor is shown in Fig. 2.

3.2.3 Clamp-Type 2C1.5-4 Motors

For the clamp-type 2C1.5-4 motors, the igniter and closure are installed in the nozzle insert, which is then pushed into the nozzle shell and secured by threading down the nozzle retaining nut. The disc-type, bevelled closure is glued in the nozzle convergent section. The squib-wire length is adjusted so that the igniter will be positioned at the motor head-end when the motor is assembled. The outside ends of the motor and the nozzle and firing-head O-rings are lightly coated with

light vacuum grease. Final assembly is made by inserting one end of the motor into the firing head, pushing the nozzle housing down over the motor end, placing the clamp lugs in the nozzle housing ears, and seating the clamps. As for the clamp-type .75C.50 motors, clamp arm tension is not critical and need only to be sufficient to provide a snug assembly. A section view of the assembled motor is shown in Fig. 3.

3.3 Ignition

3.3.1 Ignition of .75C.50 Motors

3.3.1.1 General

One of the major problem areas in the .75C.50 motor program has been the development of a satisfactory ignition system. Many different types of ignition systems have been tested, utilizing a variety of squibs, igniter materials, igniter weights, igniter positions, nozzle closures, and closure positions. Conclusions drawn as a result of these tests are summarized below.

3.3.1.2 Nozzle Closures

A nozzle closure is essential to reduce ignition delay time and rise time, and to eliminate misfires and hangfires. For best results, the closure should rupture at pressures between 80% and 120% of the motor equilibrium pressure. Nozzle closures placed in the nozzle convergent section have usually caused severe ignition-pressure spikes; much better results are obtained with a disc-type nozzle closure clamped to the nozzle exit.

Disc-type nozzle closures should fail by shearing cleanly at a diameter larger than the nozzle exit diameter. If the closure does not shear cleanly rupture pressures will be variable and thrust measurements will be affected by gas-flow disturbances produced by protrusion of jagged edges of the closure into the exit gas stream. To insure clean shearing of the nozzle closure, a special closure-retainer

is available which utilizes a coin-type slug to forcibly rupture the closure (Fig. 2). This assembly also provides much better precision of closure blowout pressure when metal closures are used.

Nominal nozzle-closure blowout pressures for regular variable-diameter retainer rings are given in Table II and nominal nozzle-closure blowout pressures for the special plug-type closure-retainer assembly are given in Table III.

Table II
Nozzle-Closure Blowout Pressures for Regular Retainers

Closure Material and Thickness	Closure Blowout Pressure ^a , psia			
	0.625" Diameter Retainer	0.75" Diameter Retainer	0.875" Diameter Retainer	1.00" Diameter Retainer
CA ^b -.010"	480	400	340	300
CA -.015"	700	590	500	440
CA -.020"	920	780	670	580
CA -.025"	1150	970	830	720
CA -.030"	1380	1160	1000	870
CA -.035"	1620	1350	1160	1010
CA -.040"	1850	1540	1320	1160
CA -.045"	2080	1730	1490	1300
CA -.050"	2310	1920	1650	1450
CA -.060"	2770	2310	1990	1730

^a1σ std. deviation ≈ 200 psia.
^bCellulose acetate sheet.

Table III
Nozzle-Closure Blowout Pressures for Plug-Type Assembly

<u>Material</u>	<u>Thickness, in</u>	<u>Blowout Pressure, psia</u>	<u>$l\sigma$, psia</u>
Aluminum ^a	0.008	480	7
Aluminum	0.010	600	27
Aluminum	0.012	700	24
Aluminum	0.016	930	33
Aluminum	0.020	1170	34
Aluminum	0.025	1400	26
CA ^b	0.020	750	202
CA	0.025	1060	139
CA	0.030	1360	115
CA	0.035	1540	247
Brass ^c	0.005	1060	60

^a 1100-0 aluminum sheet.

^b Cellulose acetate sheet.

^c Sheet shim stock.

3.3.1.3 Igniters

The optimum igniter location is at the head end of the motor with the squib wires passing through the firing head. If the igniter is toward the aft end, the squib head may be torn from the squib wires and plug the nozzle. Satisfactory ignition can usually be accomplished with an igniter positioned in the nozzle expansion cone, but the necessary piercing of the nozzle closure to permit squib-wire passage results in ragged closure rupturing and erratic rupture pressures.

For propellants which are relatively easy to ignite, the optimum igniter consists of an M-1 squib for the 1.5-inch motor, or a squib with additional RIP-1¹ or RHim-1 (Table IV) for the 2.5 and 3.5 inch long motors. The larger igniters are made by pouring the required amount of igniter powder into the small half of a number 0 gelatin capsule, inserting the squib into the capsule, and cementing the squib and capsule together with Dico³ cement. The resultant igniters are of the fast-acting, flash type.

Table IV
Composition of RHim-1 Igniter Powder

<u>Constituent</u>	<u>Weight per cent</u>
Metal Magnesium (55-100 μ)	60
KClO ₄ (~105 μ)	25
Ba(NO ₃) ₂ (<149 μ)	15

For propellants which cannot be satisfactorily ignited with the M-1 squib-RHim-1 system, a dipped Atlas Match igniter is generally satisfactory. This igniter consists of a plain Atlas Match squib which is repeatedly dipped into a slurry of RHim-1 and a solution of 5% poly(isobutylene) in n-hexane until a sufficient quantity of the mixture adheres to the squib head. The solution is then allowed to evaporate, leaving a coating of RHim-1 on the squib head. The resultant igniters are of the soft, slow-burning type, and eject burning particles.

3.3.1.4 Effect of Ignition on Specific-Impulse Measurements

Corrected specific impulse using the .75C.50 motors is markedly dependent upon ignition delay time, ignition weight, and ignition rise time. Long ignition-delay times invariably result in low values of

¹RIP-1 is a Picatinny Arsenal product consisting of 68.2% barium nitrate and 31.8% magnesium.

³E. I. DuPont de Nemours & Co., Wilmington, Delaware.

specific impulse due to propellant cook-off and increased heat losses. On the other hand, the measured specific impulse will be too high if a relatively large weight of igniter material is used, and no correction is made for the contribution of the igniter. Measurements of specific impulse of a typical plastisol propellant as a function of ignition delay time and igniter weights demonstrated the need for short ignition-delay times with minimum quantities of igniter material (Fig. 17).

The policy of this Division has been to use igniters which weigh no more than one-half per cent of the charge weight, and to make no igniter correction to specific impulse although the igniter adds about $\frac{1}{4}\%$ to total impulse. This increase is very closely matched by an apparent decrease in impulse due to the fact that motors are fired vertically and the loss of weight results in a base-line shift of the thrust cell. The M-1 squib used to ignite the 1.5-inch motor contains about 50 milligrams of combustible material, which is one-half per cent of the nominal charge weight. For 2.5- and 3.5-inch motors, RHim-1 igniter powder is added to make the total igniter weight, including the M-1 squib weight, equal one-half per cent of the charge weight.

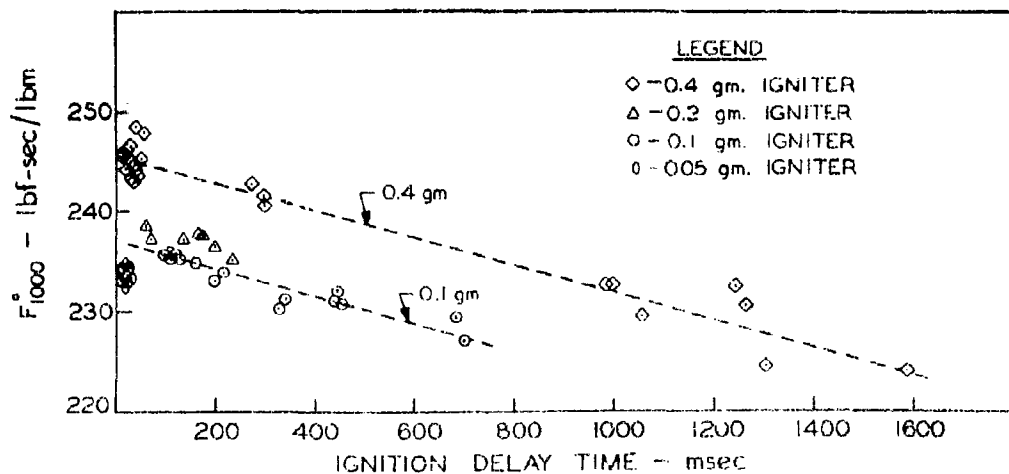


Fig 17 Effect of ignition delay and igniter weight on the specific impulse measured in the 75C 50 micro motor

If the weight of the igniter necessary to achieve ignition is greater than one-half per cent of the charge weight, an igniter correction should be applied to the measured specific impulse. The method used is discussed in Section 3.6.

3.3.1.5 Effect of Ignition on P-K-r Measurements

Ignition requirements for P-K-r measurements differ somewhat from those for specific-impulse measurements. The primary objective is a pressure trace in which the pressure builds up rapidly, end-of-burning is sharp, and pressure decays rapidly. To obtain this, an M-1 squib with additional RHIm-powder is used. Since the igniter-correction problem which must be considered in specific-impulse measurements is not critical for P-K-r measurements, any amount of additional RHIm-1 required may be used to achieve the desired trace shape. In most cases .05 to .15 grams of RHIm-1 is sufficient for ignition of the 1.5-inch motor. Clean shearing of nozzle closures is not critical.

3.3.2 Ignition of 2Cl.5-4 Motors

3.3.2.1 General

Two-inch-diameter motors are easier to ignite than the .75-inch because as much as 0.7 gram ($\frac{1}{2}\%$ of the charge weight) of igniter material can be used for specific-impulse measurements. Larger igniters may be used for P-K-r measurements.

3.3.2.2 Nozzle Closures

Closures which rupture at pressures from 20 to 100 per cent of motor operating pressure are generally acceptable for 2-inch motors. Plastic nozzle closures are usually cemented into the nozzle convergent section with an adhesive such as Pliobond^{®1}. An injection-molding process is used to fabricate these closures (Fig. 18) in three diameters and a wide range of thicknesses. Closures having a thickness between 0.035 and 0.060 inch generally provide excellent ignition for firings at a nominal pressure of 1000 psia.

¹The Goodyear Tire & Rubber Co., Akron 16, Ohio.

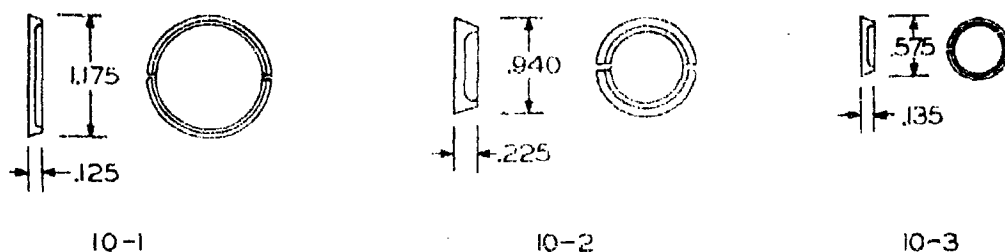


Fig.10 Nozzle closures for 2C1.5-4 motors.

3.3.2.3 igniters

Two types of igniters have been used for 2-inch motors: a fast-acting bag type and a slow-burning jelly-roll type. Both utilize the Atlas Match squib.

The bag-type igniter is made by enclosing the igniter powder (either RIP or RHim) and the Atlas Match squib head in a 2-mil polyethylene bag. The bag, cut from sheet stock, is fastened around the squib wires with a rubber band.

The jelly-roll igniter is made by rolling up a narrow rectangular strip of the previously prepared jelly-roll material around the squib head; this is then wrapped tightly with one layer of 2-mil polyethylene and secured with rubber bands. The finished product resembles a jelly-roll, with the squib head in the center. The jelly-roll material is prepared by coating a sheet of cheesecloth to a depth of about $\frac{1}{16}$ -inch with a slurry of RHim-1 and a solution of 5% poly(isobutylene) in n-hexane.

3.4 Insulation of .75C.50 Motors

Quite accurate P-K-r and temperature-coefficient data may be obtained from .75C.50 motors if the propellant temperature is accurately known. However, because of their small mass, these motors can undergo rapid temperature changes. Consequently, if firing temperatures other than ambient are required, the motors must be well-insulated to prevent

prohibitive propellant-temperature changes from occurring during the time interval between removal from the conditioning box and firing. Temperature measurements were made by inserting a thermocouple in the propellant of a .75C.50-1.5 motor. The motor was cooled to -40°F and removed from the cold box. After four minutes, the average time from box to firing, the temperature had risen 40°F with an initial temperature differential of 125°F . (Fig. 19).

Very good temperature control was achieved by insulating the loaded-motor assembly, including the pressure gauge, in a close-fitting rectangular box made of 1-inch-thick polystyrene foam (Fig. 20). The box is open on the pressure gauge end, and is closed on the nozzle end. The insulating box is left in place during firing, and upon ignition a press-fit plug is blown out of the closed end of the box.

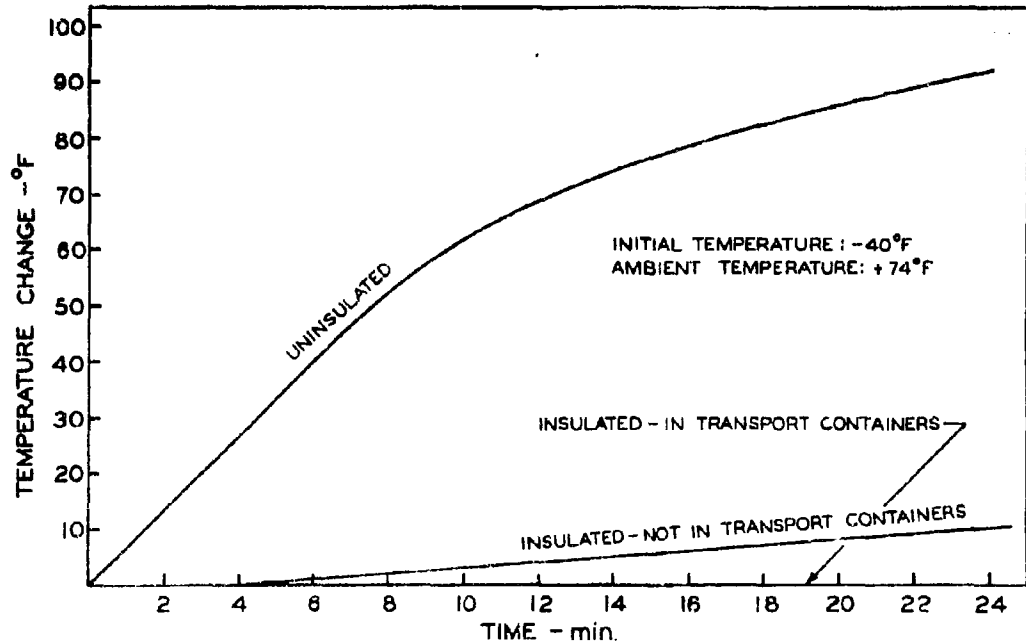


Fig 19 Change in propellant temperature in .75C.5-1.5 micro-motors as a function of time after removal from a cold box at -40°F .

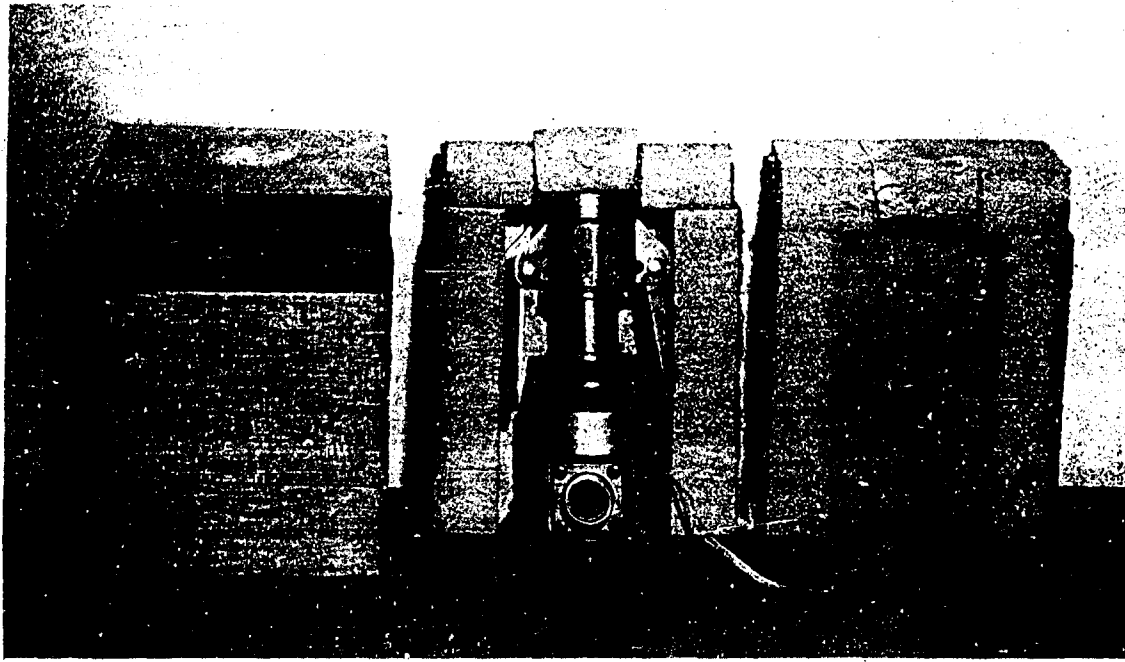


Fig.20 Insulating box for .75C.50-1.5 motor. Assembled box and motor at left. Cutaway view at center and right.

The complete insulated assembly is conditioned at the required temperature. Several of these assemblies are then placed in a larger insulated box, which has also been conditioned to the motor temperature, for transportation to the firing range. The insulated motor assemblies are removed one at a time for firing; a firing can usually be accomplished within two minutes of removal from the insulated transport box.

Temperature-time measurements made with a thermocouple embedded in the propellant showed that the insulation reduced heat transfer sufficiently that accurate estimates of the propellant temperature at the time of firing could be made (Fig. 19).

Micro-motors have been successfully fired at extreme temperatures of -40°F and $+140^{\circ}\text{F}$. Since the pressure gauges are conditioned with the motors they must be calibrated at these temperatures.

Since the standard Celvacene¹ light vacuum grease used to pack the gauges is satisfactory at +140°F but freezes at -40°F, Dow-Corning High-Vacuum Grease diluted with Dow Silicone Oil is used at -40°F.

To prevent gas leaks from occurring on cold shots utilizing the threaded-motor design, motors are assembled after the individual components have been cooled. The clamp-type motors may be assembled at ambient temperature.

3.5 Instrumentation

3.5.1 General

The basic instrumentation system used for both .75C.50 and 2C1.5-4 motors is shown schematically in Fig. 21. The thrust channel consists of a dual-thrust gauge, filter, calibrator, amplifier, and an analog and digital recording system. The pressure channel is basically the same as the thrust channel except that a filter is not used.

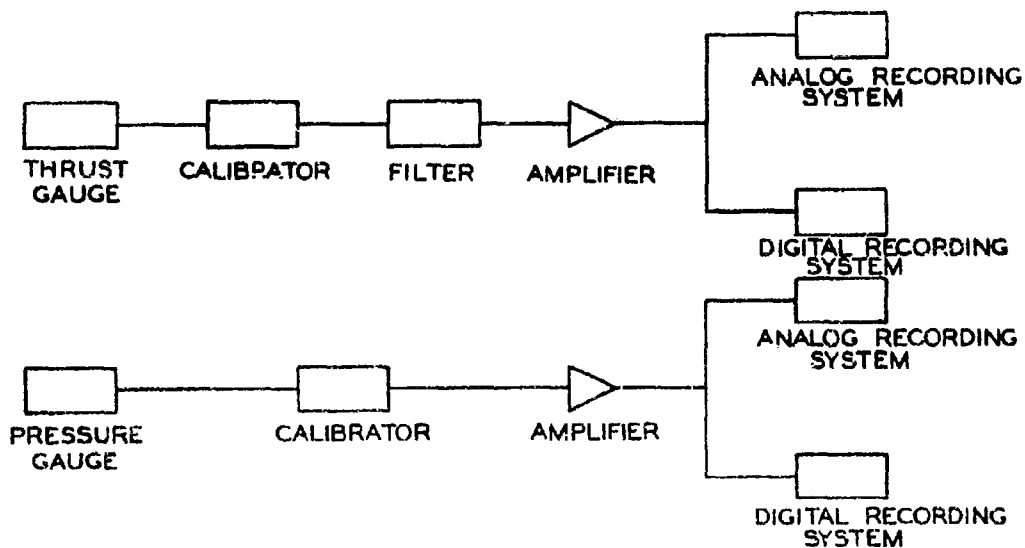


Fig 21 Thrust and pressure instrumentation used with micro-motors.

¹Consolidated Electrodynamics Corporation, Pasadena, California.

The amplifiers used are Kintel Model 112¹ which have the desirable characteristics for transient measurements of a wide frequency response and a wide linear output-voltage range. A wide frequency response is not in itself necessary but, unless the cutoff frequency of the amplifier is considerably above the cutoff frequency of the filter, it is necessary that the amplifier have the characteristics of a true filter. For example, amplifiers characterized by a slewing rate must be used with caution.

Probably the best types of integrating systems for transient data are those based upon the voltage-to-frequency type converter such as the Dymec Model 2211B.² These converters have excellent frequency response, wide linear overrange capacity, and a full-scale frequency which is high enough to provide adequate resolution for shots having a duration of 10 milliseconds or longer.

3.5.2 Special Considerations for .75C.50 Motors

In order to minimize the weight of the overall assembly, a special pressure gauge (Figs. 1 and 2) was designed for use with .75C.50 motors. This pressure gauge is the same basic design as the Rohm & Haas diaphragm gauge used by this Division for a number of years; the sensitive element of the gauge is a diaphragm to which the strain-gauge bridge and the temperature-compensating resistor are cemented. The gauge internal cavity is filled with Celvacene light vacuum grease to protect the diaphragm, reduce the motor free volume, and reduce motor heat losses. The resonant frequency of the assembly using a 50-pound load cell is approximately 130 cycles/sec.

The motor, pressure gauge, and thrust gauge constitute a highly under-damped second-order system which is shocked into appreciable oscillation by the motor thrust. This oscillation is of such magnitude that it interferes with the digital integration by causing the thrust gauge output to swing below zero. To eliminate this oscillation, a 50-cycle low-pass filter (Fig. 22) is included in the thrust-gauge circuit.

¹Cohn Electronics Inc., Kintel Div., San Diego, California.

²Dymec Div., Hewlett-Packard Co., Palo Alto, California.

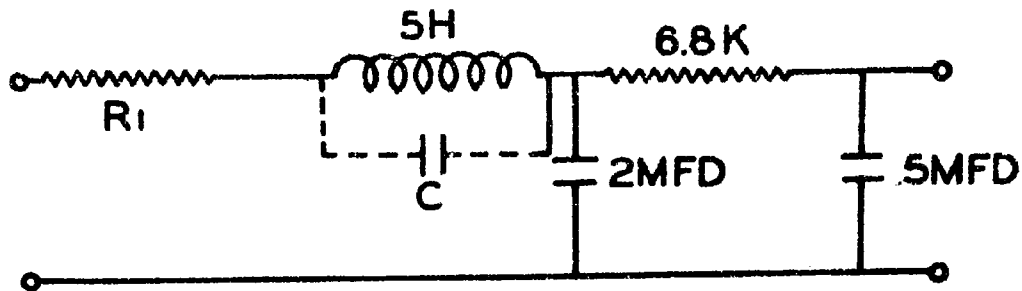


Fig.22 Low-pass filter to eliminate thrust oscillation during .75C.50 motor firings.

The filter is designed according to the Butterworth¹ condition except that R is adjusted for optimum transient response.

The attenuation of the filter above the cutoff frequency increases at a rate of nearly 18 decibels/octave, but the oscillations are not sufficiently attenuated when a 50-pound thrust gauge is used. To provide more attenuation the capacitor C was added to form a trap for the resonant frequency of the system, approximately 130 cycles. With this addition the recorded traces are oscillation-free.

The total impulse of a motor is defined as $\int F(t)dt$. In practice, however, it is not $F(t)$ that is integrated but a function, using Laplace notation

$$L^{-1}A(s)B(s)F(s)$$

¹Ernst A. Guillemin, "Synthesis of Passive Networks," John Wiley & Sons, New York, 1957.

where $F(s) = LF(t)$, $A(s)$ is the transform of the electronics of the system and $B(s)$ is the transform of the thrust stand and thrust gauge. If the measured impulse is to be valid $\int L^{-1}A(s)B(s)F(s)dt$ must equal $\int F(t)dt$ even though $L^{-1}A(s)B(s)F(s)$ only approximates $F(t)$, due to the transient nature of the thrust, the relatively low frequency of the thrust stand, and the filter.

The method used to study this problem was to assume as the thrust function $F(t)$ the pulse $\mu(t) - \mu(t-a)$, that is, a square pulse of unit amplitude and a duration, which has a very wide frequency spectrum and to evaluate $\int L^{-1}A(s)B(s)F(s)$ by integration. The frequency response of the amplifier and the digital system is very high (10,000 cycles), and the only frequency-dependent component of $A(s)$ that matters is the filter. Let $A(s) = PG(s)$ where $G(s)$ is a general low-pass filter

$$\frac{A_m s^m + A_{m-1} s^{m-1} + \dots + 1}{B_n s^n + B_{n-1} s^{n-1} + \dots + 1} \quad n > m$$

If $B(s)$, the transform of the thrust stand, is ignored, and since

$$L[u(t) - u(t-a)] = \frac{1}{s} - \frac{1}{s} e^{-as} \quad (1)$$

then

$$LA(s)F(s) = \frac{1}{s} (1 - e^{-as}) \frac{A_m s^m + A_{m-1} s^{m-1} + \dots + 1}{B_n s^n + B_{n-1} s^{n-1} + \dots + 1} P \quad (2)$$

By the theory of partial fractions the right hand side of Eq. 2 may be expanded into

$$P(1 - e^{-as}) \left(\frac{1}{s} + \frac{A}{s + \omega_1} + \frac{Bs + C}{(s + \beta_1)^2 + \omega_2^2} + \frac{Es + D}{(s + \beta_2)^2 + \omega_3^2} + \dots \right)$$

The first term of the above expression $\frac{1}{s}(1 - e^{-as})$ is $LF(t)$. Therefore if

$$\int_0^{\infty} L^{-1} \left\{ (1 - e^{-as}) \left[\frac{A}{s + \omega_1} + \frac{Bs + C}{(s + \beta_1)^2 + \omega_2^2} + \frac{Es + D}{(s + \beta_2)^2 + \omega_3^2} + \dots \right] \right\} dt = 0 \quad (3)$$

then

$$\int_0^{\infty} F(t) dt = \int_0^{\infty} L^{-1} A(s) F(s) dt \quad (4)$$

That Eq. 3 does equal zero may be shown by direct integration although this is not necessary since, by the Second Shifting Theorem, $L^{-1} e^{-as} \phi(s) = \phi(t-a)u(t-a)$, and each term of the inverse transform of Eq. 3 will contain a minus exponential, so the integral is obviously zero.

The analysis could be extended to a general $F(t)$ by dividing $F(t)$ into a succession of pulses $F_i[u(t-L_i) - u(t-L_i-a)]$ and then letting $a \rightarrow 0$.

Since the thrust stand is a second-order system with the familiar equation

$$m\ddot{x} + \rho\dot{x} + kx = F(t) \quad (5)$$

its transform $B(s)$ is

$$\frac{B}{ms^2 + \rho s + k}$$

which is mathematically the transform of a second-degree filter.

Therefore the effect of the thrust stand may be included simply by adding another term to Eq. 2 and the result is the same. Constants are automatically taken care of by the calibration procedure.

These results mean that it is possible to integrate very transient forcing functions using the same instrumentation that is used for larger motors.

To demonstrate the mathematical analysis experimentally, a series of .75C.50-1.5 micro-motors was fired at various thrust/mass ratios using a 100-pound load cell and various degrees of filtering. The precision of the measurements was not good, partly because the severe oscillations exceeded the range of the load cell. However, $\int Fdt$ seemed to be independent of the thrust/mass ratio and filtering (Table V).

Table V
Summary of Filter Check Data

<u>No.</u> <u>Rounds</u>	<u>Batch</u>	<u>Thrust/Mass</u> ^b <u>Ratio</u>	<u>Filter</u>	<u>F₁₀₀₀</u> ^a
5	A	10	50 cycle	234.8
5	A	0.5	15 cycle	233.2
6	B	10	50 cycle	236.0
5	B	10	None	235.3
4	B	0.5	15 cycle	235.5

^a See Appendix A for definition of ballistic parameters.

^b Thrust/mass ratios of 0.5 were achieved by adding 50 lbs mass to the standard motor; the standard configuration had a thrust/mass ratio of 10.

In general, the accuracy of the measurements (as distinct from the problem of motor reproducibility) should be essentially the same as with larger motors. An advantage is the ease with which low-range gauges can be calibrated with dead weights. Occasionally, some of the 50- and 100-pound thrust gauges have given trouble because of calibration instability. It is necessary to load the thrust gauges very conservatively since the high oscillation level can over-range the gauge.

Generally the capacity of the thrust gauge should be at least twice the maximum thrust expected.

Data from three ten-motor groups of .75C.50-3.5 micro-motors containing RH-P-112cb propellant are shown in Table VI to illustrate the precision of specific-impulse measurement which can be obtained when proper experimental techniques are used.

Table VI
Specific-Impulse Data from .75C.50-3.5 Micro-Motors

<u>Group No.</u>	<u>Group Size</u>	<u>Average</u> <u>F_{1000}^0</u>	<u>1 σ</u> <u>(absolute)</u>	<u>1 σ</u> <u>(per cent)</u>
1	10	241.0	1.0	0.4
2	10	241.3	0.9	0.4
3	10	240.0	0.4	0.2

3.6 Data Reduction

Except for somewhat different definitions of parameters, data-reduction methods for micro-motors are the same as those for large motors. Conventional data-reduction procedures used by this Division, as well as the exceptions required for micro-motors, are given in Appendix A.

Because ignition of micro-motors is so critical, it is possible to obtain forms of pressure-time traces which deviate considerably from those of larger motors. Application of conventional data-reduction techniques to pressure traces can result in large errors. Several exaggerated forms of pressure-time traces which might be obtained with micro-motors are given in Appendix A.

The lower trace in Fig. 23 provides an example of how erroneous data might be obtained using conventional data-reduction techniques. The conventional definition of start of action time and burning time is the time at which pressure has risen to 100 psia on the primary rise portion of the trace (point 3). This is not valid for the trace shown, since the pressure

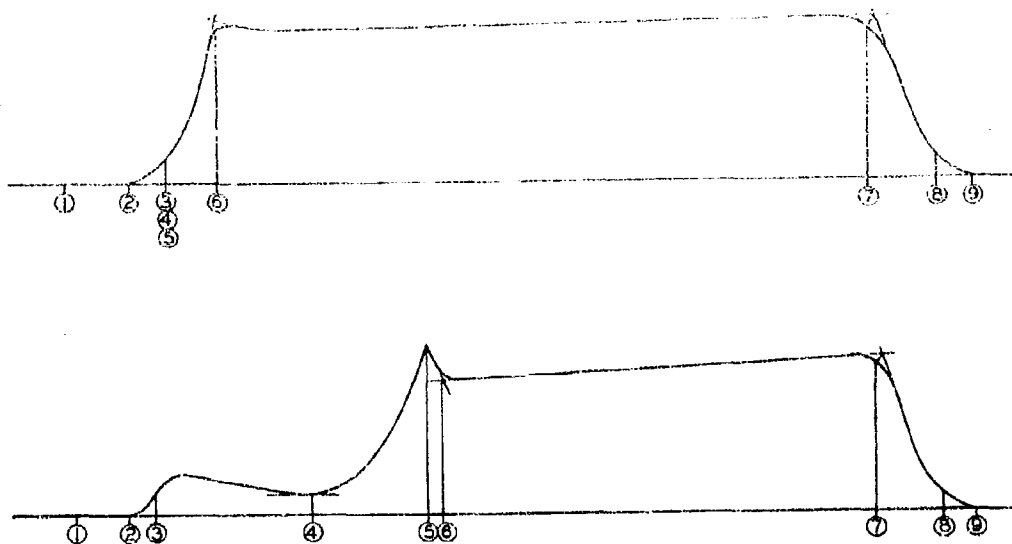


Fig. 23 Desired "square trace" (top) and an unusual pressure trace (bottom).

up to point 4 is caused by the igniter alone. Propellant begins to burn at point 4, and this should be used as the start of burning time. If beginning of action time is defined as the time at which the thrust trace begins to rise, this should correspond to point 5 (the time at which the closure ruptures). Use of the 100-psia convention would yield unrealistically long values for burning time and action time, and correspondingly low values for r_b , \bar{P}_b , and \bar{P}_a . Values of F_{1000}^0 would be too high, since the low value of P_a would be used in the $C_{F_{Test}}$ equation employed in the correction.

The most desirable pressure traces are regular as shown in Fig. 23; if enough rounds are available from individual propellant batches the ignition system can usually be adjusted to give good traces. Poor traces are then discarded if enough good traces are available. However, when only a few motors are available, all may produce irregular pressure traces. In this case the data would be reduced using procedures outlined in Appendix A.

Any correction for excessive igniter contribution should be made once F_{1000}^0 is determined by the procedures outlined in Appendix A. Defining a new term $(F_{1000}^0)_i$ as the igniter-corrected F_{1000}^0 , the following equations may be derived:

$$(F_{1000}^0)_i = F_{1000}^0 - I_{spi} \times \frac{w_i}{w_p} \quad (\text{for correction to zero igniter weight}) \quad (6)$$

$$(F_{1000}^0)_i = F_{1000}^0 - I_{spi} \left(\frac{w_i}{w_p} - 0.005 \right) \quad (\text{for correction to } 1/2\% \text{ igniter weight}) \quad (7)$$

where I_{spi} = specific impulse of igniter ($I_{spi} = 110$ for M-1 squib and RIP or RHim)

w_i = weight of combustible material of igniter

w_p = weight of propellant

Measurement of igniter specific impulse by firing igniters in motors containing dummy grains and measuring $\int Fdt^1$ is not practical for micro-motors since the $\int Fdt$ of 0.05 grams of igniter material is not measurable on a 50-ib load cell. Consequently, igniter impulse was determined by firing multiple rounds with various amounts of igniter. The resulting plot of F_{1000}^0 versus igniter weight (Fig. 24) was extrapolated to zero igniter weight, yielding $(F_{1000}^0)_i$. The specific impulse of the igniter was then deduced by comparing $(F_{1000}^0)_i$ with F_{1000}^0 for a particular igniter weight.

¹JANAF Solid Propellant Rocket Static Test Panel, "Recommended Procedures for the Measurement of Specific Impulse of Solid Propellants," SPLA Publication No. SPSTP/10B, March 1962.

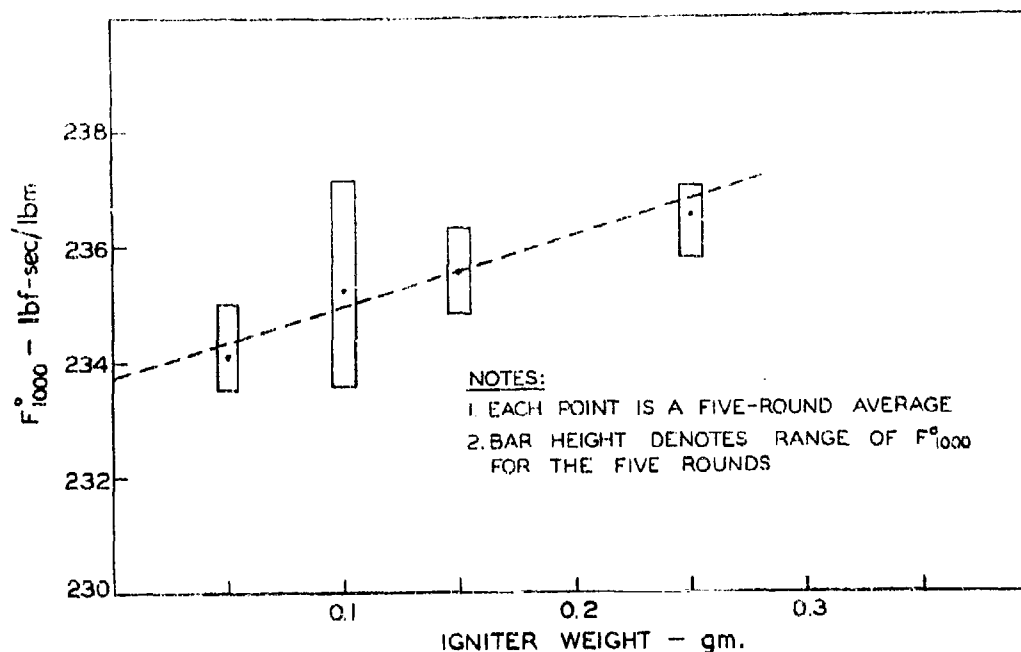


Fig.24 Specific impulse as a function of igniter weight.

The standard micro-motor grain length is $\frac{3}{32}$ inch shorter than the case. Occasionally, however, shorter grains will be encountered, either because insufficient propellant was available to fill the motor or because the cured grains were trimmed to remove end flaws. Since short grains will expose more of the motor case, heat losses will be higher and specific impulse correspondingly lower. It is generally desirable to correct specific impulse for the additional heat loss, giving a specific impulse which would have been measured with a standard grain. This correction may be accomplished by use of the following equation, which was derived from equations given in Section 4 of this report.

$$(F_{1000}^0)_f = \sqrt{(F_{1000}^0)^2 + \frac{2J\eta q}{144 g_0} \left[\left(\frac{t A}{z m} \right)_{\text{actual}} - \left(\frac{t A}{z m} \right)_{\text{nominal}} \right]} \quad (8)$$

where $(F_{1000}^0)_f = F_{1000}^0$ which should be obtained with standard length grain
 J = energy conversion factor, = 778.16 ft-lbf/Btu
 q = heat flux, Btu/sec-ft²
 g_0 = mass conversion factor = 32.174 ft-lbm/lbf-sec²
 η = theoretical thermal efficiency
 t_c = time interval during which heat is lost from propellant gases to motor hardware, sec
 A = exposed motor hardware surface area, in²
 m = propellant weight, lbm.

Data-reduction practices used to obtain P-K-r data from micro-motors are the same as those used throughout the industry, if a regular trace is obtained. For the more peculiar traces, the procedures outlined in Appendix A for micro-motors should be used to obtain $\bar{P}_b - r_b$ and $P_{eq} - K$ data.

Due to the small web thickness ($\frac{1}{8}$ inch) of .75C.50 motors, small dimensional variations along the grain have a pronounced effect on the apparent burning rate. Any variations present usually cause the propellant to burn out unevenly, resulting in lower-than-normal integral ratios ($\int P_b dt / \int P_{tot} dt$ as defined in Appendix A). In general, the lower the integral ratio the higher the apparent burning rate. Therefore, for burning-rate measurements, no trace is considered whose integral ratio is not at least 0.90, and for the most accurate rates, integral ratios of 0.95 or higher are preferred.

Data reduction for temperature-coefficient firings is handled in the same way as for P-K-r data. The propellant temperature upon firing is estimated from experimental curves such as those in Fig. 21.

Temperature coefficient of pressure at constant K, π_K , is calculated as follows:

$$\pi_K = \frac{P_2 - P_1}{\left(\frac{P_2 + P_1}{2}\right)} \times \frac{100}{T_2 - T_1} \quad (9)$$

where P_1 = average pressure over burning time at temperature T_1 .

P_2 = average pressure over burning time at temperature T_2 .

4 Data Interpretation

4.1 Specific-Impulse Data

Strict compliance with all the methods and techniques described in Section 2 of this report will yield numbers which can properly be called F_{1000}^0 in the (.75C.50-1.5, .75C.50-2.5, .75C.50-3.5, 2C1.5-4) micro-motor. These numbers in themselves have no particular significance unless they form the basis for a predicted specific impulse for the specific composition in a much larger motor which has a specific application.

4.1.1 Theoretical Scaling Considerations and Equations

Theoretically, the corrected specific impulse of a motor-propellant system is dependent upon the following factors:

- (a) the basic available combustion energy of the propellant;
- (b) the amount of energy lost from the propellant gases in the form of heat transfer to the motor components;
- (c) the degree of kinetic and thermal equilibrium attained between the gaseous and condensed phases of the combustion products during the expansion process;
- (d) combustion efficiency, or the relative completeness of combustion achieved in the motor chamber; and
- (e) the degree of dissociation and/or recombination of the product gases during the expansion process.

Items (b) through (e) can be expected to vary with motor size and configuration, and these variations are responsible for the frequently observed specific-impulse scaling effect, or the difference in F_{1000}^0 between motors of different sizes containing identical propellants.

4.1.1.1 Heat-Loss Effects

Assuming complete kinetic and thermal equilibrium between gaseous and condensed combustion products, the specific impulse equation may be written as

$$F_{1000}^0 = \sqrt{\frac{2J}{g_0} (\Delta H_c)} = \sqrt{\frac{2J}{g_0} (H_c - H_e)} \quad (10)$$

where

- J = energy conversion factor, 778.16 ft-lbf/Btu
- g_0 = mass conversion factor, 32.174 ft-lbm/lbf-sec²
- ΔH_c = isentropic enthalpy change of combustion products during expansion through the nozzle, Btu/lbm
- H_c = enthalpy of combustion products at nozzle entrance, Btu/lbm
- H_e = enthalpy of combustion products at nozzle exit, Btu/lbm

From the relation

$$\Delta H = C_p \Delta T \quad (11)$$

F_{1000}^0 may be rewritten as

$$F_{1000}^0 = \sqrt{\frac{2J}{g_0} C_{p_c} T_c \left(1 - \frac{C_{p_e} T_e}{C_{p_c} T_c} \right)} = \sqrt{\frac{2J}{g_0} H_c \eta} \quad (12)$$

where

- C_{p_c} = specific heat at constant pressure of the combustion products (in the chamber) at temperature T_c , Btu/lbm-°R
- C_{p_e} = specific heat at constant pressure of the combustion products (at the nozzle exit) at temperature T_e , Btu/lbm-°R
- T_c = chamber temperature, °R
- T_e = exit temperature, °R
- $\eta = 1 - \frac{C_{p_e} T_e}{C_{p_c} T_c}$
- $H_c = C_{p_c} T_c$

Assuming that heat q is lost from the combustion gases in the form of heat transfer to the combustion chamber, and that the chamber enthalpy would have been H_o instead of H_c had the heat loss not occurred, the heat loss may be expressed as

$$Q/m = H_o - H_c = C_{p_o} T_o - C_{p_c} T_c \quad (13)$$

where Q/m = heat lost from combustion products to the motor chamber, Btu/lbm

H_o = enthalpy of combustion products in the chamber for the case of no heat loss, Btu/lbm

C_{p_o} = specific heat at constant pressure of the combustion products at temperature T_o , Btu/lbm-°R

T_o = chamber temperature for the case of no heat loss, °R.

Substitution of Eq. 13 into Eq. 12 yields

$$F_{1000}^o = \sqrt{\frac{2J}{g_o} (H_o - Q/m)\eta} = \sqrt{\frac{2J\eta H_o}{g_o} - \frac{2J\eta}{g_o} Q/m} \quad (14)$$

The specific impulse that would have been obtained for the case of no heat loss may be expressed as

$$\begin{aligned} I_{HL}^o &= \sqrt{\frac{2J}{g_o} \Delta H_{HL}^o} = \sqrt{\frac{2J}{g_o} (H_o - H'_e)} = \sqrt{\frac{2J}{g_o} H_o \left(1 - \frac{C'_{p_e} T'_e}{C_{p_o} T_o}\right)} \\ &= \sqrt{\frac{2J}{g_o} H_o \eta_1} \end{aligned} \quad (15)$$

where C'_{p_e} = specific heat at constant pressure of the exit products at temperature T'_e , Btu/lbm-°R

ΔH_{HL}^o = isentropic enthalpy change of the combustion products during expansion through the nozzle for the case of no heat loss, Btu/lbm

H'_e = enthalpy of combustion products at nozzle exit for the case of no heat loss, Btu/lbm

T'_e = exit temperature for the case of no heat loss, °R.

$$\eta_1 = 1 - \frac{C'_{p_e} T'_e}{C_{p_o} T_o}$$

Since $\eta \approx \eta_1$, Eq. 15 may be substituted into Eq. 14 to yield

$$F_{1000}^0 = \sqrt{\left(I_{HL}^0\right)^2 - \frac{2J}{g_0} \eta \frac{Q}{m}} \quad (16)$$

Eq. 16 relates the specific impulse actually obtained when heat loss occurred (F_{1000}^0), the specific impulse which would have been obtained had heat loss not occurred (I_{HL}^0), and the amount of heat lost (Q/m).

4.1.1.2 Two-Phase-Flow Effects

The specific impulse equation may be written as

$$F_{1000}^0 = \frac{\dot{m}_g V_g + \dot{m}_s V_s}{g_0 (\dot{m}_g + \dot{m}_s)} = \frac{\dot{m}_g V_g}{g_0 (\dot{m}_g + \dot{m}_s)} + \frac{\dot{m}_s V_s}{g_0 (\dot{m}_g + \dot{m}_s)} = \frac{yV_g + xV_s}{g_0} \quad (17)$$

for a two-phase system, where

$$\begin{aligned} \dot{m}_g &= \text{mass flow rate of gaseous phase at nozzle exit, lbm/sec} \\ \dot{m}_s &= \text{mass flow rate of condensed phase at nozzle exit, lbm/sec} \\ V_g &= \text{velocity of gaseous phase at nozzle exit, ft/sec} \\ V_s &= \text{velocity of condensed phase at nozzle exit, ft/sec} \\ x &= \frac{\dot{m}_s}{\dot{m}_g + \dot{m}_s} \\ y &= \frac{\dot{m}_g}{\dot{m}_g + \dot{m}_s} \end{aligned}$$

If $V_s = V_g$ (no velocity lag of the condensed phase),

Eq. 17 reduces to

$$I_{VL}^0 = \frac{V_g}{g_0} \quad (18)$$

Dividing Eq. 17 by Eq. 18 results in

$$\frac{F_{1000}^0}{I_{VL}^0} = \frac{yV_g + xV_s}{V_g} = y + x \frac{V_s}{V_g} \quad (19)$$

The fractional velocity lag may be defined as

$$\Delta = \frac{V_g - V_s}{V_g} = 1 - \frac{V_s}{V_g} \quad (20)$$

Substitution of Eq. 20 into Eq. 19 yields

$$\frac{F_{1000}^0}{I_{VL}^0} = y + x(1 - \Delta) = y + x - x\Delta = 1 - x\Delta \quad (21)$$

Eq. 21 relates the specific impulse actually obtained when velocity lag of the condensed phase occurs (F_{1000}^0), the specific impulse which would have been obtained had no velocity lag occurred (I_{VL}^0), the weight fraction of condensed products (x), and the fractional velocity lag of the condensed products (Δ).

4.1.1.3 Combined Heat Loss and Two-Phase Flow Effects

Eq. 21 may be written in the form

$$\frac{I_{HL}^0}{I^0} = 1 - x\Delta \quad (22)$$

where I_{HL}^0 = specific impulse which should be obtained if velocity lag occurs but heat loss does not occur

I^0 = specific impulse which should be obtained if neither heat loss nor velocity lag occurs.

Substitution of Eq. 22 into Eq. 16 yields

$$F_{1000}^0 = \sqrt{(I^0)^2 (1 - x\Delta)^2 - \frac{2J}{g_0} \eta \frac{Q}{m}} \quad (23)$$

The unknown quantity I^{00} may be eliminated by writing Eq. 23 for two static test motors and solving the resulting equations simultaneously as follows:

$$(F_{1000}^0)_1^2 = (I^{00})^2 (1 - x\Delta_1)^2 - \frac{2J}{g_0} \eta (Q/m)_1 \quad (24)$$

$$(F_{1000}^0)_2^2 = (I^{00})^2 (1 - x\Delta_2)^2 - \frac{2J}{g_0} \eta (Q/m)_2 \quad (25)$$

$$(F_{1000}^0)_2 = \sqrt{\left(\frac{1 - x\Delta_2}{1 - x\Delta_1}\right)^2 \left[(F_{1000}^0)_1^2 + \frac{2J\eta}{g_0} (Q/m)_1 \right] - \frac{2J}{g_0} \eta (Q/m)_2} \quad (26)$$

The heat-loss term, Q , in Eq. 26 may be expressed as

$$Q = \frac{qt_z A}{144} \quad (27)$$

where q = heat flux, Btu/sec-ft²

t_z = time interval during which heat is lost to internal motor hardware (motor action time), sec

A = surface area of internal motor hardware to which heat is lost, in²

Substitution of Eq. 27 into Eq. 26 yields

$$(F_{1000}^0)_2 = \sqrt{\left(\frac{1 - x\Delta_2}{1 - x\Delta_1}\right)^2 \left[(F_{1000}^0)_1^2 + \frac{2J\eta q}{144g_0} \left(\frac{t_z A}{m}\right) \right] - \frac{2J\eta q}{144g_0} \left(\frac{t_z A}{m}\right)} \quad (28)$$

Eq. 28 relates the specific impulses of two arbitrary static test motors (containing identical propellants) in terms of their respective velocity lags and heat losses, and is the basic equation used by this Division to predict large-motor specific impulse and to determine scaling factors from small-motor static-test data.

Eq. 28 is not a rigorous equation; many simplifying assumptions were made in its derivation. However, it has proven to be valuable and useful in its present form, and consequently no attempts have been made to perform a more rigorous analysis.

4.1.2 Calculation of Fractional Velocity Lag (Δ)

A FORTRAN computer program developed at this Division is currently used to calculate fractional velocity lag (Δ). A simplified mathematical model is used to approximate the real flow process. This simplified model, which ignores the coupled effect of the particle lag on the flow of the gas phase, permits rapid estimation of the effects of solid particles and nozzle configuration on performance. The model is not sophisticated; however, it has been satisfactory for the determination of specific-impulse scaling factors from small-motor static tests. Description of the program and the mathematical model is given in Appendix B and a complete listing of the FORTRAN program is given in Appendix C.

Before the present program was developed, an even more simplified version programmed for a Royal-McBee LGP-30 computer was used to calculate values of Δ . For a given case, the current program sometimes yields Δ values quite different from those of the original program. Consequently, scaling factors derived from a given set of small-motor data could differ somewhat, depending on the program used to calculate Δ values. However, practically identical predictions of specific impulse in a given large motor are obtained with both velocity-lag programs.

Use of Δ values calculated for our reference RH-P-112 plastisol propellant generally result in valid predictions for other propellant compositions, even though the derived scaling factors might differ considerably from those obtained if Δ values calculated for the specific propellant are used. For this reason, a set of Δ curves generated for

RH-P-112 propellant are shown in Appendix D. Curves of Δ vs nozzle diameter at various nozzle expansion ratios and particle diameters are shown for the Rohm & Haas .75C.50, 2C1.5, and 6C5 motor nozzles, for the USAF BATES motor nozzle, and for the Aerojet 10KS-2500 motor nozzle. These curves will generally result in valid specific impulse predictions for most propellants, but, if a computer is available, use of Δ values calculated for the actual propellant is recommended. Additional computer-calculated Δ values will obviously be required for predictions in motors other than those for which curves are given in Appendix D.

4.1.3 Determination of Scaling Factors

Examination of Eq. 28 indicates that an $(F_{1000}^0)_2$ for some arbitrary motor could be calculated, based on the ballistic results obtained from static tests of some other motors, if values for Δ and q were known. The weight fraction of condensables, x , is known from thermochemical calculations; values for $(F_{1000}^0)_1$, $(F_{1000}^0)_2$ and m_1 are known from static tests; A_1 and A_2 may be calculated on the basis of the respective motor configurations; and $(A_2)_2$ and m_2 may be closely estimated, based on the ballistic results from motor 1 and the configuration of motor 2.

Further, by the procedure described in Appendices B and C, only the particle diameter (N) must be specified to calculate Δ_1 and Δ_2 . All other parameters necessary for the fractional velocity lag calculation are known, once the propellant composition and nozzle configurations have been specified. This means that $(F_{1000}^0)_2$ could be calculated, based on static test data from motor 1, if N and q were known.

Many simplifying assumptions were made in deriving Eq. 28. Probably the most questionable is the assumption that specific impulse scaling is due only to heat loss and two-phase-flow effects. Consequently, it is doubtful that use of the real values of N and q in Eq. 28, even if these values could be directly measured, would provide

proper correlation of the specific impulses of different motor configurations. For this reason, effort was directed toward a determination of the effective or apparent values of N and q which embody all questionable assumptions but, although they may differ considerably from the real values, nevertheless provide correlation between specific impulses of different motor configurations. These effective values of N and q are called scaling factors.

By assuming that the heat flux (q) is independent of motor configuration, Eq. 28 may be solved for q to yield

$$q = \frac{(F_{1000}^0)_2^2 - \left(\frac{1 - x\Delta_2}{1 - x\Delta_1}\right)^2 (F_{1000}^0)_1^2}{\frac{2J\eta}{144g_0} \left[\left(\frac{1 - x\Delta_2}{1 - x\Delta_1}\right)^2 \left(\frac{t_{zA}}{m}\right)_1 - \left(\frac{t_{zA}}{m}\right)_2 \right]} \quad (29)$$

The utility of Eq. 29 is immediately obvious. If static test data are available in two motor configurations, Eq. 29 is an equation in the two unknowns q and N . If static test data are available in three motor configurations, a total of three equations in the form of Eq. 29 may be written in the unknowns q and N ; this is more than sufficient to allow simultaneous solution for q and N .

Since the value N does not appear explicitly in Eq. 29, the method of intersecting curves must be used to effect a solution. All quantities derived from static tests and thermochemical calculations are substituted in Eq. 29 for the two motors to be compared. Various values of N are assumed and values of Δ_1 , Δ_2 , and q are calculated for each until an extensive curve of q versus N has been generated. A different combination of two motors is selected and another curve of q versus N is generated. These curves will intersect at the point of solution for the scaling factors q and N , and these scaling factors may then be used in conjunction with Eq. 28 to predict specific impulse in any other motor configuration.

Static test data must be available from a minimum of three motor configurations to allow solution for q and N by the above method, but more accurate scaling factors will result if data are available from more than three configurations. Also, more reliable scaling factors should be obtained from large motors than from small motors, due primarily to the difficulties associated with accurate measurement of ballistic parameters in small motors. Full use should be made of the maximum quantity of propellant available.

For best results, the motors used to obtain the data necessary for scaling-factor determination should be of two distinct types: (1) motors having the same grain O.D. and grain cross-sectional configuration but differing in length by at least a factor of two, and (2) motors which are linearly scaled but which differ in grain O.D. by at least a factor of two. The constant-O.D., different-length motors will have similar two-phase-flow losses but will differ significantly in heat losses, while the scaled motors will have practically the same heat loss per unit mass (Q/m) but will differ significantly in two-phase-flow losses. Thus, any F_{1000}^0 differences for the different-length motors should be primarily dependent on heat losses, whereas F_{1000}^0 differences for scaled motors should be primarily dependent on two-phase-flow losses. The q versus N curve for the scaled motors should then be much steeper than the q versus N curve for the different-length motors, providing a very definite intersection point for scaling factor determination.

The micro-motor system described in this report has been successfully used to determine scaling factors for propellants available in very limited quantities. The minimum three-motor configurations used are the .75C.50-1.5, the .75C.50-3.5, and the 2C1.5-4. Due to the difficulties associated with measurement of ballistic parameters in such small motors, multiple firings are generally conducted, using a minimum of five .75C.50-1.5, five .75C.50-3.5, and three 2C1.5-4 motors if possible. These thirteen rounds can be cast from a nominal 2-lb propellant mix.

Scaling factors can be estimated, based on a knowledge of scaling factors for similar propellants, if they cannot be determined experimentally because of propellant limitations. Estimated scaling factors will be questionable at best, but may be of some use in making approximate scale-up predictions.

If static test data are available only for one motor configuration, both q and N must be estimated. The following comments are offered as a guide in making these estimations.

Results from a series of tests of plastisolnitrocellulose propellant having aluminum concentrations from 5 to 22% by weight were correlated using Eq. 29 to determine scaling factors. For all compositions tested, q values fell between 1100-1500 Btu/sec-ft² and N values between 1.1-1.8 microns. Several NFPA compositions having aluminum concentrations from 10-15% gave q values in the same range and N values from 0.8-1.1 microns. The q values could be roughly correlated by the equation

$$q = 6.382 (T_c/1000)^4 + 156.4 (T_c/1000) \quad (30)$$

where T_c = theoretical flame temperature, °K. The empirical constants in Eq. 30 were determined using a heat flux, q , of 1300 Btu/sec-ft² for RH-P-112cb propellant ($T_c = 3325^\circ\text{K}$), and assuming that the heat flux was 60% radiative (proportional to T_c^4) and 40% convective (proportional to T_c).

If data are available for only one motor configuration, an estimated q should be calculated from Eq. 30. An estimated value for N will have to be arbitrarily selected, based on considered judgment.

If data are available for two motor configurations only, a curve of q versus N should be constructed as previously outlined. A value for q should be calculated from Eq. 30, and the N value which corresponds to the calculated q should be picked from the q versus N curve.

A detailed example illustrating scaling factor determination from .75C.50-1.5, .75C 50-3.5, and 2C1.5-4 motor static test data is presented in Appendix E. Auxiliary curves permitting rapid determination of the area term (A) for selected motors in Eqs. 28 and 29 are given in Appendix F.

4.1.4 Prediction of Large-Motor Specific Impulse

Large-motor specific impulse predictions are made using Eq. 28 and are relatively straightforward once the scaling factors have been determined. The configuration of the large motor is selected, allowing determination of t_2 , A_2 , m_2 , and Δ_2 . These parameters are substituted into Eq. 28 along with the corresponding parameters for one of the small motors for which static test data are available, and $(F_{1000}^0)_2$ is calculated for the large motor.

A detailed example illustrating the prediction procedure is given in Appendix E.

Micro-motors should not be used to make direct specific impulse comparisons. That is, specific impulses of a test propellant and a reference propellant as determined in micro-motors should not be extrapolated to some large motor; biased results will almost certainly be obtained unless the propellants being compared have similar heat losses and two-phase-flow properties. Flame temperatures, burning rates, and concentrations of condensable products in the exhaust must be about equal for the propellants before comparative specific impulses have any significance.

4.2 P-K-r and Temperature-Coefficient Data

While specific-impulse values obtained in micro-motors must be scaled to larger motors, $P-r$ and π_K data obtained in micro-motors are the same as for large motors, provided that proper experimental techniques are used in making the measurements. A scaling effect exists for P-K data, however.

The P-K-r relationships between micro-motors and larger motors were evaluated by firing a plastisol nitrocellulose composition in fourteen different motor configurations. The motors ranged in size from a .75C.50-1.5 micro-motor (10 gm) to a 9C7.5-17 (19 lb) motor. Data from three complete series are tabulated in Table VII. The propellant burning rate was varied by using ammonium perchlorate having different particle sizes.

The values of K in Table VII were obtained by correcting the actual values to 1000 psi (assuming $n = 0.5$) so that a comparison could be made between motor sizes. This correction was small in most cases, since all firings had been designed to give an average pressure of 1000 psi. At mass-discharge rates greater than 3 lb/sec K was essentially constant but at mass-discharge rates of less than 3 lb/sec K decreased with increased mass discharge (Fig. 25). The probable

Table VII

**Ballistic Data from Firings of Various-Size Motors
Containing Plastisol Propellants Having Three Different Burning Rates**

Motor Designation	Grind "a" APC ^a			Grind "b" APC ^a			Grind "c" APC ^a		
	K_m	\bar{r}_b (in/sec)	\dot{m} (lb/sec)	K_m	\bar{r}_b (in/sec)	\dot{m} (lb/sec)	K_m	\bar{r}_b (in/sec)	\dot{m} (lb/sec)
.75C.50-1.5	178.0	0.70	0.094	213.9	0.57	0.068	264.4	0.43	0.061
.75C.50-1.5	177.5	0.70	0.15	----	----	----	----	----	----
.75C.50-3.5	176.8	0.67	0.22	----	----	----	----	----	----
.75C.50-9	171.6	----	0.61	----	----	----	----	----	----
2C1.5-2	175.4	0.71	0.29	211.4	0.56	0.25	273.1	0.47	0.21
2C1.5-4	173.0	0.68	0.67	211.4	0.56	0.53	265.4	0.45	0.45
2C1.5-7.5	170.7	0.67	1.29	205.9	0.56	1.02	265.1	0.45	0.84
2C1.5-11.2	166.3	0.70	1.99	206.8	0.57	1.59	259.4	0.45	1.30
2C1.5-14.6	166.2	0.69	2.64	205.1	0.56	2.15	253.8	0.47	1.73
6C5-6	165.3	0.69	3.60	198.5	0.56	2.92	243.1	0.46	2.45
6C5-11.4	164.6	0.68	7.06	196.2	0.55	5.75	243.1	0.45	4.68
6C5-24	164.5	0.73	14.38	197.1	0.55	11.68	248.1	0.45	9.71
6C5-33	164.3	0.69	19.76	199.4	0.55	15.80	247.7	0.45	13.42
9C7.5-17.1	164.9	0.69	15.98	198.3	0.55	12.60	247.7	0.45	10.59

^a Each number is the average from five rounds fired at a given K value.
^b All K_m and \bar{r}_b have been corrected to $\bar{P}_b = 1000$ psi.

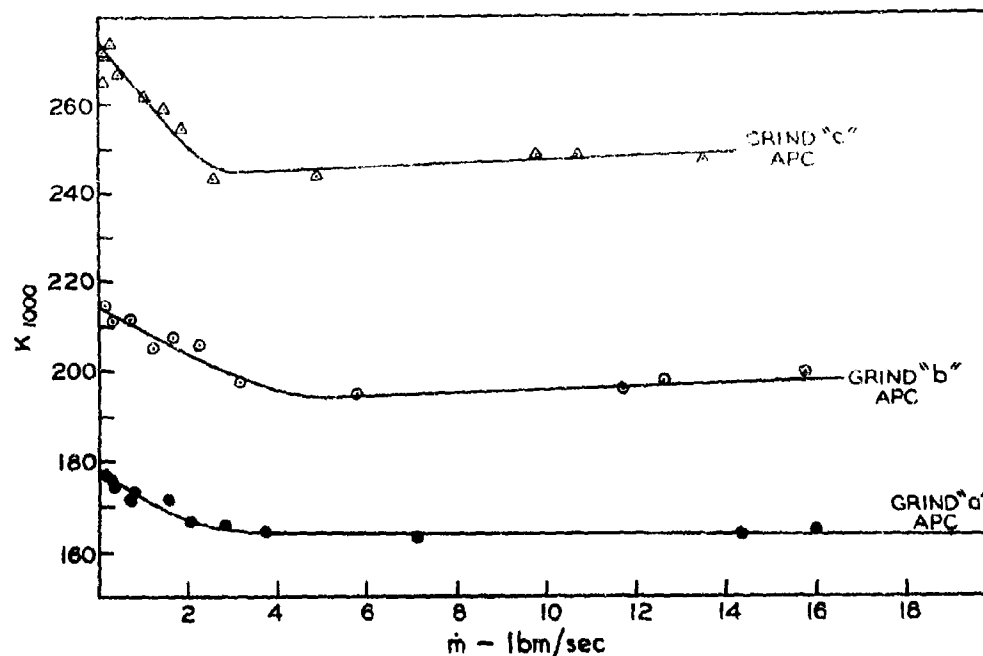


Fig. 25 K_{1000} as a function of \dot{m} and ammonium perchlorate particle size for plastisol propellant.

cause is a combination of heat loss and poor combustion efficiency. Curves of K_m as a function of

$$\sqrt{\frac{tA}{m}}$$

a heat-loss term, in which t is burning time, A is area of hardware exposed, and m is the propellant weight are shown in Fig. 26 for propellant containing 70% ammonium perchlorate. A different curve was obtained for each motor diameter, indicating that heat-loss variations alone are not responsible for the change in K_m . As motor length increased K_m tended to become constant.

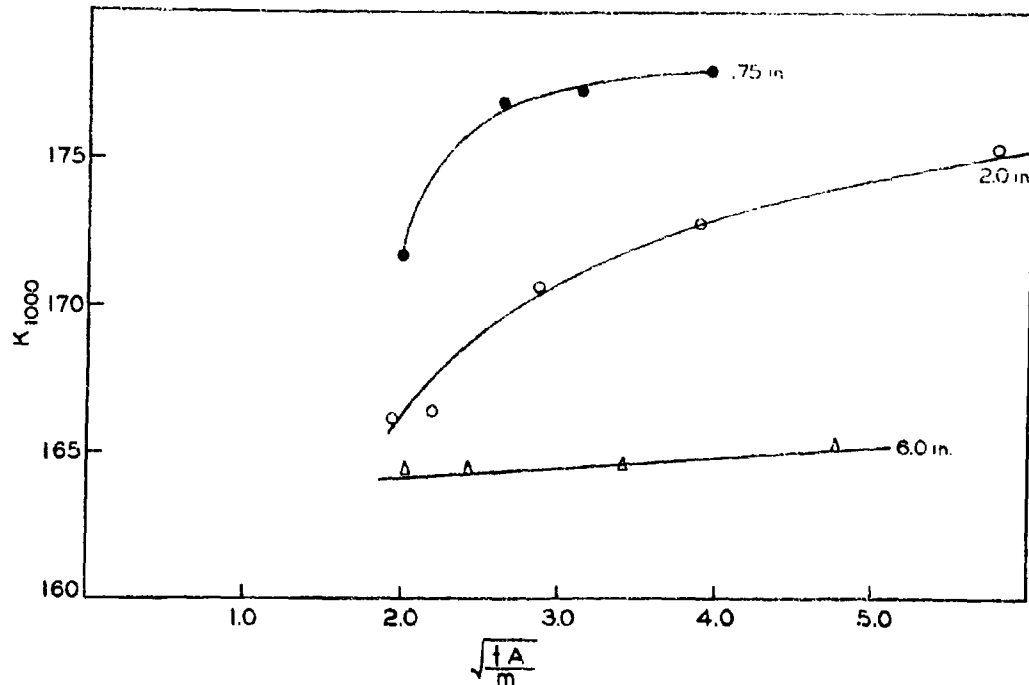


Fig. 25 K_{1000} for plastisol propellant as a function of $\sqrt{\frac{tA}{m}}$.

The burning rates, \bar{P}_b for the fourteen motor sizes in each series were corrected to 1000 psi (Table VII). These burning rates were, within experimental error, independent of mass discharge rate or propellant web thickness.

The results indicate that micro-motor P-K-r data can be very useful on new propellant compositions. Burning-rate data can be used directly, and P-K data can be used after the proper corrections have been made.

A pressure value corresponding closely to the equilibrium pressure of the rocket motor would be most meaningful in P-K relationships. The average pressures, \bar{P}_b , for two motors having the same amplitude pressure trace but different burning times are different since the aspect ratio of the pressure-time trace varies with motor size. Use of points 5 and 7 on the pressure-time trace (see Appendix A) as the limits of the equilibrium pressure integral is recommended. This pressure should be essentially constant for a given K regardless of the initial rise time or the total burning time of the propellant and should be used in P-K calculations.

The average pressure, \bar{P}_b , would still be used for burning rate measurements.

The data of Tables VIII and IX illustrate temperature coefficient relationships between micro-motors and 6C5-11.4 motors. Data obtained from firing a series of .75C.50-1.5 micro-motors with a typical plastisol propellant at the extremes of ambient temperature (35°F to 71°F) are shown in Table VIII. Using these data, π_K (35°F to 71°F) = 0.21%/°F. The temperature coefficient for this propellant as determined in the 6C5-11.4 motor was π_K (-40°F to 135°F) = 0.23%/°F while the temperature coefficient determined in insulated micro-motors was π_K (-33°F to 97°F) = 0.25%/°F.

Table VIII
Temperature Coefficient Data from .75C.50-1.5 Micro-Motors
at Ambient Temperatures

K = 164

<u>Temperature, °F</u>	<u>\bar{P}_b</u>	<u>\bar{r}_b</u>	<u>$\int P_b dt / \int P_{total} dt$</u>	<u>P_{max} / \bar{P}_b</u>
37	983	0.601	0.94	1.19
37	997	0.603	0.95	1.17
37	981	0.601	0.95	1.19
37	1004	0.590	0.96	1.16
37	983	0.609	0.95	1.19
37	1005	0.594	0.96	1.14
Avg 37	992	0.600	0.95	1.17
71	1059	0.643	0.96	1.13
71	1072	0.654	0.95	1.15
71	1072	0.672	0.95	1.13
71	1068	0.652	0.94	1.14
71	1063	----	0.92	1.13
71	1049	----	0.92	1.14
Avg 71	1064	0.655	0.94	1.14

$$\pi_K = 0.21\%/^{\circ}\text{F}$$

Table IX
Temperature Coefficient Data from Insulated .75C.50-1.5 Micro-Motors

K = 186

<u>Temperature, °F</u>	<u>\bar{P}_b</u>	<u>r_b</u>	<u>$\int \bar{P}_b dt / \int P_{total} dt$</u>
-33	758	0.470	0.95
-33	717	0.449	0.95
-33	820	0.530	0.92
-33	779	0.501	0.92
Avg	769	0.488	0.94
97	1078	0.705	0.88
97	1061	0.660	0.92
Avg	1069	0.682	0.90

$$\pi_K = 0.25\% / ^\circ F.$$

These results indicate that good temperature-coefficient data can be obtained in micro-motors.

Bibliography

1. B. L. Cockrell, "Ballistic Scaling of Specific Impulse," Bulletin of the 10th Meeting of the JANAF Solid Propellant Rocket Static Test Panel, October 1961.
2. L. M. Brown and B. L. Cockrell, "Micro-Motor Evaluation of Specific Impulse," Bulletin of the 18th Meeting of the JANAF-ARPA-NASA Solid Propellant Group, Volume III, June 1962.
3. L. M. Brown, J. L. Chaille, B. L. Cockrell, J. E. DeMore, "Micro-Motors--Instrumentation and Test Problems," Bulletin of the 11th Meeting of the JANAF Solid Propellant Rocket Static Test Panel, October 1962.
4. R. C. Petry, M. G. Baldwin, P. H. Gehlhaus, J. S. Foster, B. K. Nipp, J. W. Parrott, L. M. Brown, B. L. Cockrell, "Experimental High Energy Propellants," Bulletin of the 19th Mtg. of the Interagency Solid Propellant Group, Volume II, July 1963.
5. L. M. Brown and W. W. Seaton, "The Comparative Evaluation of State-of-the-Art Propellants," Bulletin of the 19th Mtg. of the Interagency Solid Propellant Group, Volume II, July 1963.
6. B. L. Cockrell, L. M. Brown, B. E. Sturgis, "Evaluation of Hazardous Propellants," Bulletin of the Annual Meeting of the ICRPG Working Group on Static Testing, October 1963.
7. L. M. Brown, J. S. Foster, R. C. Petry, "Experimental Difluoramino Propellants," Bulletin of the 20th Mtg. of the Interagency Solid Propellant Group, Volume II, July 1964.
8. Ernst A. Gullemmin, "Synthesis of Passive Networks," John Wiley & Sons, New York, 1957.
9. JANAF Solid Propellant Rocket Static Test Panel, "Recommended Procedures for the Measurement of Specific Impulse of Solid Propellants," SPIA Publication No. SPSTP/10B, March 1962.
10. Rohm & Haas Company, Quarterly Progress Report on Interior Ballistics, No. P-60-7, December 1960.
11. Rohm & Haas Company, Quarterly Progress Report on Interior Ballistics, No. P-60-19, January 27, 1961.
12. Rohm & Haas Company, Quarterly Progress Report on Interior Ballistics, No. P-61-1, June 1961.
13. Rohm & Haas Company, Quarterly Progress Report on Interior Ballistics, No. P-61-7, October 1961.
14. Rohm & Haas Company, Quarterly Progress Report on Interior Ballistics, No. P-61-13, December 1961.

Bibliography, continued

15. Rohm & Haas Company, Quarterly Progress Report on Interior Ballistics, No. P-62-1, August 1962.
16. Rohm & Haas Company, Quarterly Progress Report on Interior Ballistics, No. P-62-22, July 1963.
17. Rohm & Haas Company, Quarterly Progress Report on Interior Ballistics, No. P-63-1, October 1963.
18. Rohm & Haas Company, Quarterly Progress Report on Interior Ballistics, No. P-63-8, January 1964.
19. Rohm & Haas Company, Quarterly Progress Report on A.R.P.A. Projects, No. P-61-21, October 1961.
20. Rohm & Haas Company, Quarterly Progress Report on A.R.P.A. Projects, No. P-61-27, January 1962.
21. Rohm & Haas Company, Quarterly Progress Report on A.R.P.A. Projects, No. P-62-5, April 1962.
22. Rohm & Haas Company, Quarterly Progress Report on A.R.P.A. Projects, No. P-62-12, July 1962.
23. Rohm & Haas Company, Quarterly Progress Report on A.R.P.A. Projects, No. P-62-26, January 1963.
24. Rohm & Haas Company, Quarterly Progress Report on A.R.P.A. Projects, No. P-63-5, April 1963.
25. Rohm & Haas Company, Quarterly Progress Report on A.R.P.A. Projects, No. P-63-19, October 1963.
26. Rohm & Haas Company, Quarterly Progress Report on Engineering Research, No. P-60-17, December 1960.
27. United Technology Center, "High Performance Nozzles for Solid Propellant Rocket Motors," ITR-2025, November 1963.
28. J. H. Perry, ed., "Chemical Engineer's Handbook," 3rd ed., McGraw-Hill, New York (1950).
29. C. E. Lapple, "Fluid and Particle Mechanics," 1st ed., University of Delaware, Newark, Delaware (1954).
30. Sir James Jeans, "An Introduction to the Kinetic Theory of Gases," University Press, Cambridge (1948).
31. J. O. Hirschfelder, C. F. Curtiss, and R. B. Bird, "Molecular Theory of Gases and Liquids," John Wiley & Sons, New York, (1954).

Appendix A

Data Reduction Definitions and Procedures

Typical pressure-time and thrust-time traces are shown in Fig. A-1. While actual oscillograph traces have heavy vertical bars every 100 msec, lighter vertical bars every 10 msec, and a 1000-cycle sine wave to provide 1-msec timing, these extraneous features have been omitted for clarity. Also deleted from the traces is a train of "blips" which indicate cumulative instantaneous pressure-time and thrust-time integrals.

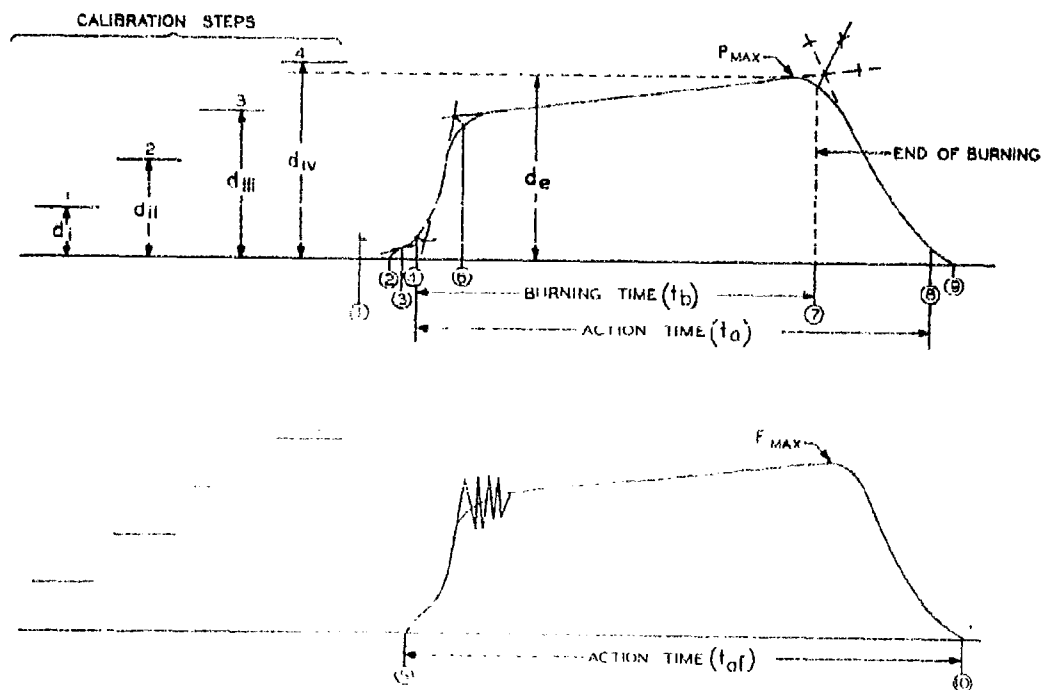


Fig A-1 Typical pressure-time trace (top) and thrust-time trace (bottom).

The following time points in Fig. A-1 are defined as follows:

- t_1 = time of current application to squib
- t_2 = time of initial pressure rise
- t_3 = time when pressure has increased to 100 psia
- t_4 = time when propellant begins to burn
- t_5 = time when thrust begins to rise
- t_6 = time when equilibrium pressure is attained
- t_7 = time of end of burning
- t_8 = time when pressure has decayed to 100 psia
- t_9 = time when pressure has decayed to zero psig
- t_{10} = time when thrust has decayed to zero lbf.

The following definitions and formulas describe the calculations performed from the static-test oscillograph records and from the digital instrumentation to determine ballistic data.

1. Standard Calculations from Oscillograph Traces

$$Z_P(\text{psi/in}) = \text{pressure factor} = \frac{(\text{calibration value of step}) \times (\text{value of pressure gauge, psi})}{(\text{height of step, in}) \times (\text{gauge calibration factor})}$$

$$Z_F(\text{lb/in}) = \text{thrust factor} - \text{obtained in the same way as } Z_P.$$

Interpolation between two calibration steps is as follows (see Fig. A-1):

$$Z = Z_3 + \frac{(d_e - d_{iii})(Z_4 - Z_3)}{(d_{iv} - d_{iii})}$$

(NOTE: Numerical subscripts and integral limits are abbreviated designations of times shown in Fig. A-1. Thus F_3 is the instantaneous thrust at t_3)

$$\text{Ignition Delay(msec)} = t_3 - t_1$$

$$t_{eq}(\text{msec}) = \text{equilibrium pressure time} = t_7 - t_6$$

$$t_b(\text{sec}) = \text{burning time} = t_7 - t_3$$

$$r_b(\text{in/sec}) = \text{average burning rate over burning time} = \frac{\text{web (in)} \times 1000}{t_b(\text{msec})}$$

$$t_{ap} \text{ (msec)} = \text{pressure action time} = t_0 - t_3$$

$$t_{af} \text{ (msec)} = \text{thrust action time} = t_{10} - t_5$$

$$\bar{r}_a \text{ (in/sec)} = \text{average burning rate over action time} = \frac{\text{web (in)} \times 1000}{t_{af} \text{ (msec)}}$$

$$P_{ig} \text{ (psia)} = \text{ignition pressure} = P_{ig} \text{ (in)} \times Z_P \text{ (psi/in)} + 14.4^1$$

$$P_{max} \text{ (psia)} = \text{maximum pressure} = P_{max} \text{ (in)} \times Z_P \text{ (psi/in)} + 14.4$$

$$F_{max} \text{ (lbf)} = \text{maximum thrust} = F_{max} \text{ (in)} \times Z_F \text{ (lbf/in)}$$

¹Average atmospheric pressure at test facility.

2. Special Calculations from Oscillograph Traces

If digital data are not obtained or are unsatisfactory, the areas under the pressure-time and thrust-time traces are manually integrated with a planimeter and the following calculations are performed.

$$Z_t \text{ (msec/in)} = \text{time factor}$$

$$= \frac{\text{total number of 1-msec timing marks in an interval}}{\text{length of the interval (in)}}$$

$$\bar{P}_{eq} \text{ (psia)} = \text{equilibrium pressure}$$

$$= \frac{\int_6^7 P dt \text{ (in}^2) \times Z_t \text{ (msec/in)} \times Z_P \text{ (psi/in)}}{(t_7 - t_6) \text{ (msec)}} + 14.4$$

$$\bar{P}_b \text{ (psia)} = \text{average pressure over burning time}$$

$$= \frac{\int_2^7 P dt \text{ (in}^2) \times Z_t \text{ (msec/in)} \times Z_P \text{ (psi/in)}}{(t_7 - t_2) \text{ (msec)}} + 14.4$$

$$\bar{P}_a \text{ (psia)} = \text{average pressure over action time}$$

$$= \frac{\int_3^8 P dt \text{ (in}^2) \times Z_t \text{ (msec/in)} \times Z_P \text{ (psi/in)}}{(t_8 - t_3) \text{ (msec)}} + 14.4$$

$$\int P_{\text{total}} dt \text{ (psia-sec)} = \text{total pressure-time integral}$$

$$= \frac{\int_0^{t_2} P dt \text{ (in}^2) \times Z_t \text{ (msec/in)} \times Z_P \text{ (psi/in)} + 14.4 \times (t_2 - t_1) \text{ (msec)}}{1000}$$

$$\int F dt \text{ (lbf-sec)} = \text{thrust-time integral}$$

$$= \frac{\int_0^{t_2} F dt \text{ (in}^2) \times Z_t \text{ (msec/in)} \times Z_F \text{ (lbf/in)}}{1000}$$

$$F_a \text{ (lbf)} = \text{average thrust over action time} = \frac{\int_0^{t_2} F dt \text{ (lbf-sec)}}{(t_2 - t_1) \text{ (msec)}} \times 1000$$

3. Calculations from Digital Integrals

3.1 Calculation of Total Integrals

The following data are printed out from the Dymec digital instrumentation system for both pressure and thrust channels:

Zero (baseline), counts/sec

All calibration steps, counts/sec

Gross integral, counts

Gate-open time, sec

The following calculations are made using these data:

Net full scale (c/sec) = gross full scale (c/sec) - zero (c/sec)

Base area (counts) = gate open time (counts) \times zero (c/sec)

Net integral (counts) = gross integral - base area

Top-step pressure value (psi)

$$= \frac{(\text{calibration value of top step}) \times (\text{value of pressure gauge, psi})}{\text{gauge calibration factor}}$$

Top-step thrust value (lbf)

$$= \frac{(\text{calibration value of top step}) \times (\text{value of thrust gauge, psi})}{\text{gauge calibration factor}}$$

$$\int F dt \text{ (lbf-sec)} = \text{thrust-time integral}$$

$$= \frac{(\text{top-step thrust value, lbf}) \times (\text{net integral, counts})}{(\text{net full scale, c/sec})}$$

$$\int P_{\text{total}} dt \text{ (psia-sec)} = \text{total pressure-time integral}$$

$$= \frac{(\text{top-step pressure value, psia}) \times (\text{net integral, counts})}{(\text{net full scale, c/sec})}$$

$$+ 14.4 \times (\text{gate open time, sec})$$

3.2 Calculation of \bar{P}_{eq} , \bar{P}_{b} , and \bar{P}_{a}

$$\bar{P}_{\text{eq}} \text{ (psia)} = \text{equilibrium pressure} = \frac{\int_{t_6}^{t_7} P dt \text{ (psi-sec)}}{(t_7 - t_6) \text{ (sec)}} + 14.4$$

$$\bar{P}_{\text{b}} \text{ (psia)} = \text{average pressure over burning time} = \frac{\int_{t_3}^{t_7} P dt \text{ (psi-sec)}}{(t_7 - t_3) \text{ (sec)}} + 14.4$$

$$\bar{P}_{\text{a}} \text{ (psia)} = \text{average pressure over action time} = \frac{\int_{t_2}^{t_8} P dt \text{ (psi-sec)}}{(t_8 - t_2) \text{ (sec)}} + 14.4$$

The respective pressure-time integrals required to calculate \bar{P}_{eq} , \bar{P}_{b} , and \bar{P}_{a} are determined in a manner completely analogous to that outlined for determining the total pressure-time integral. However, the respective gross integrals in counts are not printed out and must be determined by counting "blips" representing the instantaneous cumulative integral. These blips, generated by the digital instrumentation, are visually displayed on the oscillograph traces in groups of 5, 50, and 500. Each blip is equivalent to two counts. Also, the respective proper time intervals in sec ($t_7 - t_6$, $t_7 - t_3$, $t_8 - t_2$) must be used in place of gate-open time.

4. Subsequent Calculations

$K_m = S_m / \bar{A}_T$, where S_m is an integral average surface area and \bar{A}_T is the arithmetic average of throat area before and after firing. Throat diameter after firing is measured before any accumulated deposit is removed.

XR = Nozzle expansion ratio = $(\bar{D}_E / \bar{D}_T)^2$, where \bar{D}_T and \bar{D}_E are the respective arithmetic average values of nozzle throat diameter before and after firing and nozzle exit diameter before and after firing.

$$C_D \text{ (lbm/lbf-sec)} = \text{Discharge coefficient} = \frac{\text{charge weight (lbm)}}{A_T \times \int_{\text{total}} P dt}$$

Charge weight is the difference between weight before firing (before inhibitor is applied) and weight after firing.

C_{D_o} = Discharge coefficient corrected for pressure drop along the length of the grain = $C_D (P_h / P_c)$, where P_h is the head-end pressure and P_c is the stagnation pressure at the entrance to the converging section of the nozzle.

Calculate J_o (initial ratio of throat area to port area) and from Fig. A-2 find the corresponding Mach number (M_{LO}). Calculate J_F (final J) and from Fig. A-2 find M_{LF} . Calculate an average M_L by means of the following formula.

$$M_L = 0.03 (M_{LO}^2 - M_{LF}^2) + 0.5 (M_{LO} + M_{LF})$$

where M_L is the Mach number at the end of the grain, and the subscripts "O" and "F" again refer to initial and final conditions, respectively.

From Fig. A-3 find the value of P_h / P_c corresponding to M_L and substitute in the formula for C_{D_o} .

$$S_m = \frac{\int_{x=0}^{x=\text{web}} S dx}{\text{web}}, \text{ where } S = \text{surface area (in}^2\text{) and web = burning distance (in). For cylindrical grains, } S_m = \frac{\text{Grain volume (in}^3\text{)}}{\text{web (in)}}$$

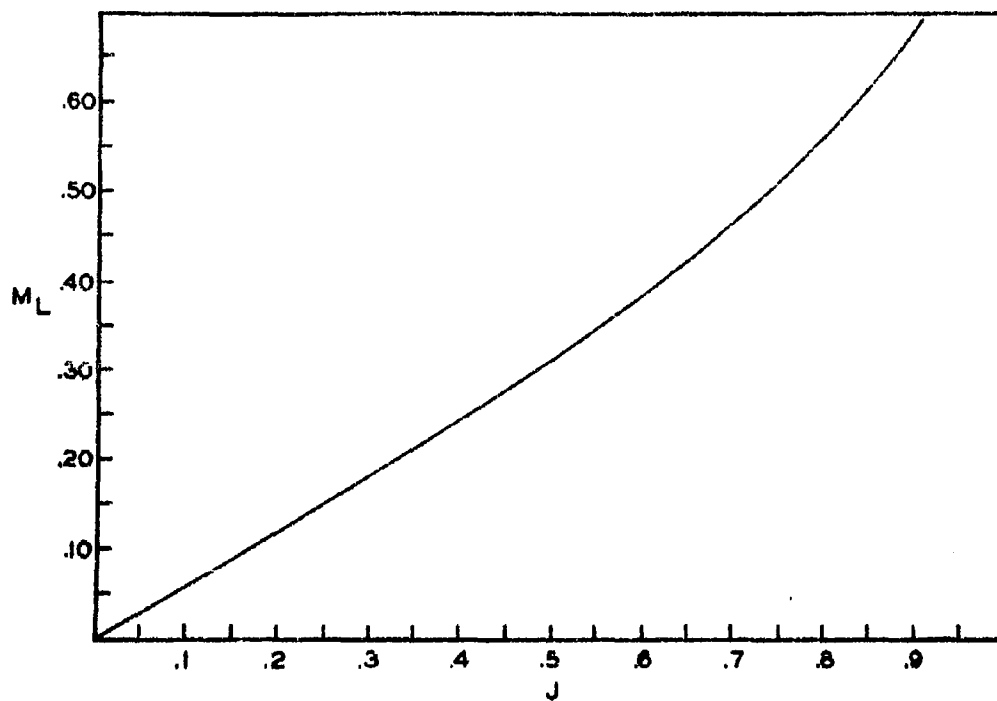


Fig. A-2 Mach number as a function of J for $\gamma=1.2$.

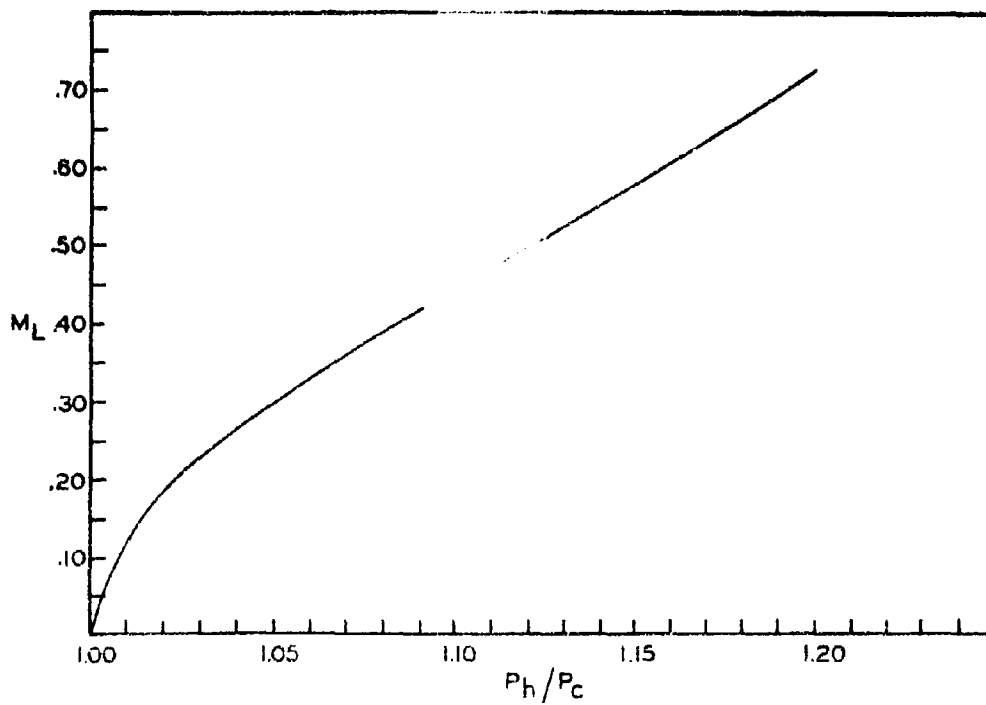


Fig. A-3 M_L as a function of P_h/P_c .

$$c^* \text{ (ft/sec)} = \text{characteristic exhaust velocity} = \frac{32.16 \text{ (ft-lbm/lbf-sec}^2\text{)}}{C_{D_0} \text{ (lbm/lbf-sec)}}$$

$$I_{\text{spd}} \text{ (lbf-sec/lbm)} = \text{delivered specific impulse} = \frac{\int F dt \text{ (lbf-sec)}}{\text{charge wt. (lbm)}}$$

$$\dot{m} \text{ (lbm/sec)} = \text{mass discharge rate} = \frac{\text{charge wt. (lbm)} \times 1000}{t_{\text{af}} \text{ (msec)}}$$

$$C_F = \text{measured thrust coefficient} = I_{\text{spd}} \text{ (lbf-sec/lbm)} \times C_{D_0} \text{ (lbm/lbf-sec)}$$

$$C_{F_{1000}} = \text{corrected thrust coefficient} = F_{1000}^0 \text{ (lbf-sec/lbm)} \times C_{D_0} \text{ (lbm/lbf-sec)}$$

F_{1000}^0 = specific impulse corrected to 1000 psia chamber pressure, optimum expansion ratio at sea level atmospheric pressure (14.7 psia), and 0° nozzle exit divergence angle.

$$= I_{\text{spd}} \left[\frac{C_F \text{ (std)}}{C_F \text{ (test)}} \right]$$

$C_F \text{ (std)}$ is a function only of specific heat ratio (γ) and is taken from a table of such values.

$C_F \text{ (test)}$ is calculated from the relationship

$$C_F \text{ (test)} = \lambda C_F \text{ (vac)} + (1 - \lambda) \left(\frac{P_e}{P_a} \right) XR - \left(\frac{P_{\text{atm}}}{P_a} \right) XR$$

where $C_F \text{ (vac)}$ and P_e/\bar{P}_a are functions only of γ and XR (nozzle expansion ratio) and are obtained from tables of such values; P_{atm} is the average atmospheric pressure at which the firing is made (14.4 psia at Huntsville, Alabama); \bar{P}_a is the actual motor average pressure over the action time, and λ is the nozzle divergence angle correction factor defined by

$$\lambda = \frac{1}{2} (1 + \cos \beta)$$

where β is the divergence half-angle at the nozzle exit.

$I_{sp}^1 = F_{1000}^0$ when the following additional conditions have been met:

- (a) the trace is neutral within the limits

$$0.90 \leq \frac{P}{P_b} \leq 1.10$$

over the equilibrium portion of the trace,

- (b) $800 \leq \bar{P}_a \leq 1200$

- (c) the tail-off portion of the trace is limited by the following:

$$t_b \geq 0.87 t_{ap}$$

$$\frac{\int P_b dt}{\int P_{total} dt} \geq 0.95$$

$I_{1000}^0 = I_{sp}^0 = F_{1000}^0$ when the following additional conditions have been met:

- (a) $900 \leq \bar{P}_a \leq 1100$

- (b) $8 \leq XR \leq 11$

- (c) the record is obtained from a 6C5-11.4 static-test motor.

4. Exceptions for Micro-Motors

Some definitions must be revised to provide additional flexibility for application to micro-motors. The trace time-points are still applicable, but, the location of these points will depend on the shape of the trace to be reduced. Several possible forms of pressure-time traces which may be obtained from micro-motors are shown in Fig. A-4.

The exceptions for micro-motors are outlined below; other data-reduction procedures remain unchanged.

¹JANAF Solid Propellant Rocket Static Test Panel, "Recommended Procedures for the Measurement of Specific Impulse of Solid Propellants," SPJA Publication No. SPSTP/10B, March 1962.

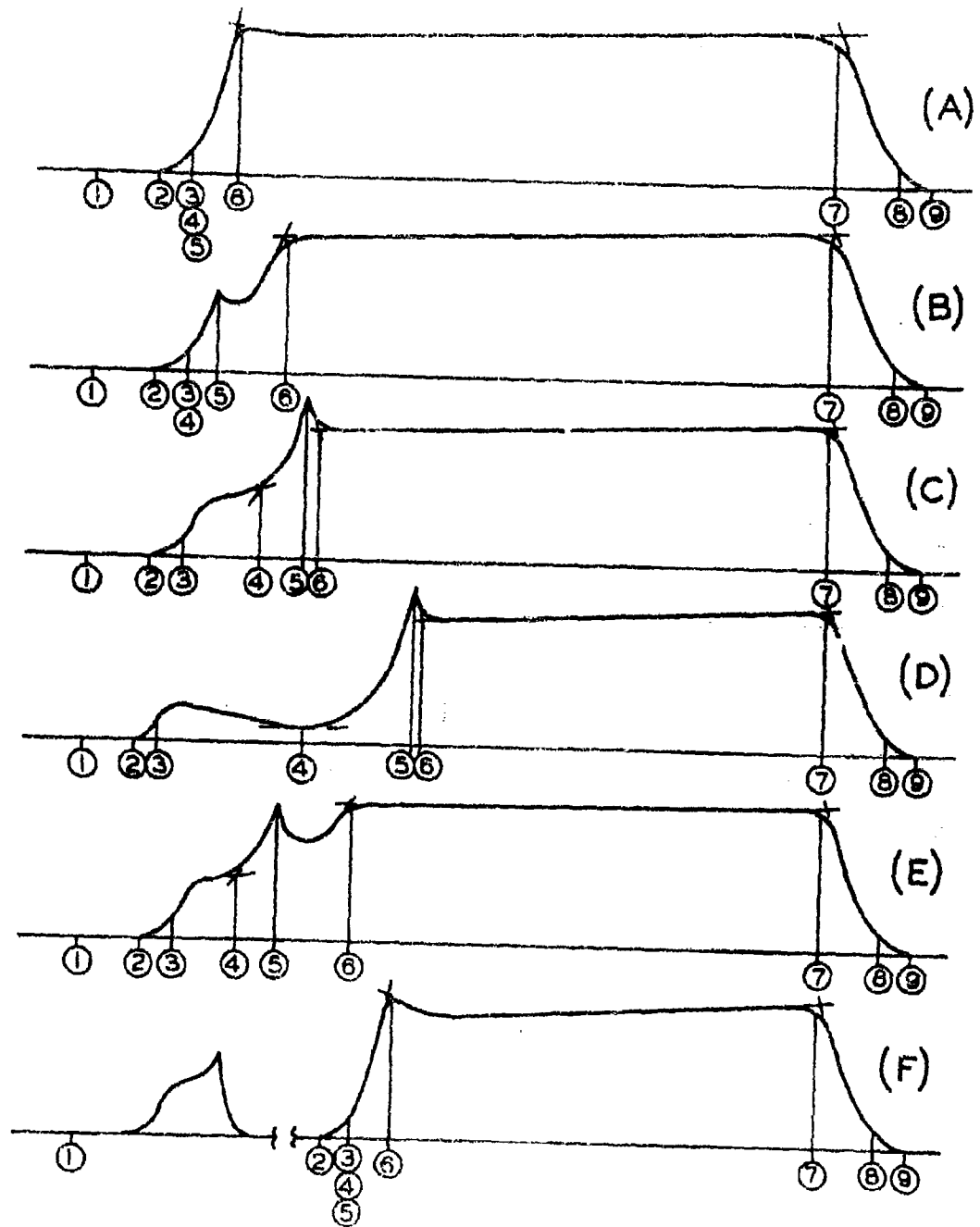


Fig A-4 Typical forms of pressure traces obtained with micro-motors

Parameter	Definition and Comments
Ignition delay time (msec)	$t_2 - t_1$
t_b (msec) = burning time	$t_7 - t_4$ (use for burning rate and P_b calculations)
t_{ap} (msec) = action time	$t_8 - t_5$ (use for P_a calculations)
t_c (msec) = correction time	$t_8 - t_4$ (use for heat loss correction)
\bar{P}_b (psia) = burning-time-average pressure	$\frac{\int_4^7 P dt}{t_7 - t_4} + 14.4$ (use for P-r correlations)
\bar{P}_a (psia) = action-time-average pressure	$\frac{\int_5^8 P dt}{t_8 - t_5} + 14.4$ (use for C_F test calculation)
\bar{P}_{eq} (psia) = equilibrium pressure	$\frac{\int_4^7 P dt}{t_7 - t_4} + 14.4$ (use for P-K correlations)
Integral ratio	$\frac{\int_4^7 P dt}{\int_2^7 P dt}$ (indication of "square" trace)
Rise-time factor	$\frac{t_6 - t_2}{t_7 - t_2}$ (indication of poor ignition)
Decay-time factor	$\frac{t_9 - t_7}{t_9 - t_6}$ (indication of poor ignition and/or off-center mandrel)

Appendix B

Calculation of Velocity Lag in Two-Phase Flow

A digital computer program written in FORTRAN for calculating particle-velocity lags in two-phase flow through nozzles of specified geometry was developed using a simple mathematical model to approximate the flow process. The mathematical model is described and procedures for using the computer program are outlined. A listing of the program and an example problem are given in Appendix C. Source decks for the program are available on request.

1. Mathematical Model

The mathematical model describing two-phase flow through nozzles was obtained from a simplification of a previous study at this Division¹. In this simple model, the combustion and expansion processes were assumed to be adiabatic. Dynamic non-equilibrium effects were determined by treating the particle-velocity lag as a perturbation of a system in which the particles were assumed to be gas-like. The one-dimensional, isentropic expansion of the gas-like system was first determined through the use of an effective specific-heat ratio and an effective gas molecular weight based on a chemical composition frozen at the combustion-chamber conditions. The velocity of the condensed-phase particles, which were assumed to be spherical, was then approximated by calculating the velocity of a single particle introduced into the gas-like system. The coupled effect of the particle lag on the flow of the gas-like system was ignored.

The specific-heat ratio of the gas-like system is given²

¹Rohm & Haas Company, Quarterly Progress Report on Engineering Research, No. P-60-17, December 1960.

²United Technology Center, "High Performance Nozzles for Solid Propellant Rocket Motors," ITR-2025, November 1963.

by

$$\gamma_e = \frac{\gamma_g (1 + z\gamma)}{1 + \gamma_g z\gamma} , \quad \text{B-1}$$

where γ_g is the specific heat ratio of the gas phase in the chamber, z is the ratio of the mass flow rate of the particles to that of the gas, and γ is the ratio of the particle specific heat at constant pressure to that of the gas. The effective molecular weight of the gas-like system is given by

$$M_e = M_g (1 + z) , \quad \text{B-2}$$

where M_g is the molecular weight of the gas in the chamber.

Motion of the particle was assumed to be governed by the differential equation

$$\left[\frac{\pi}{6} D_p^3 \rho_p \right] u_p \frac{du_p}{dx} = \frac{C_D}{2} \rho_g \left[\frac{\pi}{4} D_p^2 \right] \phi (u_g - u_p) |u_g - u_p| \quad \text{B-3}$$

where u_p is the particle velocity, u_g is the velocity of the gas-like system, p_g is the pressure of the gas-like system, x is the distance along the nozzle center line, D_p is the particle diameter, ρ_p is the particle density, ρ_g is the density of the gas-like system, C_D is the drag coefficient, and ϕ is the Cunningham correction for molecular mean-free-path effects. The positive direction is assigned to the direction of flow of the gas-like system.

A least-squares fit to the drag coefficient tabulation for spheres given in Perry¹ was used in the computer program. This expression is

¹J. H. Perry, ed., "Chemical Engineer's Handbook," 3rd ed., McGraw-Hill, New York (1950).

$$\ln C_D = 3.271 - 0.8893 (\ln Re) + 0.03417 (\ln Re)^2 + 0.001443 (\ln Re)^3, \quad B-4$$

$$0.1 \leq Re \leq 2000$$

where the particle Reynolds number is given by

$$Re = \frac{D (u_g - u_p) \rho_g}{\mu_g} \quad B-5$$

The viscosity of the gas-like system, μ_g , was determined as a function of temperature using a mole fraction weighted average of the viscosities of the major gaseous constituents of the combustion products of a typical C-H-O-N-Cl-Al propellant¹. The viscosity so determined is represented by the polynomial

$$\ln(\mu_g \times 10^5) = 0.3757 + 0.8629 \ln \left[\frac{T_g}{1000} \right] - 0.05446 \left[\ln \left(\frac{T_g}{1000} \right) \right]^2, \quad B-6$$

$$1000^\circ R \leq T_g \leq 6500^\circ R,$$

where viscosity is in $\text{lbm-ft}^{-1}\text{-sec}^{-1}$ and T_g is the gas temperature in $^\circ R$.

The Cunningham correction is given by^{2,3}

$$\phi = \frac{1}{1 + \frac{\lambda}{D_p} \left[1.644 + 0.552 \exp(-0.656 D_p / \lambda) \right]} \quad B-7$$

where the units for the particle diameter, D_p , and the mean free path of the gas-like system, λ , must be identical.

The mean free path of the gas-like system was based on a mole fraction weighted average of the gaseous-phase constituents.

¹Rohm & Haas Company, Quarterly Progress Report on Engineering Research, P-60-17, December 1960.

²J. H. Perry, ed., "Chemical Engineer's Handbook," 3rd ed., McGraw-Hill, New York (1950).

³C. E. Lapple, "Fluid and Particle Mechanics," 1st ed., University of Delaware, Newark, Delaware (1954).

The mean free path so determined is given by^{1,2}

$$\lambda = 1.025 \times 10^{-6} \frac{T_g}{P_g} ,$$

B-8

where mean free path is in ft, temperature T_g is in °R, and pressure P_g is in lbf-ft⁻².

The nozzle geometry employed in this analysis is shown in Fig. B-1. The nozzle is composed of a conical converging section having an inlet diameter D_o and a half-angle α , a rounded throat section having a radius of curvature R and a throat diameter D_t , and a conical diverging section having a half-angle β and an exit diameter D_e . The coordinates of several reference points in the nozzle are shown in parentheses. Similar nomenclature is used to describe the nozzle in the computer program.

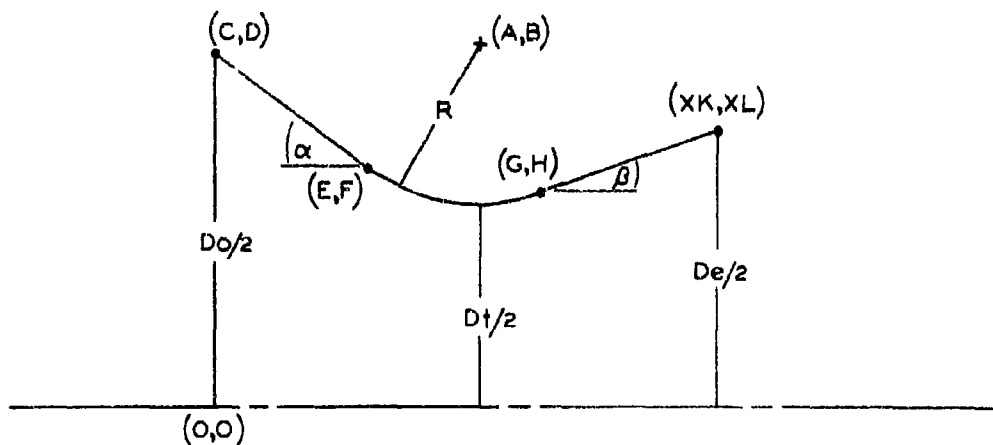


Fig. B-1 Nozzle geometry.

¹Sir James Jeans, "An Introduction to the Kinetic Theory of Gases," University Press, Cambridge (1948).

²J. O. Hirschfelder, C. F. Curtiss, and R. B. Bird, "Molecular Theory of Gases and Liquids," Wiley, New York (1954).

2. Computer Program

Solutions to Eq. B-3 were obtained by numerical integration using a Runge-Kutta method. The space in the conical converging section was divided into unequal increments using a weighted Mach number increment to provide smooth starting for the integration. The space in the rounded converging section was similarly divided. The space in the rounded diverging section was divided into unequal increments such that the area ratio at each successive interval increased by 0.05. The space in the conical diverging section was similarly divided, except that the area ratio at each successive interval increased by 0.25.

The units of the input data for the computer program are those commonly employed in internal ballistics; the computer program converts the data to an internally consistent set for calculation. The data required by the computer program are described below.

<u>Mnemonic Symbol</u>	<u>Description</u>
DZERO	Nozzle inlet diameter, in.
R	Throat radius of curvature, in.
ALPHA	Converging section half-angle, degrees
BETA	Diverging section half-angle, degrees
GAMMA	Effective specific heat ratio (Eq. B-1)
TZERO	Chamber temperature, °K
PZERO	Chamber pressure, psia
XMW	Effective molecular weight (Eq. B-2)
CINTV	Number of integration intervals in conical converging section (usually 20)
XR	Expansion ratio at exit plane
DP	Particle diameter, microns
DT	Throat diameter, in.

The output format consists of a heading, a listing of the data, and a tabulation giving the particle velocity in ft-sec^{-1} , the local expansion ratio, and the relative velocity lag $(u_g - u_p)/u_g$ as a function of the distance in inches from the nozzle inlet.

Appendix C

FORTRAN Program for the Calculation of Velocity Lag

```

00000 * VELOCITY LAG IN TWO PHASE FLOW
00000 C
00000 C PROGRAMMED BY L. E. STONECYPHER
00000 C ROHM AND HAAS COMPANY
00000 C HUNTSVILLE, ALABAMA
00000 C
00001 C
00001 C COMMON ETA1, ETA2, ETA3, ETA4, ETA5, ETA6, ETA7,
00001 C 2 ETAB, TZERO, RHOZE, DP, FNCM1, ROOT, ITESI, UGAS,
00001 C 2 XMACH, HMACH, YMACH, X1, X2, Y1, Y2, XXR, YXR, XUP
00001 1 READ2,DZERO,R,ALPHA,BETA,GAMMA,TZERO,PZERO,
00001 2XMW,CINTV,XR,DP,DT
00034 2 FORMAT (5E14.8)
00043 S1 = DZERO
00047 S2 = R
00053 S3 = ALPHA
00057 S4 = BETA
00063 S5 = GAMMA
00067 S6 = TZERO
00073 S7 = PZERO
00077 S8 = XMW
00103 DZERO = DZERO/12.0
00111 R = R/12.0
00117 ALPHA = ALPHA/57.29578
00125 BETA = BETA/57.29578
00133 TZERO = TZERO*1.8
00141 PZERO = PZERO*144.0
00147 3 PRINT4,S1,S2,S3,S4,S5,S6,S7,S8
00172 4 FORMAT(1H120X25H VELOCITY LAG CALCULATION ///
00172 2 4H DZERO = F9.5, 6X5H R = F9.5, 2X9H ALPHA = F9.5,
00172 2 4X8H BETA = F9.5 / 9H GAMMA = F9.5, 2X9H TZERO = F9.2,
00172 2 2X9H PZERO = F9.2, 6X6H MW = F9.5)
00356 S9 = DT
00362 S10 = DP
00366 DT = DT/12.0
00374 DP = DP*3.281/100000.0
00404 PRINT7,CINTV,XR,S10,S9
00417 7 FORMAT(1X8HCINTV = F9.1, 6X5HXR = F9.5, 6X5HDP = F9.5,
00417 27X5HDT = F9.5 //)
00470 C PERFORM PRECOMPUTATIONS
00470 RHOP = 3.97*62.4
00476 PI = 3.1415927
00507 RHOZE = (PZERO*XMW)/(TZERO*1546.0)
00520 ETA1 = 2.0/(GAMMA + 1.0)
00534 ETA2 = (GAMMA - 1.0)/(GAMMA + 1.0)
00552 ETA3 = (GAMMA + 1.0)/(2.0 * (GAMMA - 1.0))
00572 ETA4 = ETA3 - 1.0
00588 ETA5 = (GAMMA - 1.0)/2.0
00610 ETA6 = 1.0/(GAMMA - 1.0)
00624 ETA7 = (1546.0*32.17/XMW)*2.0*GAMMA*ETA6
00642 ETAB = 3.0/(4.0*DP*RHOP)
00660 C CALCULATE NOZZLE PARAMETERS
00660 CALFA = COS(ALPHA)
00666 SALFA = SIN(ALPHA)
00674 TALFA = SALFA/CALFA

```

Best Available Copy

```

00762 CBETA = COS(BETA)
00710 SBETA = SIN(BETA)
00716 TBETA = SBETA/CBETA
00724 A = (DZERO - DT + 2.0 * R * (1.0 / CALFA - 1.0)) /
00724 2 (2.0 * TALFA)
00764 R = R + DT / 2.0
00774 E = A - R * SALFA
01005 F = B - R * CALFA
01016 G = A + R * SBETA
01026 H = B - R * CBETA
01037 XL = (DT/2.0)*SORT(XR)
01055 XK = G + (XL - H)/TBETA
01067 C CALCULATE AREA RATIOS
01067 AREAU = (PI/4.0)*DZERO**2
01113 AREAF = PI*F**2
01131 AREAT = (PI/4.0)*DT**2
01155 AREAH = PI*H**2
01173 AREAL=PI*XL**2
01211 XRO = AREAU/AREAT
01217 XRF = AREAF/AREAT
01225 XRH = AREAH/AREAT
01253 XRL = XR
01237 GO TO 45
01241 C SET UP PRINT FOR ERROR WHEN MACH SUBROUTINE ITERATION
01241 C COUNTER IS EXCEEDED. THEN TEST FOR NEW PROBLEM
01241 8 PRINT9
01244 9 FORMAT(26H ITERATION COUNTER EXCEEDED)
01267 GO TO 44
01271 C BEGIN CALCULATIONS IN CONVERGING SECTION OF NOZZLE
01271 45 ITEST = 1
01275 GUESS = 0.01
01301 CALL MACH(GUESS, XRO)
01306 IF(ROOT-1.)46,46,46
01316 46 PRINT47
01321 47 FORMAT(1X17HCONVERGENCE ERROR)
01340 GO TO 44
01342 48 IF(ITEST)8,8,10
01350 10 OMACH = ROOT
01354 CALL MACH(GUESS, XRF)
01361 IF(ROOT-1.0)49,44,46
01371 49 IF(ITEST)8,8,11
01377 11 FMACH = ROOT
01403 C CALCULATE WEIGHTED INCREMENT SIZE IN CONVERGING SECTION
01403 DELX=CINTV*(CINTV+1.)/2.
01415 DELM1*(FMACH-OMACH)/DELX
01425 DELM2*(1.-FMACH)/DELX
01435 C PREFIX X DENOTES PRESENT PARTICLE LOCATION, PREFIX Y
01435 C DENOTES INCREMENTED LOCATION, PREFIX M DENOTES MID
01435 C POINT OF X-Y INTERVAL. SUFFIX 1 AND 2 CORRESPOND TO
01435 C X AND Y POSITIONS, RESPECTIVELY.
01435 C SET DATA FOR INITIAL LOCATION
01435 X1 = 0.0
01441 Y1 = DZERO/2.0
01447 XXR = XRO
01453 XMACH = OMACH
01457 MM = 1

```

Best Available Copy

```

01463 C CALCULATE AND PRINT FIRST LINE
01463 TERM = 1.0 + ETA5 * OMACH ** 2
01503 TEMP = TZERO/TERM
01511 UGAS = SORT(ETA7*(TZERO-TEMP))
01527 DELTA = 0.001
01533 XJP = 0.999*UGAS
01541 PRINT12,X1,XUP,XXR,DELTA
01554 12 FORMAT(20X1HX,10X2HUP,10X2HXR,9X5HDELTA/18X5H(IN.),7X5H(FPS)/17XF6
01554 2.3,F12.1, F12.3, F12.5 )
01630 C BEGIN DO LOOP FOR CONVERGING SECTION
01630 L=CINTV
01635 13 DO 24 I=1,L
01641 XI = I
01646 GO TO (14,15),MM
01654 14 YHACH = XMACH + DELH1*XI
01664 GO TO 16
01666 15 YHACH = XMACH + DELH2*XI
01676 16 AREA2 = (AREAT/YHACH)*(ETA1+ETA2*YHACH**2)
01735 2**ETA3
01735 Y2 = SORT(AREA2/P1)
01781 GO TO (17,18),MM
01787 17 X2 = X1 + (Y1 - Y2)/TALFA
01771 GO TO 19
01773 18 X2=A-SORT(ABS(R**2-(B-Y2)**2))
02053 19 YXR = AREA2/AREAT
02061 HX = (X2 - X1)/2.0 + X1
02073 GO TO (20,21),MM
02101 20 HY = Y1 - TALFA*(HX - X1)
02114 GO TO 22
02116 21 HY = B - SORT(R**2-(A-HX)**2)
02170 22 HXR = (PI*HY**2)/AREAT
02210 GUESS=XMACH
02214 CALL WACH(GUESS,HXR)
02221 IF(ROOT-1.0)/50,46,46
02231 30 IF(ITEST)8,8,23
02237 23 MMACH = ROOT
02243 C USE SUBROUTINE TO CALCULATE UP AT Y AND PRINT RESULTS
02243 CALL FINAL
02246 24 CONTINUE
02253 C END OF CONVERGING SECTION DO LOOP
02253 IF(MM-1)25,25,26
02263 25 MM = MM + 1
02271 GO TO 13
02273 C TWO AREA INCREMENT SIZES ARE USED IN DIVERGING
02273 SECTION OF NOZZLE
02273 26 XN = (XRH - 1.0)/0.25 + 1.0
02309 XRN = (XRC - 1.0)/0.25 - XN
02317 N = XN
02324 NN = 5 * N
02332 MM = 1
02336 27 DO 30 J=1,NN
02342 GO TO(28,29,30),MM
02351 28 YXR = XXR + 0.05
02357 GO TO 30
02361 29 YXR = XXR + 0.25
02367 30 Y2 = SORT(YXR*AREAT/P1)

```

Best Available Copy

```

02405      GUESS = XMACH + 0.01
02413      CALL MACH(GUESS, YXR)
02420      IF(1.0-ROOT)51,46.46
02430 51    IF(ITEST)8,8.31
02436 31    YHACH = ROOT
02442      IF(Y2 - H)32,32.33
02452 32    X2 = A + SQRT(H**2 - (B - Y2)**2)
02453      GO TO 34
02455 33    Y2 = G + (Y2 - H)/TBETA
02457 34    HX = (Y2 - Y1)/2.0 + X1
02459      IF(HY - G)35,36.36
02461 35    HY = B - SQRT(R**2 - (A-HX)**2)
02463      GO TO 37
02465 36    HY = H + TBETA * (HX - G)
02467 37    HXR = (PI*HY**2)/AREAT
02467      GUESS=(XMACH+YHACH)/2.0
02477      CALL MACH(GUESS, HXR)
02704      IF(1.0-ROOT)52,46.46
02714 52    IF(ITEST)8,8.38
02722 38    HMACH = ROOT
02726      CALL FINAL
02731 39    CONTINUE
02736 C    END OF DIVERGING SECTION DO LOOP
02736      IF(HH-2)40,60.44
02746 40    NN = NN + 1
02754      NN = XNN
02761      GO TO 27
02763 60    MM=MM+1
02771      YXR=XR
02775      NN=1
03001      GO TO 27
03003 44    GO TO 1
03005 *    END

```

Best Available Copy

Final Subroutine

```

00000 *   FINAL SUBROUTINE
00001   SUBROUTINE FINAL
00001   COMMON ETA1, ETA2, ETA3, ETA4, ETA5, ETA6, ETA7, ETAB,
00001   2 YZERO, RHOZE, DP, FNCN1, ROOT, ITEST, UGAS, XMACH,
00001   2 HMACH, YMACH, X1, X2, Y1, Y2, XXR, YXR, XUP
00001 C   BEGIN RUNGE - KUTTA INTEGRATION PROCEDURE
00001   CALL FNCN(XMACH, XUP)
00006   C1 = (X2 - X1)*FNCN1
00016   ARG1=C1*XUP**2
00034   IF(ARG1)200,203,203
00042 203   HUP = SQRT(C1*XUP**2)
00066   CALL FNCN(HMACH, HUP)
00073   C2 = (X2 - X1)*FNCN1
00103   ARG2=4.0*C2-2.0*C1*XUP**2
00137   IF(ARG2)200,204,204
00145 204   YUP1=SQRT(2.0*(2.0*C2-C1)*XUP**2)
00203   CALL FNCN(YMACH, YUP1)
00210   C3 = (X2 - X1)*FNCN1
00220   ARG3=XUP**2*(C1+4.0*C2+C3)/3.0
00252   IF(ARG3)200,205,205
00260 205   YUP=SQRT(XUP**2+(C1+4.0*C2+C3)/3.0)
00320 C   END OF INTEGRATION PROCEDURE. CHECK FOR UP GREATER THAN UC
00320   IF(UGAS - YUP)200,200,201
00330 200   YUP = 0.999* UGAS
00336 201   DELTA = (UGAS - YUP)/UGAS
00346   XP = X2+12.0
00354 C   PRINT FROM Y LINE. NOTE X UNIT CHANGE FOR PRINT
00354   PRINT202,XP,YUP,YXR,DELTA
00367 202   FORMAT(17XF6.3, F12.1, F12.3, F12.5)
00410 C   DATA TRANSFER FROM Y LINE TO X LINE
00410   X1 = X2
00414   Y1 = Y2
00420   XUP = YUP
00424   XXR = YXR
00430   XMACH = YMACH
00434   RETURN
00440 *   END

```

Best Available Copy

Function Subroutine

```

00000 *   FUNCTION SUBROUTINE
00001   SUBROUTINE FNCN(XMOCK, UP)
00001   COMMON ETA1, ETA2, ETA3, ETA4, ETA5, ETA6, ETA7,
00001   2 ETA8, TZERO, RHOZE, DP, FNCN1, ROOY, ITEST, UGAS,
00001   2 XMACH, HMACH, YMACH, X1, X2, Y1, Y2, XXR, YXR, XUP
00001 C   EVALUATE RUNGE - KUTTA FUNCTION IN EQ 3
00001   TERM = 1.0 + ETA5 * XMOCK **2
00030   TEMP = TZERO/TERM
00036   RHO = RHOZE/TERM**ETA6
00053   UGAS = SQRT(ETA7*(TZERO - TEMP))
00071   TERM1=ELOG(TEMP/1000.)
00105   XMU = EXP(0.3757 * 0.8629 * TERM1 - 0.05446)
00105   2 TERM1**2)/100000.0
00146   XLAMB = 2.052/(RHO*1.0E08)
00162   RATIO = XLAMB/DP
00170   PHI = 1.0/(1.0 + RATIO*(1.644 + 0.552 * EXP(-0.656
00170   2 /RATIO)))
00223   RE = ABS(DP*(UGAS - UP)*RHO/XMU)
00250   RELOG=ELOG(RE)
00256   DRAG = EXP(3.271 - 0.8893 * RELOG + 0.03417 *
00256   2 RELOG **2 + 0.001443 * RELOG **3)
00334   FNCN1 = ETA8 * DRAG * RHO *(UGAS - UP) * PHI *
00334   2 ABS(UGAS - UP)
00402   RETURN
00406 *   END

```

Best Available Copy

Mach Subroutine

```

00000 *      MACH SUBROUTINE
00001 SUBROUTINE MACH(ROOT1, RATIO)
00001 COMMON ETA1, ETA2, ETA3, ETA4, ETA5, ETA6, ETA7,
00001 2 ETA8, TZERO, RHOZE, DP, FNCN1, HOOT, ITEST, UGAS,
00001 2 XMACH, MMACH, YMACH, X1, X2, Y1, Y2, XXR, YXR, XUP
00001 C      CALCULATE MACH NUMBER
00001 K = 1
00005 100 TERM = (ETA1 + ETA2 * ROOT1 **2)
00034 TERM1 = TERM**ETA3
00043 ROOT = ROOT1 - (RATIO - TERM1/ROOT1)/(TERM1 /
00043 2 ROOT1 **2 - TERM**ETA4)
00133 C      TEST FOR CONVERGENCE TO REQUIRED ACCURACY
00133 IF(ABS(ROOT - HOOT1) - 0.0001)101,101,102
00156 101 RETURN
00162 102 ROOT1 = ROOT
00171 K = K + 1
00177 C      RETURN TO PROGRAM IF ITERATIONS EXCEED 100
00177 IF(100 - K)103,100,100
00207 103 ITEST = -1
00214 GO TO 101
00216 *      END

```

Best Available Copy

Example Problem

VELOCITY LAG CALCULATION

UZERO = 1.22143 R = 0.03000 ALPHA = 45.00000 BETA = 15.00000
 GAMMA = 1.17300 TZERO = 3705.62 PZERO = 1000.00 MW = 30.94359
 CINTV = 20.0 XR = 9.41311 DP = 1.00000 DT = 0.50000

X (IN.)	UP (FPS)	XR	DELTA
0.000	354.1	5.971	0.00100
0.009	357.6	5.796	0.02096
0.025	373.3	5.475	0.03540
0.048	402.5	5.056	0.04054
0.075	441.5	4.589	0.04611
0.103	489.7	4.117	0.05276
0.132	546.9	3.668	0.06016
0.159	612.6	3.259	0.06842
0.185	686.3	2.894	0.07749
0.209	767.5	2.575	0.08739
0.231	855.6	2.301	0.09810
0.251	949.0	2.066	0.10962
0.269	1049.7	1.865	0.12191
0.285	1154.1	1.695	0.13496
0.299	1262.4	1.551	0.14880
0.312	1373.4	1.429	0.16349
0.322	1485.9	1.327	0.17912
0.332	1598.5	1.242	0.19585
0.340	1709.4	1.172	0.21391
0.347	1816.2	1.115	0.23364
0.352	1916.0	1.071	0.25547
0.352	1917.9	1.070	0.25591
0.352	1921.0	1.069	0.25679
0.352	1927.3	1.067	0.25807
0.353	1935.1	1.064	0.25970
0.353	1945.0	1.060	0.26163
0.354	1957.1	1.056	0.26378
0.354	1971.6	1.052	0.26609
0.355	1988.7	1.047	0.26849
0.356	2008.4	1.042	0.27091
0.357	2031.0	1.037	0.27329
0.358	2056.4	1.031	0.27557
0.359	2084.8	1.024	0.27771
0.361	2116.3	1.021	0.27968
0.362	2150.8	1.016	0.28148
0.364	2188.3	1.011	0.28310
0.366	2228.8	1.007	0.28454
0.367	2272.2	1.004	0.28584
0.369	2318.3	1.002	0.28703
0.371	2367.0	1.000	0.28815
0.373	2414.6	1.000	0.28925
0.380	3058.1	1.056	0.29067
0.422	3448.6	1.100	0.29214
0.444	3743.8	1.150	0.29365
0.466	3980.4	1.200	0.29525
0.487	4177.9	1.250	0.29691
0.587	4466.4	1.500	0.29837
0.678	5293.1	1.750	0.29954
0.763	5606.2	2.000	0.29953
0.843	5852.4	2.250	0.29899
0.919	6054.3	2.500	0.29865
0.991	6224.4	2.750	0.29847
1.060	6370.9	3.000	0.29848
1.126	6498.0	3.250	0.29828
1.189	6612.3	3.500	0.29891
1.251	6713.6	3.750	0.29768
1.310	6805.4	4.000	0.29612
1.367	6888.8	4.250	0.29456
1.423	6964.8	4.500	0.29313
1.477	7034.9	4.750	0.29203
1.530	7099.6	5.000	0.29196
1.582	7153.7	5.250	0.29200
1.632	7215.8	5.500	0.29214
1.681	7268.1	5.750	0.29236
1.729	7317.3	6.000	0.29265
1.776	7363.5	6.250	0.29281
1.823	7407.0	6.500	0.29243
1.868	7448.7	6.750	0.29259
1.912	7487.3	7.000	0.29241
1.955	7524.1	7.250	0.29249
1.999	7559.4	7.500	0.29256
2.041	7593.9	7.750	0.29248
2.083	7627.9	8.000	0.29218
2.124	7661.4	8.250	0.29252
2.164	7684.6	8.500	0.29223
2.204	7710.6	8.750	0.29297
2.243	7739.5	9.000	0.29272
2.281	7765.3	9.250	0.29249
2.319	7791.1	9.500	0.29256

Best Available Copy

Appendix D
Velocity Lag Curves for RH-P-112 Propellant

Curves of Δ versus nozzle throat diameter for particle diameter (N) values of 0.5, 1.0, 1.5, and 2.0 μ and nozzle expansion ratio (XR) values of 6, 8, 10, and 12 are shown in Figs. D-1 through D-6 for the Rohm & Haas .75C.50, 2C1.5, and 6C5 motor nozzles; for the USAF BATES motor nozzles; and for the Aerojet 10KS-2500 motor nozzles. These curves were generated using the FORTRAN program described in Appendices B and C. The thermodynamic input parameters used were those determined for RH-P-112 propellant (GAMMA = 1.141, TZERO = 3389°K, XMW = 27.452). The parameter PZERO = 1000 psia was used in all cases. The nozzle configuration parameters used are listed in Table D-I.

Table D-I
Nozzle Configuration Parameters

<u>Motor</u>	<u>.75C.50</u>	<u>2C1.5</u>	<u>6C5</u>	<u>BATES</u>	<u>10KS-2500¹</u>
DZERO	0.75	2.00	6.00	11.73	7.125
R	0.4375	1.167	3.50	3.00	4.0
ALPHA	45	45	45	45	30
BETA	15	15	15	15	15

¹Estimated from non-dimensioned drawings.

1

NOZZLE TROAT DIAMETER - in

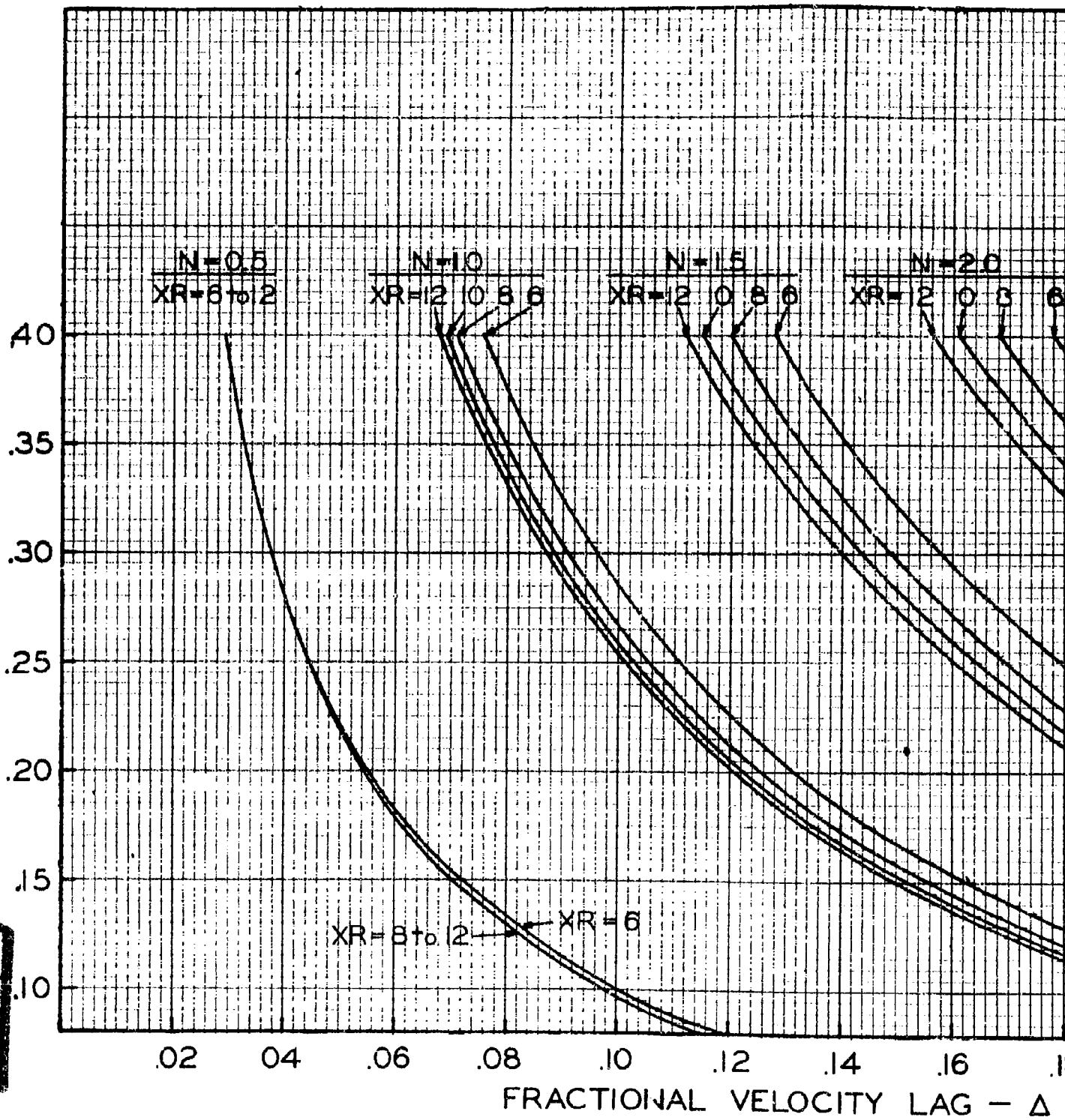
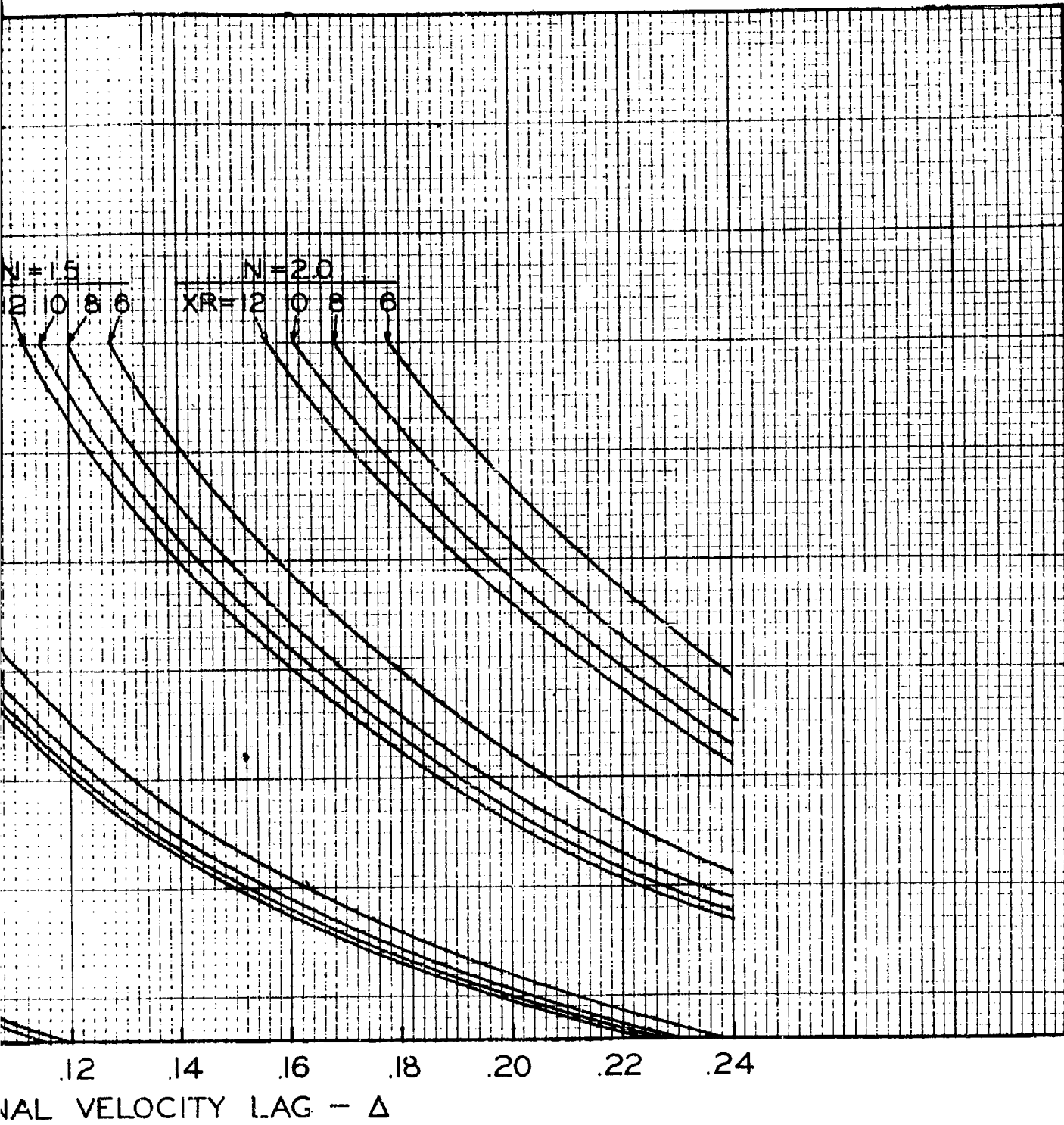
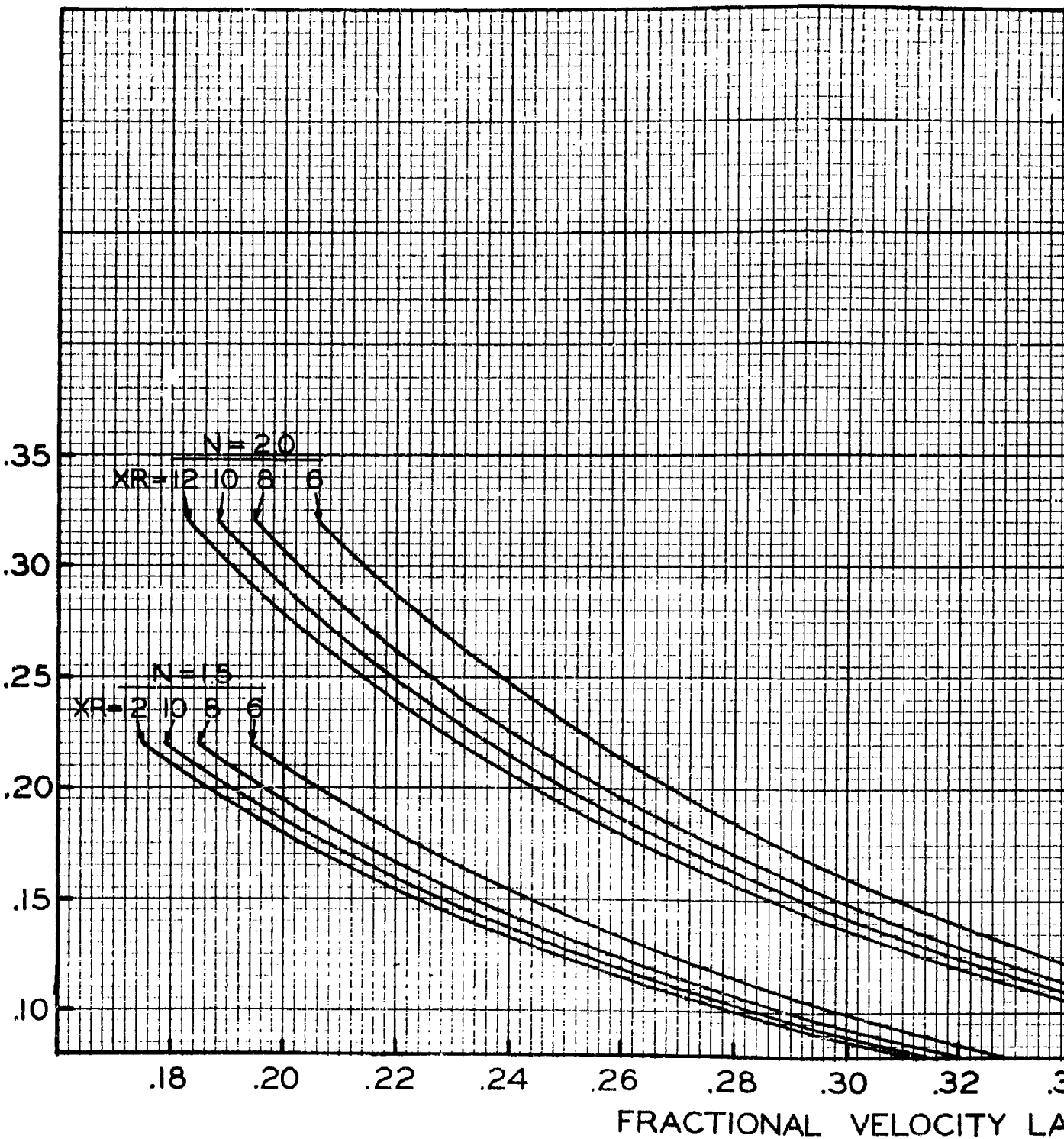


Fig. D-1 Velocity lag curves for .75C.50 motor nozzles.

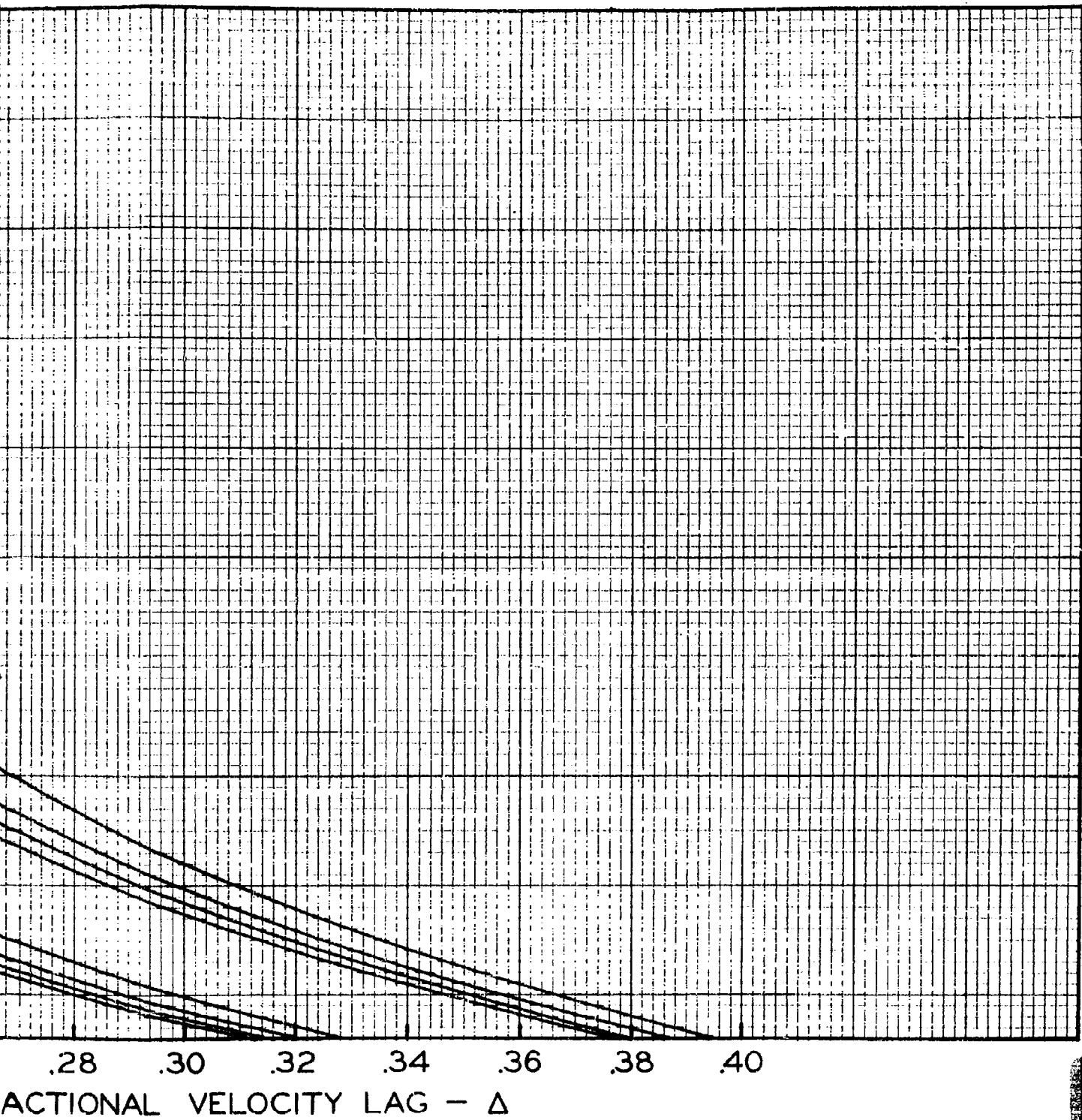
**2**

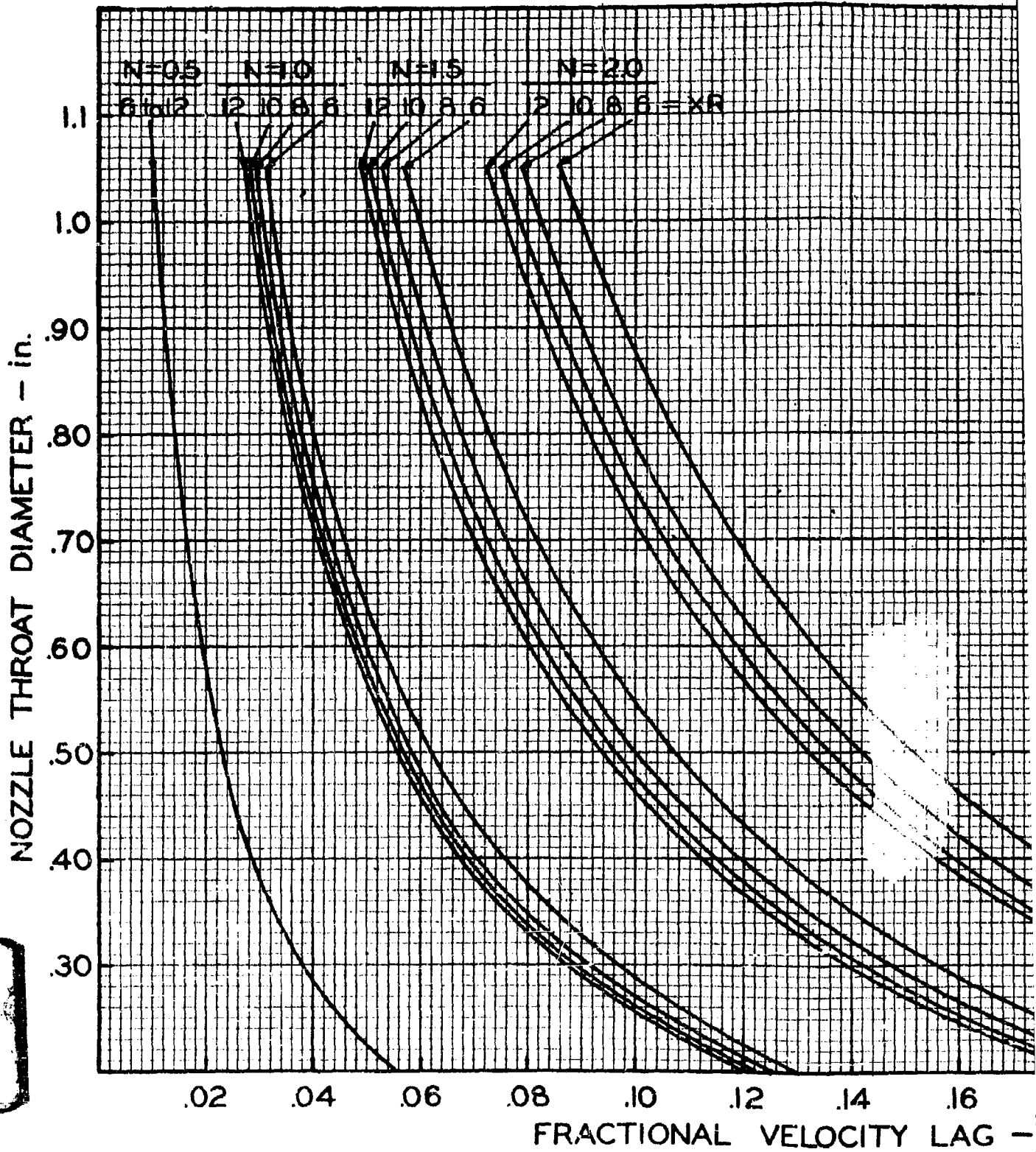
NOZZLE THROAT DIAMETER - in



1

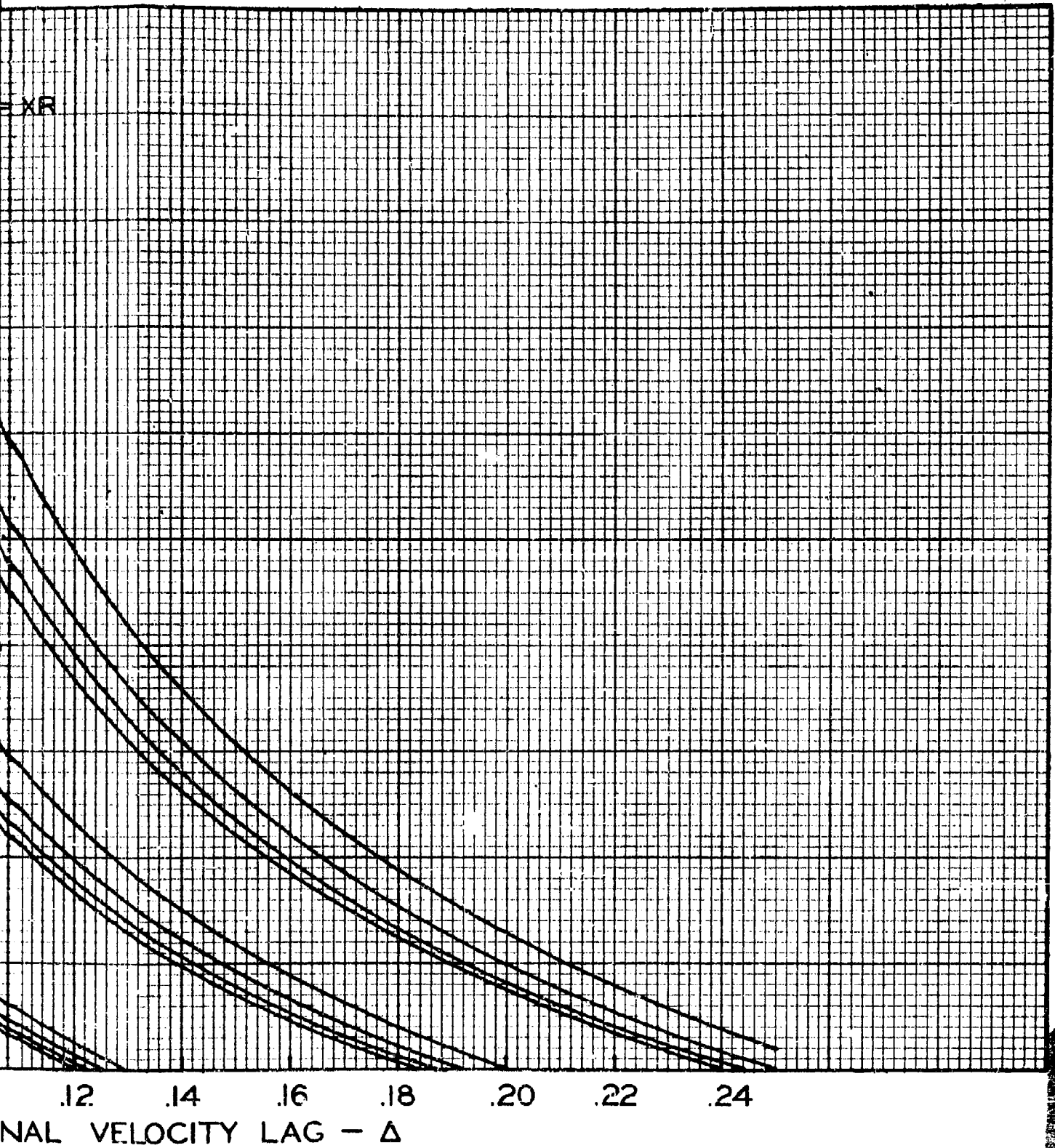
Fig. D-2 Velocity log curves for .75C.50 motor nozzles.

**2**



1

Fig. D-3 Velocity lag curves for 2C1.5 motor nozzles.

**2**

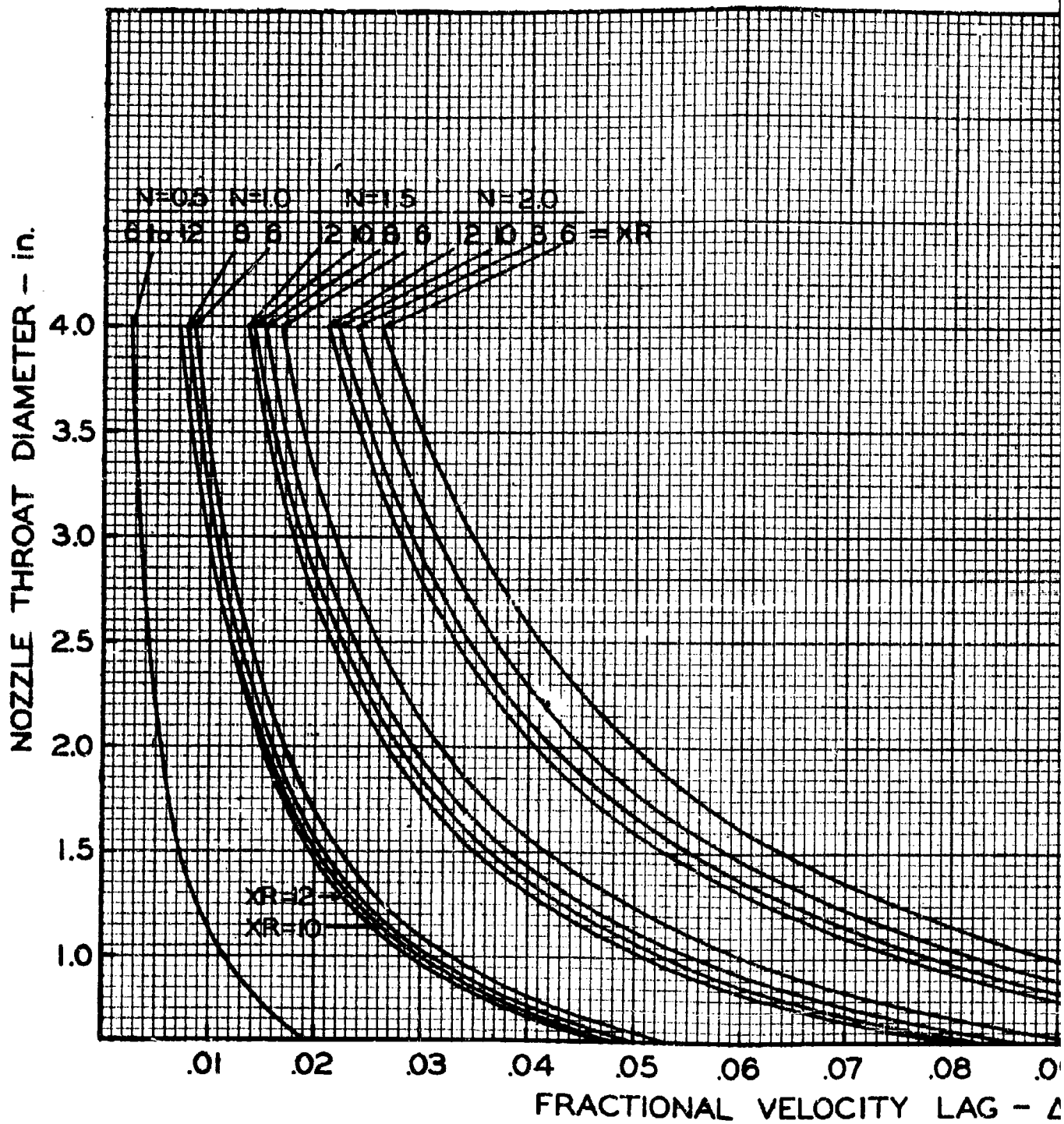
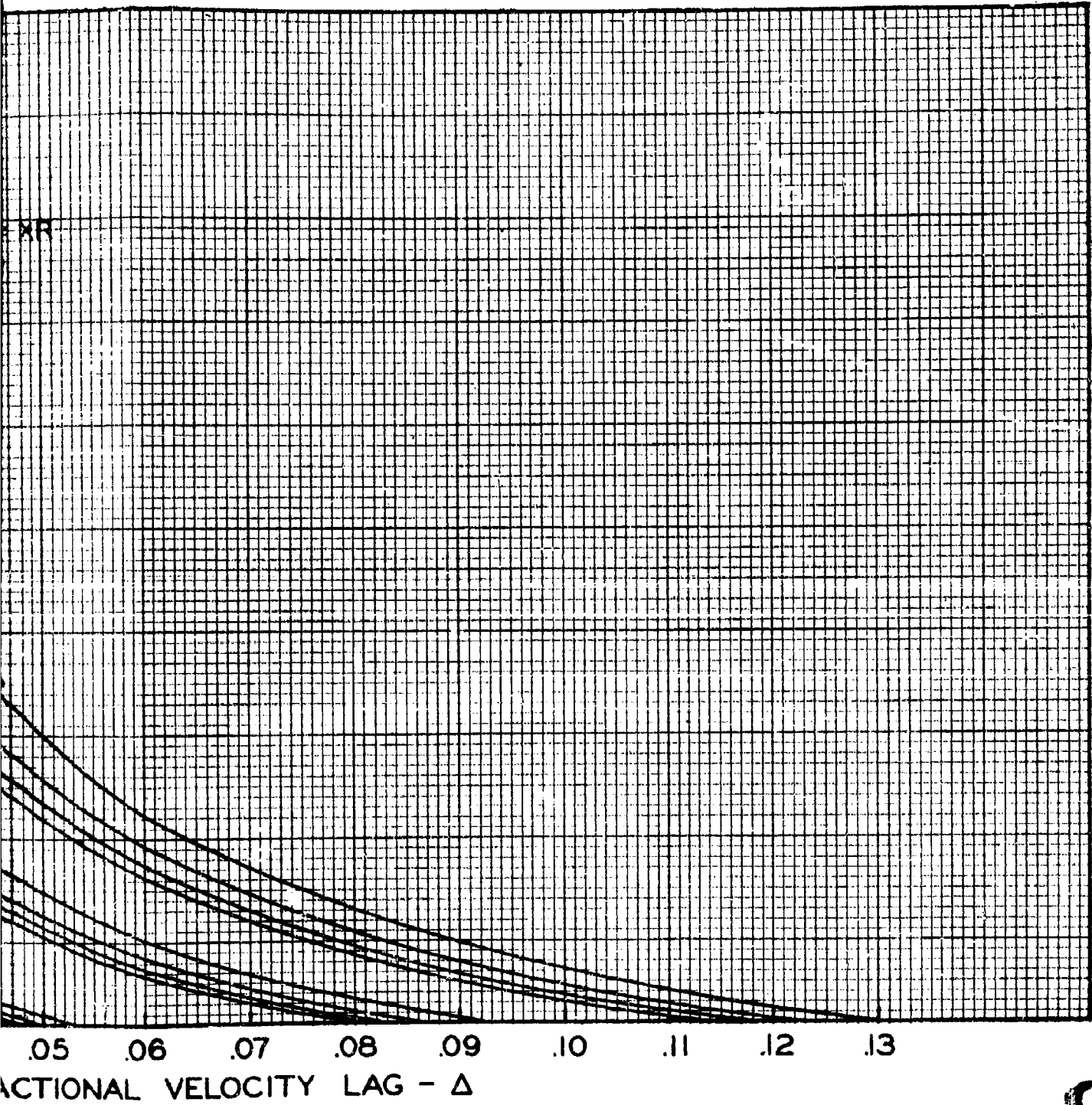


Fig. D-4 Velocity lag curves for 6C5 motor nozzles.

1

**2**

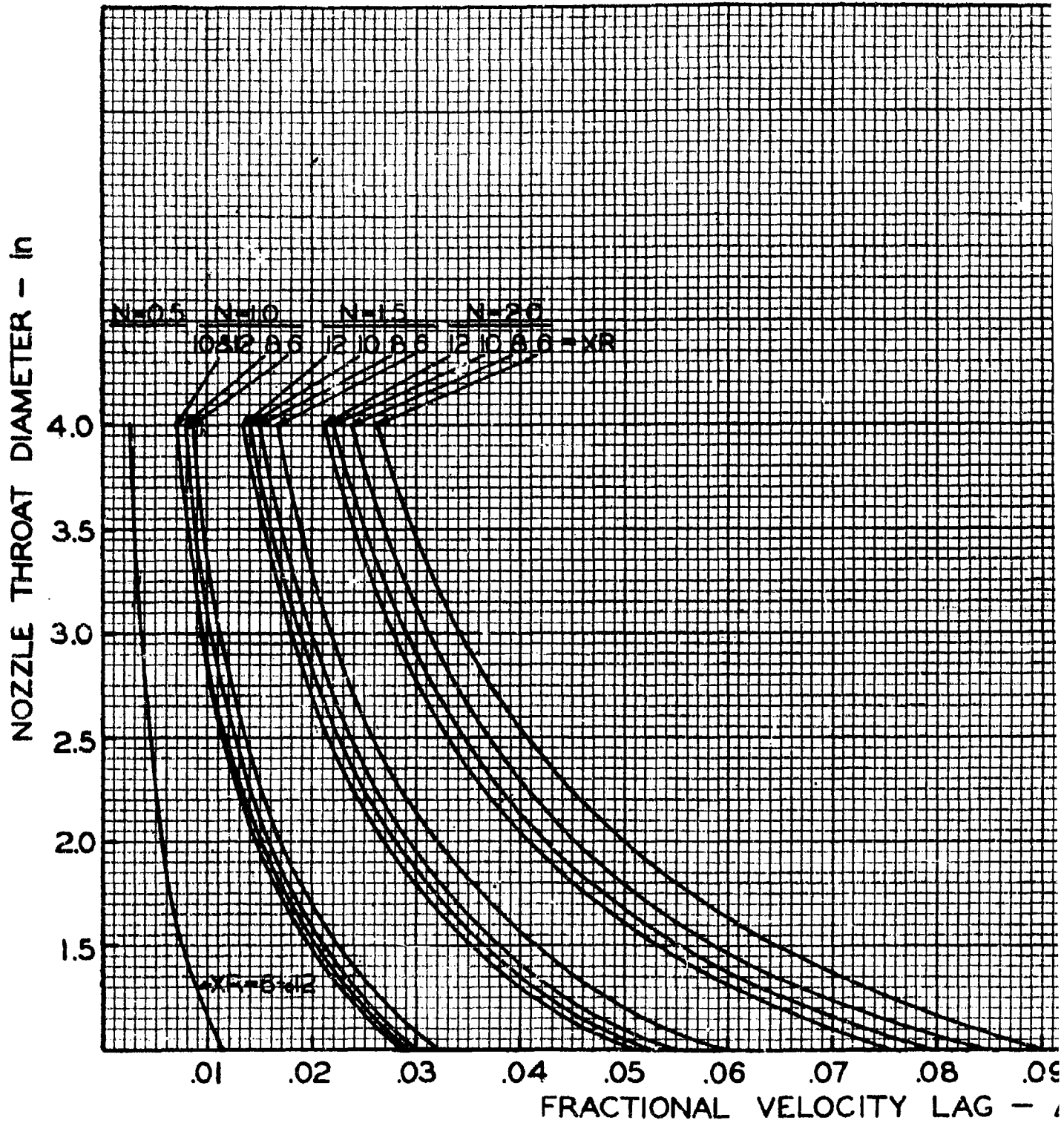


Fig. D-5 Velocity lag curves for BATES motor nozzles.



RACTIONAL VELOCITY LAG - Δ

nozzles.

2

1

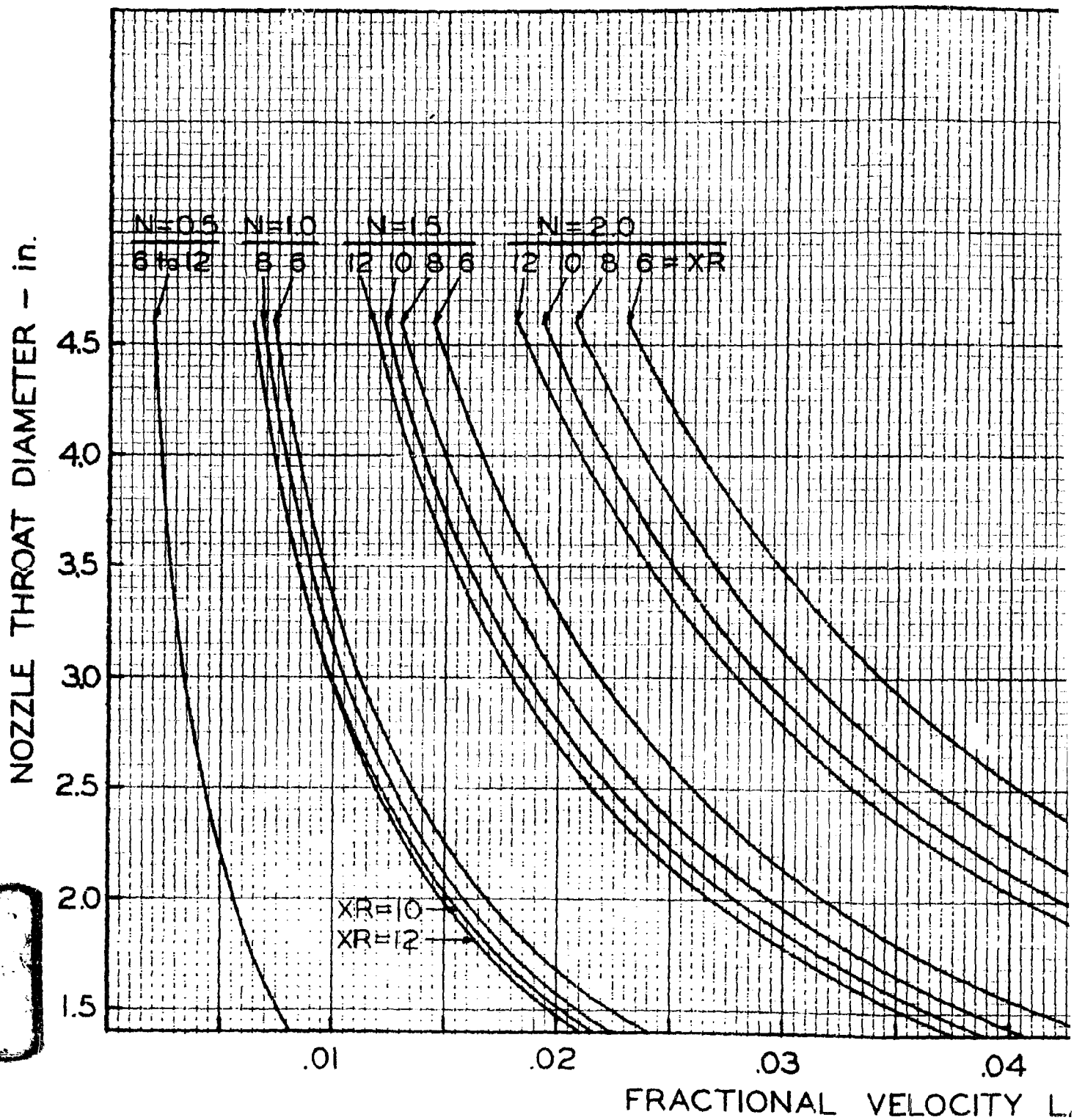
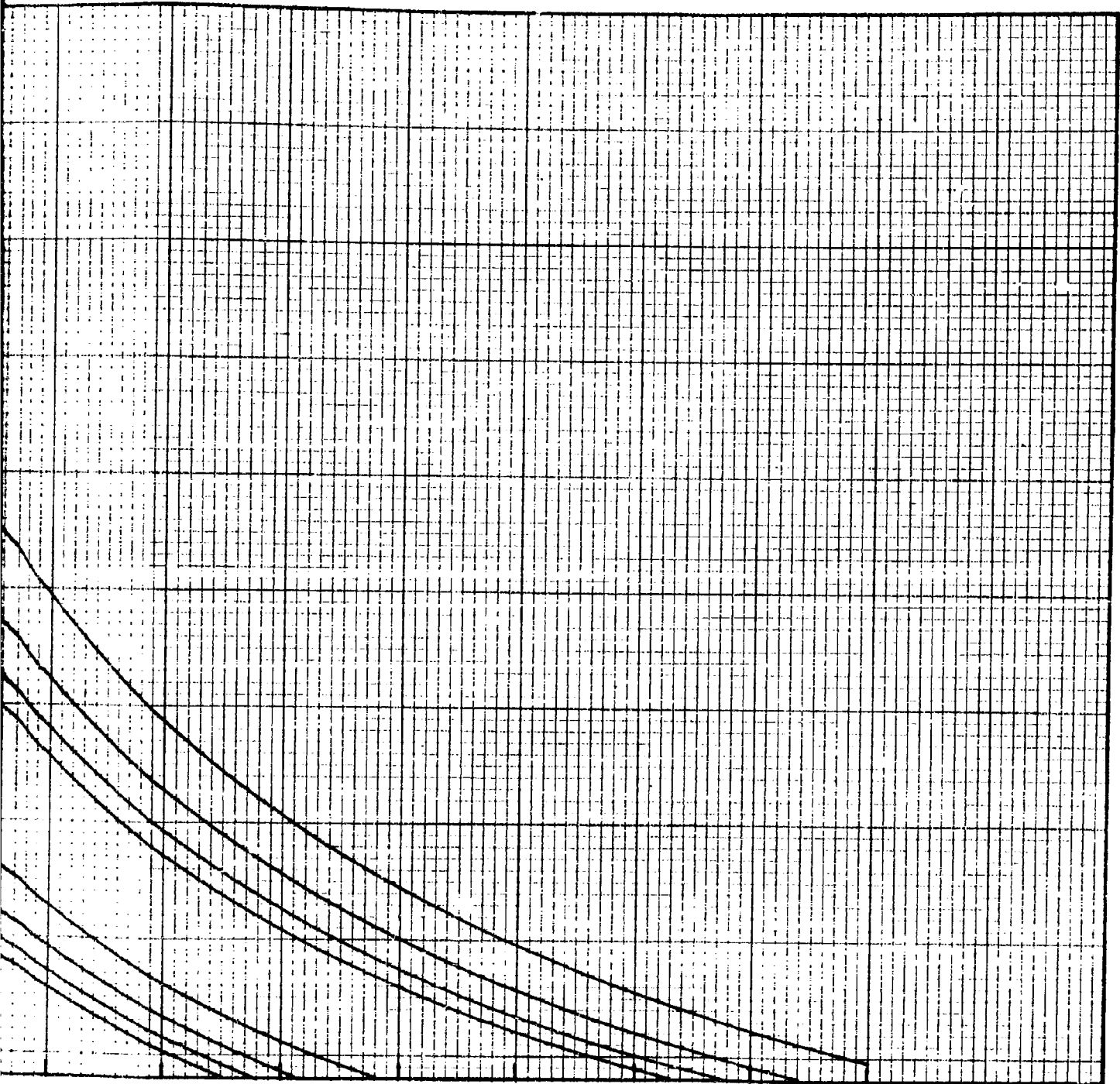


Fig D-6 Velocity lag curves for 10KS-2500 motor nozzles.



.03 .04 .05 .06
RELATIONAL VELOCITY LAG - Δ

2

Appendix E

Example of Scaling Factor Determination and Specific Impulse Prediction1. Scaling Factor Determination

Assume that the data shown in Table E-1 has been obtained for a certain propellant through static tests of micro-motors at $\bar{P}_b = 1000$ psia.

Table E-I
Micro-Motor Static Test Data

Motor	Grain Length in	K_m	D_t in	\bar{F}_b in/sec	XR	t_z sec	A_1^a in ²	m lbm	F_{1000}^o
.75C.50-1.5	1.41	173	0.146	0.60	8.5	0.234	1.645	0.02189	246.4
.75C.50-3.5	3.41	171	0.225	0.60	8.2	0.237	1.653	0.05241	252.2
2C1.5-4	3.88	170	0.386	0.60	8.0	0.470	10.42	0.3306	252.6

^aObtained as outlined in Appendix F.

Assume further that the values listed in Table E-II have been obtained from thermochemical calculations for the propellant.

Table E-II
Thermochemical Data

T_c , °K	Equilibrium T_e , °K	Chamber γ_g	Chamber mols gas/100 g	Chamber mols Al_2O_3 /100 g
3629	2224	1.20	3.65818	0.21239

The following parameters necessary for the calculation of fractional velocity lag (Δ) and for scaling-factor determination may

now be determined:

$$\eta = 1 - \frac{T_e}{T_c} = 1 - \frac{2224}{3629} = 0.38716 \quad (\text{assuming } C_{p_c} = C_{p_e})$$

$$x = \frac{\dot{m}_s}{\dot{m}_s + \dot{m}_g} = 1.0196 \text{ (mols Al}_2\text{O}_3\text{/100 g)} = 1.0196 (0.21239) = 0.21655$$

$$z = \frac{x}{1-x} = \frac{0.21655}{1-0.21655} = 0.27640$$

$$C_{p_g} = \left(\frac{\gamma_g}{\gamma_g - 1} \right) \frac{1.986 \times (\text{mols gas/100 g})}{100} = \left(\frac{1.2}{1.2 - 1} \right) \left(\frac{1.986 \times 3.65818}{100} \right) = 0.4359$$

$$\gamma = \frac{C_{p_g}}{C_{p_{\text{Al}_2\text{O}_3}}} = \frac{0.4359}{0.344} = 1.2672$$

$$\text{GAMMA} = \frac{\gamma_g (1 + z\gamma)}{1 + \gamma_g z\gamma} = \frac{1.2 (1 + 0.2764 \times 1.2672)}{1 + 1.2 \times 0.2764 \times 1.2672} = 1.141$$

$$\text{XMW} = \frac{100}{\text{mols gas/100 g}} = \frac{100}{3.65818} = 27.336$$

The preceding information, together with the nozzle configuration parameters listed in Table D-1 would provide the required input data necessary to calculate Δ values for this propellant using the FORTRAN program described in Appendices B and C. However, the curves of Appendix D will be used to obtain Δ values for this example.

From curves D-1 through D-3 Table E-III may be formed.

Table E-III
Δ Value from Curves of Appendix D

Motor	D ₁	XR	Δ Values			
			N = 0.5	N = 1.0	N = 1.5	N = 2.0
.75C.50-1.5	0.146	8.5	0.0722	0.1582	0.2356	0.3025
.75C.50-3.5	0.225	8.2	0.0490	0.1143	0.1811	0.2398
2C1.5-4	0.386	8.0	0.0298	0.0738	0.1228	0.1703

We are now in a position to calculate q values from Eq. 29 in the text, thereby generating the q-versus-N curves necessary for scaling-factor determination.

$$q = \frac{(F_{1000}^0)^2 - \left(\frac{1 - x\Delta_2}{1 - x\Delta_1} \right)^2 (F_{1000}^0)^2}{\frac{2J\eta}{144g_0} \left[\left(\frac{1 - x\Delta_2}{1 - x\Delta_1} \right)^2 \left(\frac{t_z A_1}{m} \right) - \left(\frac{t_z A_2}{m} \right) \right]}$$

Taking motor 1 as the .75C.50-1.5 motor and motor 2 as the .75C.50-3.5 motor,

$$q = \frac{(252.2)^2 - \left(\frac{1 - 0.21655 \times 0.0490}{1 - 0.21655 \times 0.0722} \right)^2 (246.4)^2}{\frac{2 \times 778.16 \times 0.38716}{144 \times 32.174} \left[\left(\frac{1 - 0.21655 \times 0.0490}{1 - 0.21655 \times 0.0722} \right)^2 \left(\frac{0.234 \times 1.645}{0.02189} \right) - \left(\frac{0.237 \times 1.653}{0.05241} \right) \right]}$$

$$q = \frac{63,604.84 - (1.01021)(60,712.96)}{0.13005 [(1.01021)(17.58474) - 7.47492]}$$

$$q = 1697.9$$

For $N = 1.0\mu$,

$$q = \frac{63,604.84 - \left[\frac{1 - 0.21655 \times 0.1143}{1 - 0.21655 \times 0.1582} \right]^2 (60,712.96)}{0.13005 \left[\left[\frac{1 - 0.21655 \times 0.1143}{1 - 0.21655 \times 0.1582} \right]^2 (17.58474) - (7.47492) \right]}$$

$$q = 1243.3$$

For $N = 1.5\mu$,

$$q = \frac{63,604.84 - 1.02501 \times 60,712.96}{0.13005 (1.02501 \times 17.58474 - 7.47492)}$$

$$q = 1001.1$$

For $N = 2.0\mu$,

$$q = \frac{63,604.84 - 1.02927 \times 60,712.96}{0.13005 (1.02927 \times 17.58474 - 7.47492)}$$

$$q = 806.8$$

We now take motor 1 as the .75C.50-1.5 motor and motor 2 as the 2C1.5-4 motor.

For $N = 0.5\mu$,

$$q = \frac{(252.6)^2 - \left[\frac{1 - 0.21655 \times 0.0298}{1 - 0.21655 \times 0.0722} \right]^2 (60,712.96)}{0.13005 \left[\left[\frac{1 - 0.21655 \times 0.0298}{1 - 0.21655 \times 0.0722} \right]^2 (17.58474) - \left(\frac{0.470 \times 10.42}{0.3306} \right) \right]}$$

$$q = \frac{63,806.76 - 1.01873 \times 60,712.96}{0.13005 (1.01873 \times 17.58474 - 14.81367)} = 4852.7$$

For $N = 1.0\mu$,

$$q = \frac{63,806.76 - 1.03820 \times 60,712.96}{0.13005 (1.0382 \times 17.58474 - 14.81367)}$$

$$q = 1729.9$$

For $N = 1.5\mu$,

$$q = \frac{63,806.76 - 1.05214 \times 60,712.96}{0.13005 (1.05214 \times 17.58474 - 14.81367)}$$

$$q = -149.6$$

For $N = 2.0\mu$,

$$q = \frac{63,806.76 - 1.06220 \times 60,712.96}{0.13005 (1.06220 \times 17.58474 - 14.81367)}$$

$$q = -1358.0$$

The q values calculated above are plotted against the respective assumed N values in Fig. E-1. Two curves result, one for the .75C.50-1.5 and the .75C.50-3.5 motors, and one for the .75C.50-1.5 and 2C1.5-4 motors. The curves intersect at $q = 1180$ Btu/sec-ft² and $N = 1.12\mu$. These values represent the scaling factors for this particular propellant.

2. Specific-Impulse Prediction

Assume that specific-impulse predictions are desired for the propellant in the 6C5-11.4, BATES, and 10KS-2500 motors. Estimates made for the parameters \bar{D}_t , XR , t_2 , A , and m for these motors ($\bar{P}_b = 1000$ psia, $K_m = 170$, $\bar{r}_b = 0.60$ in/sec, density = 0.062 lbm/in³) are summarized in Table E-IV.

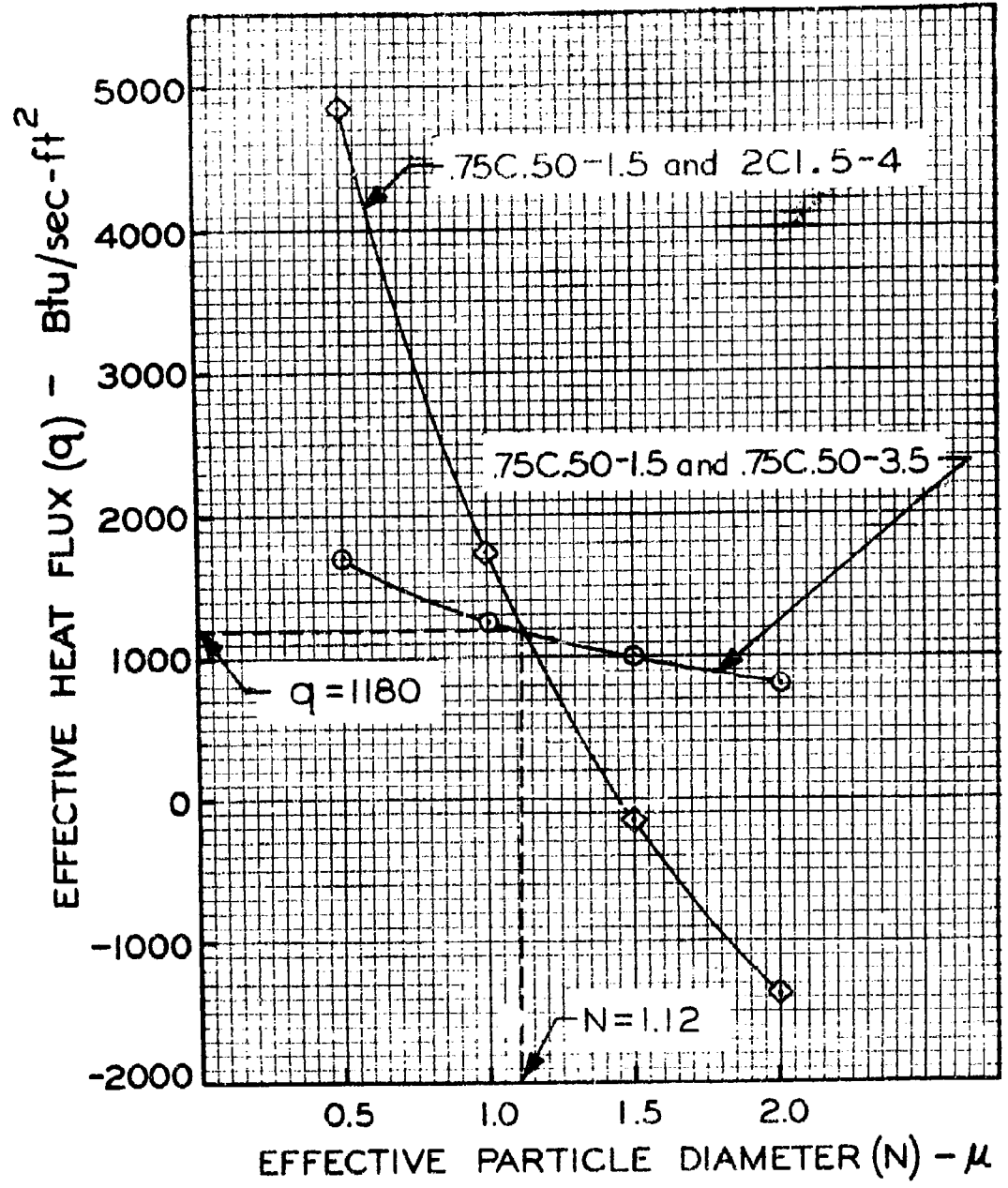


Fig E-1 q-N curves for scaling factor determination

Table E-IV
Estimated Ballistic Parameters

Motor	S_m , in ²	\bar{D}_t , in	XR	web, in	t_z , sec	A , in ²	Volume, in ³	m , lbm
6C5-11.4.	194.78	1.21	8.0	0.50	0.94	85.19 ^a	97.19	6.026
BATES	620.48	2.16	8.0	1.875	3.53	345.89 ^a	1163.4	77.13
10KS-2500	915 ^b	2.62	8.0	1.7 ^b	3.20	102.1 ^b	1570	97.34

^aObtained as outlined in Appendix F.

^bEstimated from non-dimensioned drawings.

The next step is the determination of Δ values for the .75C.50-1.5, 6C5-11.4, BATES, and 10KS-2500 motors at the previously determined effective particle diameter of $N = 1.12\mu$. This may be accomplished by plotting Δ values obtained from the curves of Appendix D (for the specific nozzle configurations) versus N , as shown in Fig. E-2. From Fig. E-2 the following Δ values are read at $N = 1.12\mu$:

For the .75C.50-1.5 motor,	$\Delta = 0.1785$
For the 6C5-11.4 motor,	$\Delta = 0.030$
For the BATES motor,	$\Delta = 0.017$
For the 10KS-2500 motor,	$\Delta = 0.014.$

Taking motor 1 as the .75C.50-1.5 motor and motor 2 as the larger motor, we may now calculate predicted specific impulse of the propellant in the larger motor from Eq. 28, for $N = 1.12\mu$ and $q = 1180$ Btu/sec-ft².

Best Available Copy

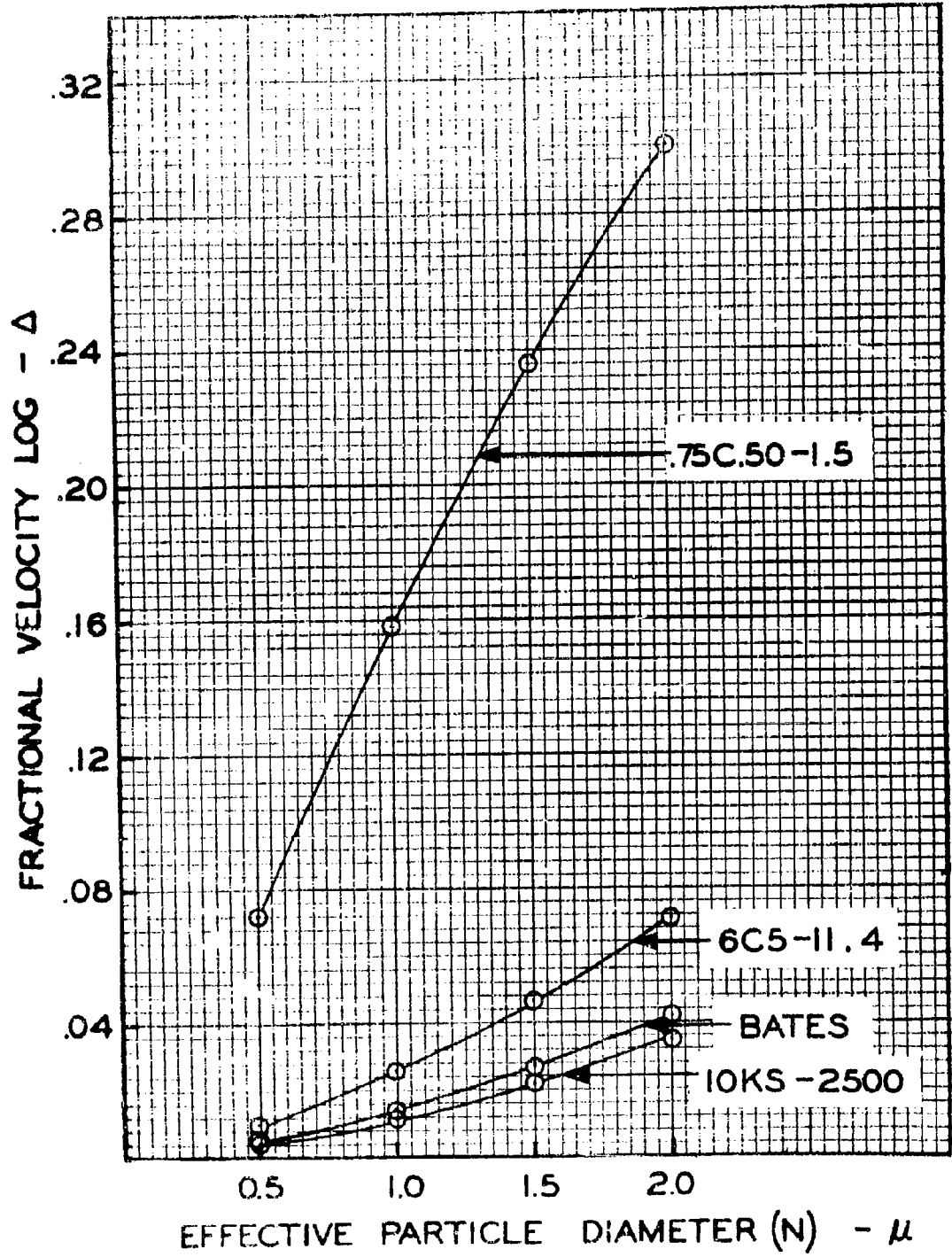


Fig. 1. Fractional velocity for specific particle prediction.

$$(F_{1000}^0)_2 = \sqrt{\left(\frac{1 - x\Delta_2}{1 - x\Delta_1}\right)^2 \left[(F_{1000}^0)_1^2 + \frac{2J\eta g}{144g_0} \left(\frac{t \cdot A}{m}\right)_1 \right] - \frac{2J\eta g}{144g_0} \left(\frac{t \cdot A}{m}\right)_2}$$

For the 6C5-11.4 Motor:

$$(F_{1000}^0)_2 = \sqrt{\left(\frac{1 - 0.21655 \times 0.030}{1 - 0.21655 \times 0.1785}\right)^2 \left[(246.4)^2 + (0.13005)(1180)(17.58474) \right] - (0.13005)(1180) \left(\frac{0.94 \times 85.19}{6.026}\right)}$$

$$(F_{1000}^0)_2 = \sqrt{1.06800 (60,712.96 + 153.459 \times 17.58474) - 153.459 \times 13.28884}$$

$$(F_{1000}^0)_2 = \sqrt{1.06800 (63,411.500) - 2039.292}$$

$$(F_{1000}^0)_2 = 256.3$$

For the BATES Motor:

$$(F_{1000}^0)_2 = \sqrt{\left(\frac{1 - 0.21655 \times 0.017}{1 - 0.21655 \times 0.1785}\right)^2 (63,411.500) - 153.459 \times \left(\frac{3.53 \times 345.89}{72.13}\right)}$$

$$(F_{1000}^0)_2 = \sqrt{1.07406 (63,411.500) - 153.459 (16.92765)}$$

$$(F_{1000}^0)_2 = 256.0$$

For the 10KS-2500 Motor:

$$(F_{1000}^0)_2 = \sqrt{\left(\frac{1 - 0.21655 \times 0.014}{1 - 0.21655 \times 0.1785}\right)^2 (63,411.500) - 153.459 \left(\frac{3.20 \times 102.1}{97.34}\right)}$$

$$(F_{1000}^0)_2 = \sqrt{1.07547 (63,411.500) - 153.459 (3.35648)}$$

$$(F_{1000}^0)_2 = 260.2$$

To summarize, based on previously determined scaling factors of $q = 1180$ Btu/sec-ft² and $N = 1.12\mu$, specific-impulse values of 256.3 would be predicted for the 6C5-11.4 motor, 256.0 for the BATES motor, and 260.2 for the 10KS-2500 motor.

Appendix F

Heat-Loss-Surface-Area Determination

As an aid in determining the heat-loss-surface-area term (A) used in Eqs. 28 and 29, Figs. F-1 through F-4 have been generated. These curves show nozzle surface area versus nozzle throat diameter for the .75C.50, 2C1.5, 6C5, and BATES motor nozzles. Nozzle surface area as used here is defined as the number of square inches exposed to hot gases in the nozzle convergent section only, beginning at the nozzle entrance and ending at the nozzle throat. Nozzle surface area downstream of the nozzle throat is ignored. The total surface area (A) exposed to hot gases is the sum of the area of the firing head, area of initial motor-case ends (not covered by propellant), average motor-case area exposed as the grain ends burn back, and the nozzle surface area.

As an example of the use of the curves, consider a 6C5 motor having a nozzle throat diameter (D_t) of 1.210 inch, a motor-case length (L_m) of 11.40 inch, and an initial grain length (L_g) of 11.25 inch. From Fig. F-3, nozzle surface area = 44.66 in², firing head area = 28.274 in², area of motor case ends = 18.850 (11.40 - 11.25) = 2.828 in², and average area exposed by burning grain ends = 9.425 in². The total exposed area (A) = 44.66 + 28.274 + 2.828 + 9.425 = 85.19 in².

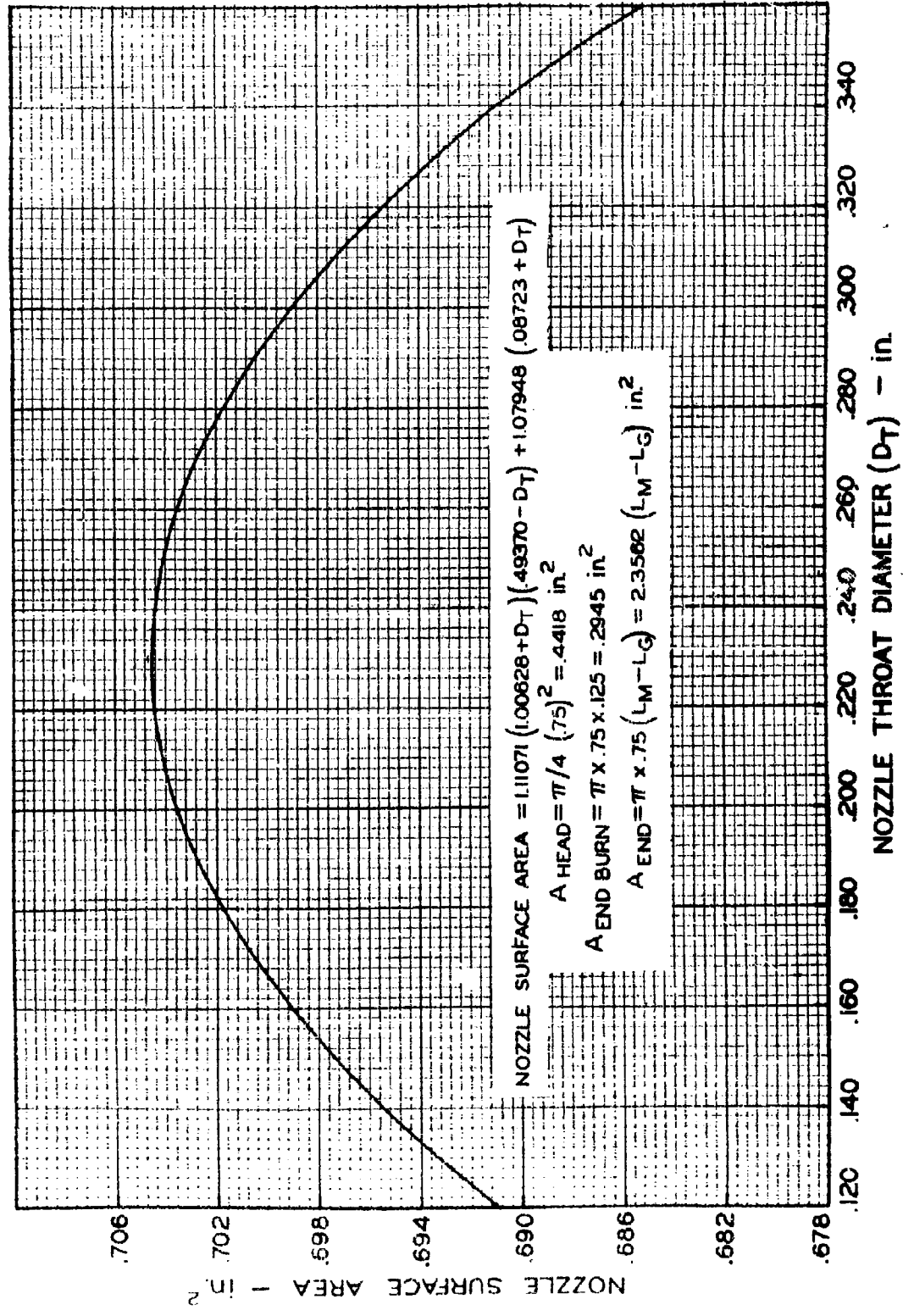


Fig F-1 Nozzle surface area as a function of nozzle throat diameter for .75C.50 motor nozzles.

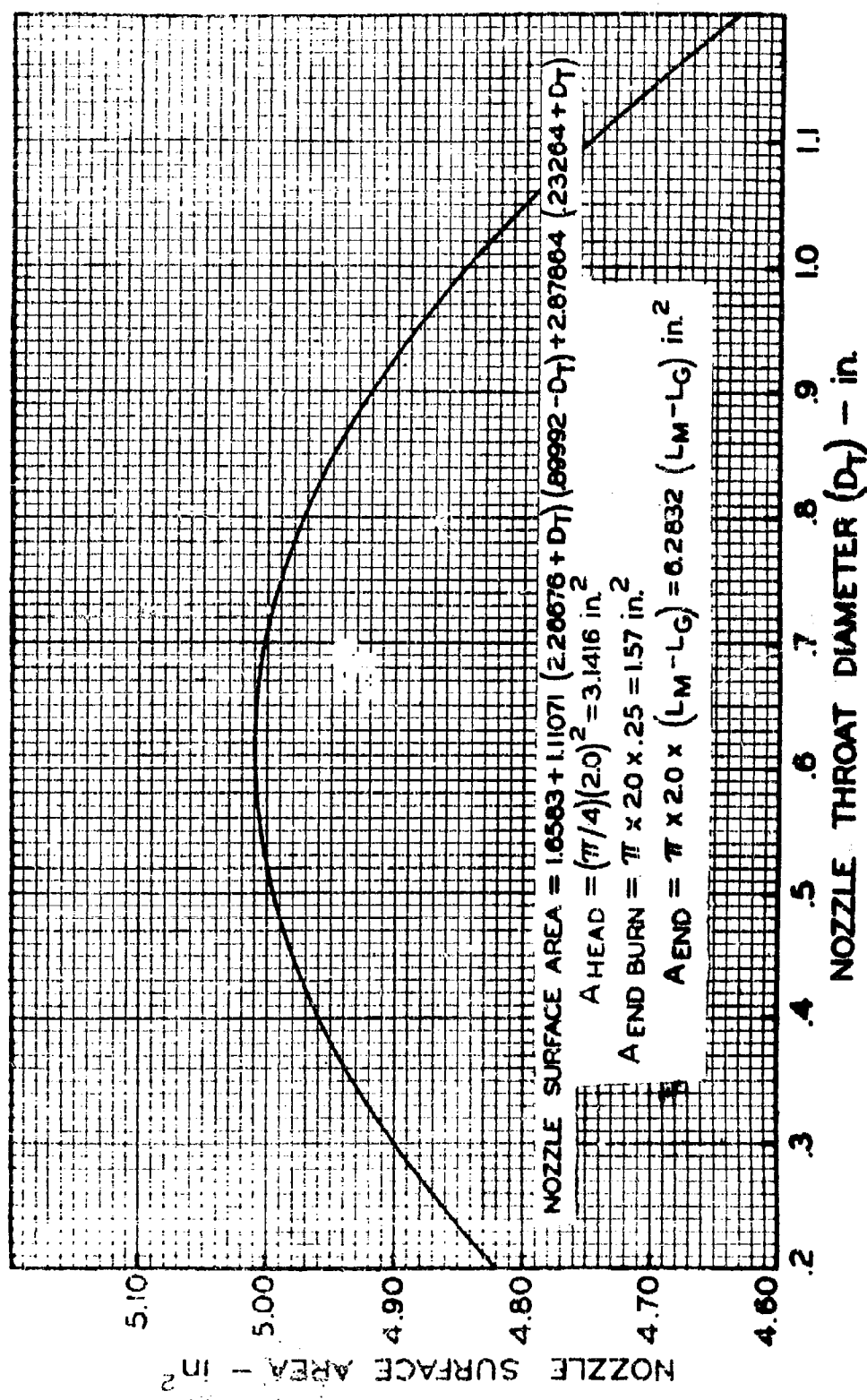


Fig F-2 Nozzle surface area as a function of nozzle throat diameter for 2C1.5 motor nozzles.

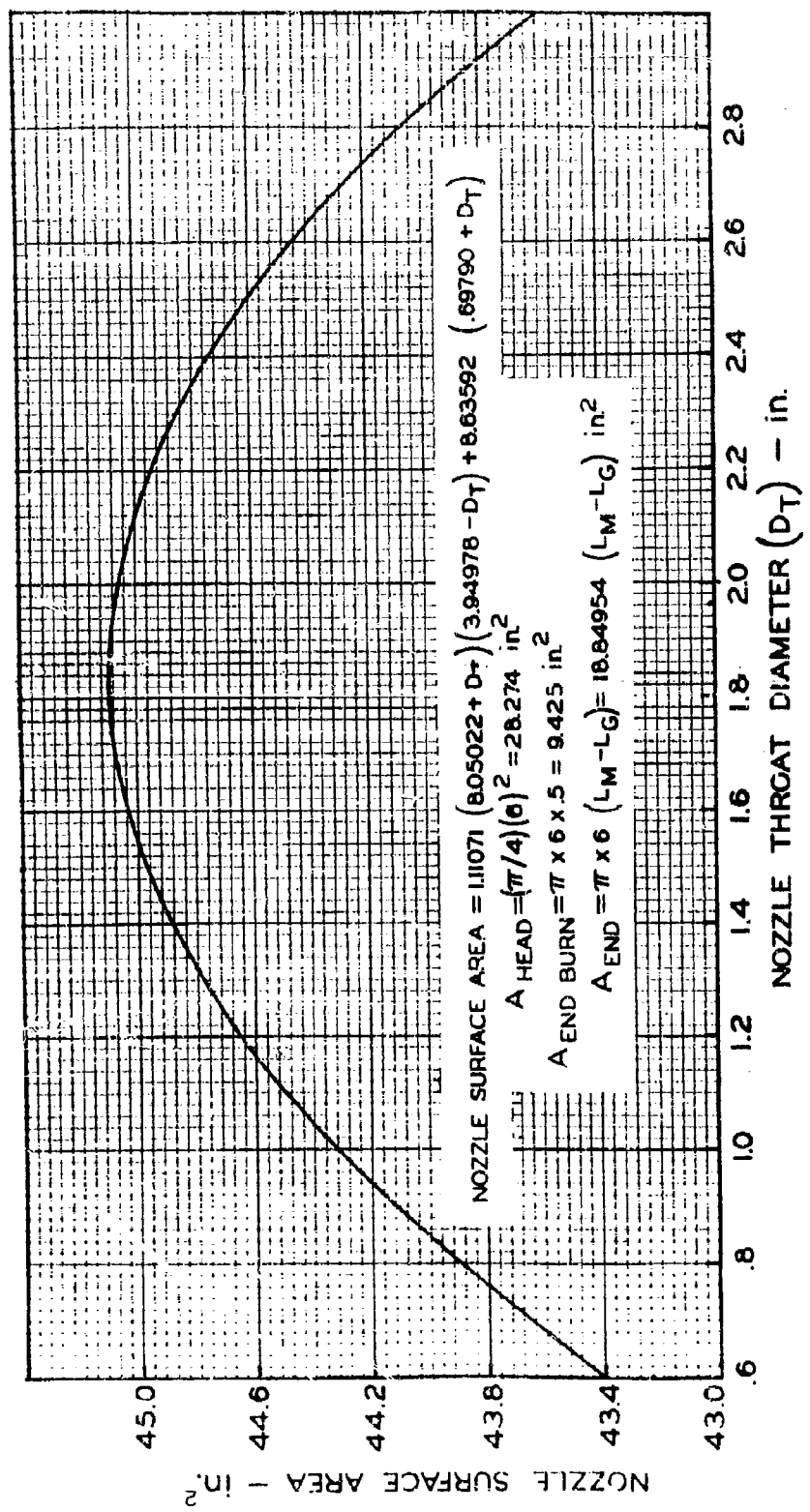


Fig F-3 Nozzle surface area as a function of nozzle throat diameter for 6C5 motor nozzles.

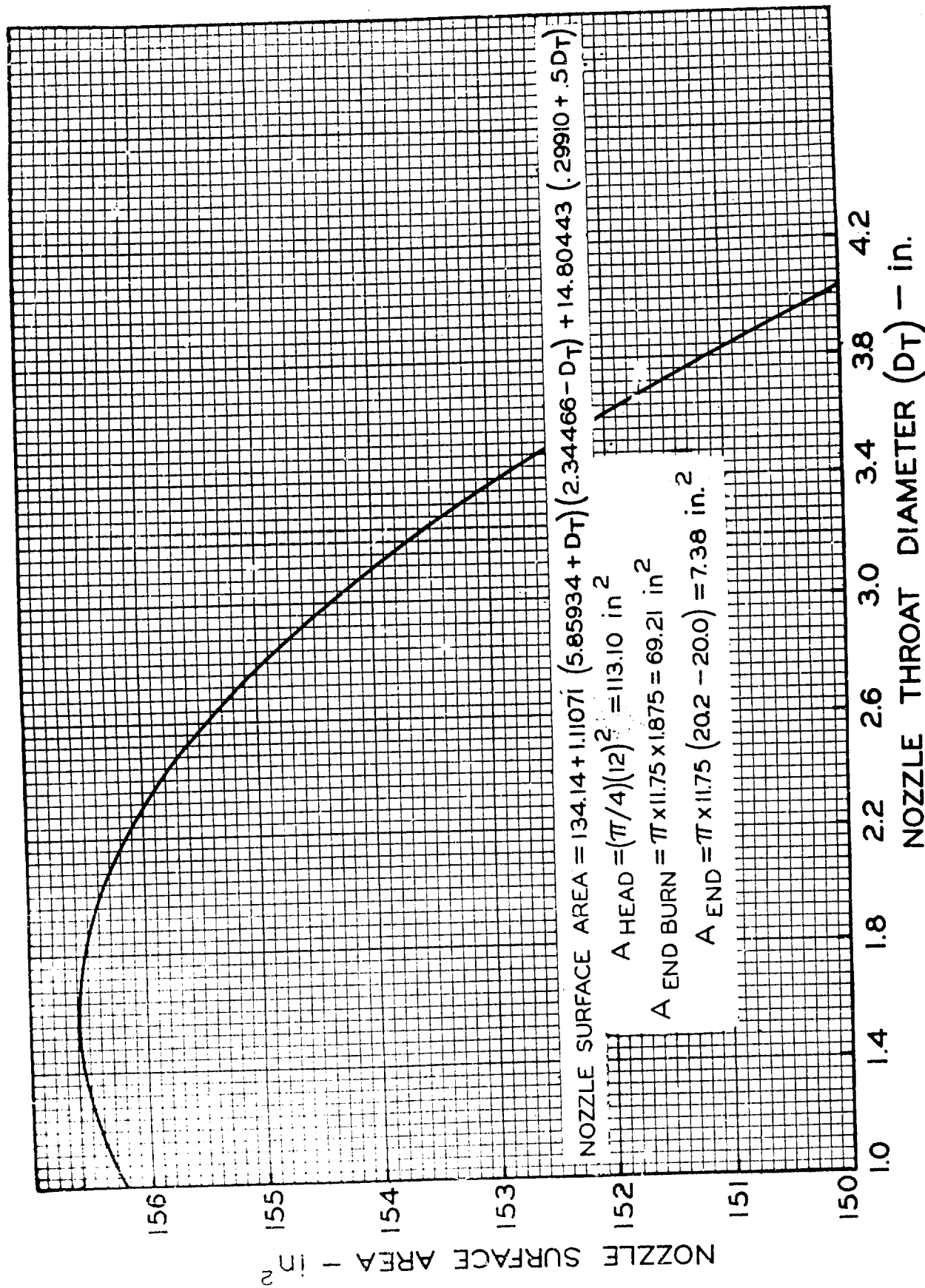


Fig. F-4 Nozzle surface area as a function of nozzle throat diameter for BATES motor nozzles.